ABSTRACT

Polymer thin films are ubiquitous in everyday life, playing a role in fields such as electronics, optics, space science, aircrafts, defense, medicine, sensors, and biotechnology. Thin film stability is a property that describes whether a film forms a continuous layer or ruptures into a morphology often characterized by holes, polygons, or droplets. This latter process, termed dewetting, has traditionally been considered an obstacle to avoid, but more recently it has been harnessed as a tool for producing patterned thin films with features on the nanoscopic scale. Regardless of its desirability, an understanding of the mechanisms that underlie dewetting is critical for tailoring the morphologies of thin films to the specifications of their applications.

The stability of a thin film to some extent depends on its thickness, and spin coating offers a convenient and affordable means for producing thin films of tunable thickness. However, existing models for predicting the film thickness of spin coated films are based primarily on nonpolar polymer thin films and often fail to accurately predict experimentally obtained results. Therefore, the goal of this independent study is to uncover the mechanisms of the polymer deposition and film formation processes for hydrophilic polymers and to work towards a model that predicts the thickness and stability of spin coated hydrophilic thin films. Various hydrophilic polymers were selected as the focus of this investigation on the basis of their crystallinity, degree of hydrophilicity, and polymer charge. Poly(vinyl alcohol) (PVOH) is a semicrystalline polymer that exists in various degrees of hydrolysis corresponding to varying hydrophilicities. PVOH 99%H (more hydrophilic and crystalline) and PVOH 88%H (more hydrophobic and less crystalline) were studied in this work. Additionally, poly(acrylic acid) (PAA) and poly(allylamine hydrochloride) are two amorphous polyelectrolytes whose pH-tunable electrostatic charge and lack of crystallinity offer an insightful point of comparison to the neutral and crystalline PVOH polymers. Poly(sodium 4-styrenesulfonate) (PSS) is a polyanion bearing a permanent negative charge that was selected for this investigation to serve as a pH-resistant point of comparison as well as a slightly more hydrophobic water soluble polymer due to its styrene moiety. Poly(vinyl pyrrolidone) (PVP) is a neutral and amorphous polymer, which makes it similar to PVOH except for its lack of crystallinity. This makes it possible to isolate the effects of crystallinity on the polymer deposition process.

Building on the research of previous lab members, a model for thin film formation that decouples total film thickness into a spontaneously deposited (h_1) layer and a spin deposited (h_2) layer was investigated in order to probe the relative contributions of polymer-substrate and polymer-polymer interactions, respectively, on thin film total thickness and stability. Static adsorption experiments were used to obtain h_1 values for each polymer. These were then subtracted from the total thickness of the spin coated film of the corresponding polymer to determine the thickness of the h_2 layer at various spin rates. Film morphologies under atomic force microscopy (AFM) were used to determine the stability of spin coated films. This information, combined with h_1 and h_2 values, allowed for an analysis of how the film formation process results in stability or lack thereof in the context of each polymer's combination of properties.

PVOH 99%H, PVOH 88%H, and PVP spin coated on silicon wafer are stable systems, forming films that do not dewet at any spin rate. Meanwhile, PAA, PAH, PSS, and PAA^- spin coated on a silicon substrate are metastable systems because they dewet at some or all spin rates. PVOH 88%H, PVP, and PAA^- formed relatively thicker films at the highest spin rates, indicating the presence of a thicker h_1 layer. In the case of PVOH 88%H and PVP, this was attributed to the

hydrophobicity of the polymer. In the case of PAA^-, this was attributed to the aggregates that formed upon titration of PAA with NaOH to produce PAA^-. At the lower spin rates, PVOH 99%H and PVOH 88%H formed relatively thicker films, which is evidence of a thicker h_2 layer. This was attributed to the crystallinity of the polymers and, in the case of PVOH 88%H which was the thickest film at the lowest spin rate, polymer hydrophobicity. PAA, PAH, PSS, and PAA^- all yielded shallow spin curves that were thinner than the stable systems at all spin rates (except PVOH 99%H at the highest spin rate). This is indicative of both weak cohesive forces and weak adhesive forces. However, the dewetting observed for these four systems implies that the cohesive forces dominate over the adhesive forces. Only PAH and PSS had spin curve exponents near -0.5, predicted by the well-known Meyerhofer model. The other exponents ranged from -1.3 to -0.2. The h_1 thicknesses obtained from static adsorption experiments did not align with what was expected based on the properties of each system and the spin coated thickness at the highest spin rates. Only PVP formed a significant h_1 layer, and all polymers including PVP formed thinner h_1 layers than anticipated. This discrepancy was attributed to the presence of a loosely bound layer within the h_1 layer that was rinsed off during the rinse steps associated with the static adsorption procedure. Repeating static adsorption with fewer rinse steps using PAA and PAA^- showed that reducing the number of rinse steps produced h_1 layers more similar in thickness to the h_1 thickness projected by spin coated film thickness at the highest spin rate.

The insights achieved through this work lay the foundation for future efforts to identify an experimental procedure that can produce h_1 layers of reliable thickness. This will allow for a validation of the proposed decoupled thickness model. Additionally, this work has continued the ongoing effort to probe the effects of crystallinity, hydrophobicity, and electrostatic charge on adhesive and cohesive forces within polymer thin films. However, future work is still needed to explore some of the nuances of these polymer systems, particularly the apparent absence of hydrogen bonding as a driving force for polymer adhesion to the silicon substrate.

AN INVESTIGATION OF THE STABILITY OF HYDROPHILIC POLYMER THIN FILMS: CRYSTALLINITY, HYDROPHILICITY, AND ELECTROSTATIC CHARGE

Carolina Shippey Alvarez

A thesis presented to the faculty of Mount Holyoke College in partial fulfillment of the requirements for the degree of Bachelor of Arts with Honors

Department of Chemistry

South Hadley, Massachusetts

April 2023

This thesis was prepared under the direction of Dr. Wei Chen for 8 credits of independent study

ACKNOWLEDGEMENTS

The work presented in this thesis reflects the efforts of a team of people, and neither the research process detailed here, nor the writing of this thesis would have been possible without the contributions of each of these people. I would like to begin by thanking Professor Wei Chen for all the support she has provided me over the past four years. She has pushed me to set and achieve goals I could not have imagined before I set foot on the campus of Mount Holyoke College, while also reminding me to be patient with myself and strive for a balanced lifestyle that maximizes productivity and happiness. It has been a privilege to work with and learn from someone so dedicated to the development of her students.

I also would like to thank Professor Himali Jayathilake for her contribution to my development as a student and researcher. I appreciate her dedication to teaching me how to think critically about results and helping me develop my scientific communication skills. She plays an integral part in creating a welcoming lab environment where I have felt comfortable asking questions, learning from mistakes, and displaying the vulnerability that is often part of the learning process.

I am also extremely grateful to Professor Kyle Broaders and Professor Tori Day for serving on my thesis committee. I have very fond memories of taking courses with both of them and am so lucky to be able to conclude my undergraduate experience with their dedication to helping me prepare the best possible version of my thesis.

The work detailed in the following pages has taken place over hundreds of days, many of which I have spent alongside my lab mates. I am so grateful to be surrounded by a team of hard working, kind, and bright peers. I would like to thank Katie Kolozsvari, who served as a thoughtful and patient mentor during my first semester in the lab. I also appreciate the welcoming lab environment created by Maggie Minett, Yuxin Jiang, Anya Chinniah, and Carlie Poworoznek, who served as excellent role models and whom I have looked up to since my first day in the lab. This supportive environment has lived on through the current members of the lab, Julia Griffin, Nancy Jiang, Eliza Butler, Mackenzie Windus, Isabel Xu, Sophie Lee, Mamie Mulder, Wenqi Zhou, and Gracie Wilkinson, who are amazing collaborators and friends.

I have learned that research is not always perfect and rarely easy. A large part of why I am able to rise to the challenges that come with navigating the research environment is because I have an amazing support system among my friends at Mount Holyoke, who have helped me through tough times and joined me in celebrating the brighter ones.

Finally, I would like to thank my family for the support they have given me for the past 21 years. Without them, I could not have accomplished the task of writing this thesis, let alone all the other goals I have set for myself since the earliest days of my education. I am extremely lucky to have parents who are so dedicated to my personal and academic growth and a sister who always manages to put a smile on my face.

TABLE OF CONTENTS

Page Number

LIST OF FIGURES AND TABLES

Page Number

1. INTRODUCTION

1.1 Surface Modification and Context/Relevancy

Surface modification is a process that is relevant to a variety of fields and has far-reaching applications. Motivations for modifying the surface of a bulk material include but are not limited to altering wettability to tailor the material to a specific application, reducing surface energy to minimize contamination, increasing surface energy to facilitate further modification or adhesion, or imparting specific chemical functionality to the surface of a material. Surface modification offers the benefit of retaining the desired properties of the bulk material while achieving the application-relevant properties of the surface, as opposed to searching for a material that possesses both the desired bulk and surface properties, which can often be challenging.

A common approach for surface modification is the use of thin films, which have found a home in fields such as electronics, optics, space science, aircrafts, defense, medicine, sensors, biotechnology, and others.[1,2] Thin films have been incorporated into devices or components such as flat panel displays, computer chips, semiconductors, antireflective coatings, and solar cells as well as utilized for techniques such as lithography and chromatography.[1] Thin films can be composed of a range of materials such as metals, ceramics, or carbon-based compounds, but polymer thin films are of value due to their cost-effectiveness, lightness, and flexibility.[2]

There is a rich body of literature focused on the preparation of nonpolar, nonvolatile van der Waals thin films on hydrophobic substrates. However, less is known about hydrophilic thin films prepared from aqueous solution despite their importance for technological applications and the additional benefit of their environmental friendliness. The presence of destabilizing polar

interactions adds a layer of complication to their behavior, requiring more in-depth investigation. In an effort to contribute to the ongoing effort to elucidate the behavior and properties of hydrophilic polymer thin films, the work described here focuses on the preparation of water-soluble polymer thin films using spin coating with the aim of developing a model to conceptually describe the deposition process and quantitatively predict film thickness and stability.

1.2 Poly(vinyl alcohol)

Poly(vinyl alcohol) (PVOH) is a versatile polymer that has garnered much attention due to its ability to adsorb to and form stable films on a range of substrates.[3,4,5,6,7] PVOH is a water-soluble, amphiphilic polymer synthesized by the hydrolysis of poly(vinyl acetate) (PVA) (**Figure 1**).

The hydrolysis of PVA to produce PVOH allows for control over the degree of hydrolysis of PVOH. Degree of hydrolysis refers to the percentage of acetate groups that are hydrolyzed to alcohol groups. A higher degree of hydrolysis corresponds to a greater percentage of alcohol groups, increased hydrophilicity, and increased crystallinity. The two degrees of hydrolysis used in this work are 88% hydrolyzed (88%H) and 99% hydrolyzed (99%H) PVOH. The degree of hydrolysis influences the adsorption behavior of PVOH and therefore the thickness and potential stability of the resulting thin films.[5,6]

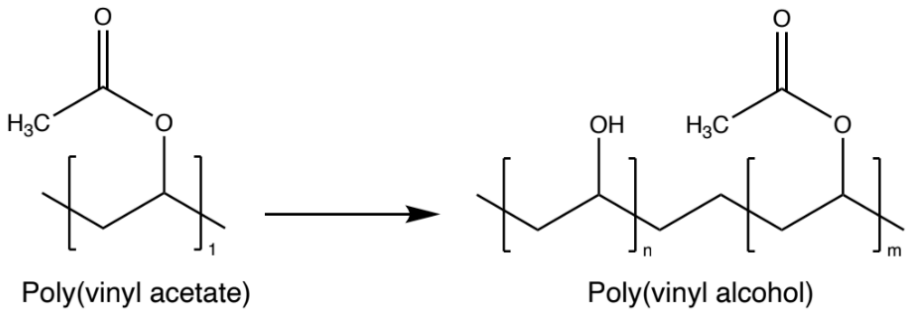

Figure 1. Poly(vinyl alcohol) is synthesized via the hydrolysis of poly(vinyl acetate)

PVOH is comprised of a repeating vinyl alcohol monoclinic unit cell (**Figure 2**) with a repeat unit length of 2.52 Å, which has been cited as evidence of a zig zag carbon backbone.[8,9,10] Its amphiphilicity arises from the hydrophobicity of its carbon backbone and the hydrophilicity of its hydroxyl groups. The hydroxyl groups can occupy either D or L positions, giving rise to two stereochemical possibilities. There is a random distribution of syndiotactic and isotactic repeat units, so there is approximately a 50% occupancy of either the D or L positions.[8] Despite this atacticity, which results from the atacticity of its PVA precursor, PVOH is semicrystalline[8,11,12,13] while atactic PVA is not. The ability of PVOH to crystallize is attributed to the small size of the hydroxyl groups, which allows PVOH to adopt a similar crystal lattice structure to that of polyethylene without disrupting the lattice structure.[8,14] This crystallinity arises from the extensive hydrogen bonding between adjacent PVOH chains,[8,10,12,15] which is also responsible for the relatively high melting point (T_M 230 ^oC) compared to similar polymers such as polyethylene (T_M 117-135 ^oC). PVOH can be anywhere from 18% to 75% crystalline depending on the presence of ions such as LiCl (which interfere with crystallization)[16] or thermal annealing (which increases crystallinity).[11,12,16]

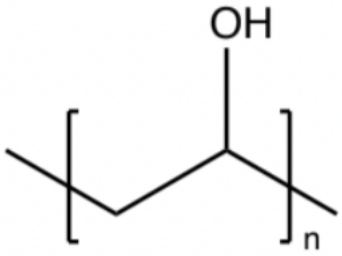

Figure 2. The structure of a repeat unit of poly(vinyl alcohol)

The mechanism for PVOH adsorption to hydrophobic substrates is a two-stage process that begins with the physisorption of PVOH chains to the surface of the hydrophobic substrate.[4,5] The hydrophobic effect has been implicated as the primary driving force for this step,[4,5,6,7] which is made possible by the amphiphilic nature of PVOH. Because the acetate groups adsorb to the hydrophobic substrate, DeWitt et. al. proposed that the energy barrier to PVOH deposition is the hydration of acetate groups.[3] Following deposition of PVOH onto the substrate, crystallization occurs via the formation of inter- and intramolecular hydrogen bonds that stabilize the polymer chains at the hydrophobic substrate-aqueous solution interface.[4,5] In addition to adsorbing to hydrophobic substrates, PVOH has also been shown to adsorb to hydrophilic substrates such as silicon wafers. Adsorption of PVOH to silicon wafers is driven by hydrogen bonding between the hydroxyl groups on PVOH and the silanol and silanolate groups on the silicon wafer.[17,18,19,20]

1.3 The Silicon Substrate

The substrate used for this work is silicon, or silicon wafer. Silicon is the most commonly used material in semiconductors, which are used to make many of the critical components of electronic devices such as memory storage chips and microprocessors.[21] Silicon is an ideal

material to serve this role because of its ability to conduct electricity at room temperature as well as higher temperatures.[22] Additionally, silicon is the second most abundant element on Earth, making the mass production of silicon-based semiconductors economically feasible.

Silicon wafers are atomically smooth (root-mean-square (rms) roughness around or below 1 nm),[23] which makes them ideal for characterization using atomic force microscopy (AFM), and the high refractive index (n = 3.88) of silicon allows for the use of ellipsometry to measure the thickness of thin films prepared on silicon wafers. Their surfaces are characterized by the presence of silanol groups, which offer the potential for chemical functionalization. This combination of properties makes silicon wafers ideal for use in academic research labs such as the work with PVOH thin films described here.

Silicon wafers are comprised of three layers (**Figure 3**):

(1) Silicon bulk – crystalline silicon, which exists in the diamond cubic crystal structure.

(2) Silica (silicon dioxide) – in the presence of oxygen and humidity in the air, a native oxide layer of thickness on the order of 10 Å forms in a layer-by-layer manner.[24]

(3) Surface silanol and siloxane groups – dotting the surface of the native oxide layer are silanol and siloxane groups that form spontaneously during surface reconstruction to reduce the high surface energy of the silicon dioxide layer.[25] Silanol groups make the surface of silicon wafers hydrophilic and have a pKa of 5.6, which allows them to be deprotonated to form silanolate groups.[26]

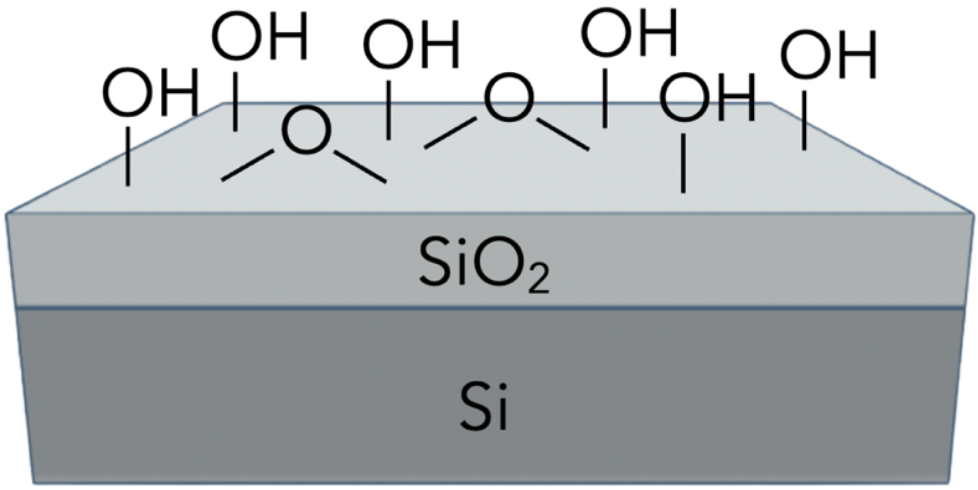

Figure 3. Silicon wafers consist of three layers: a bulk layer of crystalline silicon, whose high surface energy is reduced by the spontaneous formation of a silicon dioxide layer. This native oxide layer is dotted with surface silanol and siloxane groups that render the wafer hydrophilic.

1.4 Comparison Polymers

In order to investigate the role that crystallinity plays in the adsorption and stability of polar thin films, several amorphous water-soluble polymers were investigated. Information regarding each of these polymers is summarized in **Table I**.

1.4.1 Poly(acrylic acid) (PAA)

Poly(acrylic acid) (PAA) is an amphiphilic, water-soluble, synthetic weak polyelectrolyte prepared via the radical polymerization of acrylic acid.[27] Each repeat unit (**Figure 4**) consists of a carboxylic acid that can be deprotonated (pKa 4.5-6.5),[28,29,30] rendering the polymer negatively

charged. This results in electrostatic repulsion of nearby polymer chains. Unlike PVOH, PAA is amorphous.[29]

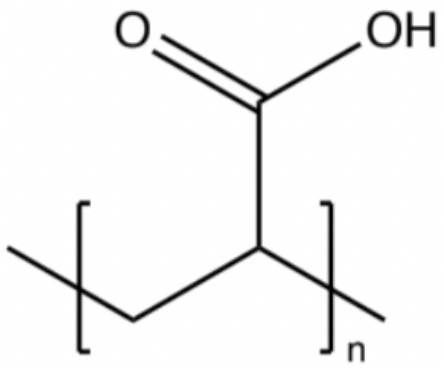

Figure 4. The structure of a repeat unit of poly(acrylic acid)

PAA is non-toxic, biocompatible, adhesive (due to the presence of carboxylic acid groups), and can be crosslinked to improve its mechanical properties, which makes it an ideal candidate for use in medical adhesives, biomedical nanocomposites, drug storage and delivery materials, packaging materials, and pharmacology, among other biological and medical purposes.[31]

1.4.2 Poly(allylamine hydrochloride) (PAH)

Poly(allylamine hydrochloride) is also an amphiphilic, water-soluble, synthetic, weak polyelectrolyte prepared via the polymerization of the allylamine monomer (**Figure 5**), which contains a primary amine that is responsible for many of the characteristic properties and behaviors of PAH. PAH cannot be prepared via radical polymerization due to a phenomenon termed degradative chain transfer, in which the allylic hydrogen is transferred to the radical at the growing ends of the polymer, thus terminating the polymerization process.[32,33,34] Instead,

PAH can be prepared by polymerizing an inorganic salt of allylamine via bulk or solution polymerization followed by swapping of the salt used during synthesis for hydrochloride.[35,36,37] Like PAA, PAH is amorphous,[37] offering a good point of comparison to PVOH. At neutral pH, the amine group is protonated, and the polymer is positively charged; however, the amine group can be deprotonated (pKa ~8.7),[30,38] rendering the polymer neutral.

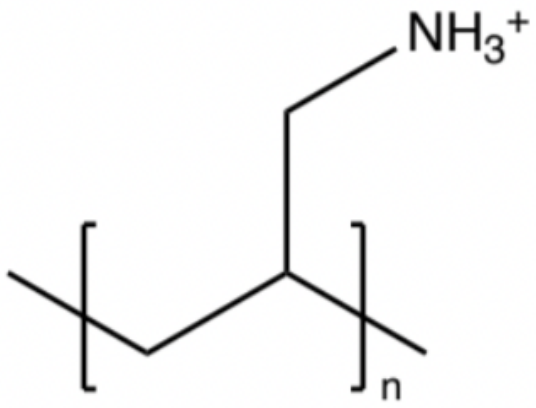

Figure 5. The structure of the repeat unit of poly(allylamine hydrochloride)

The most common application for PAH is in layer-by-layer (LBL) engineered capsules, which are hollow capsules on the order of microns or nanometers. These capsules can be prepared using a number of synthetic or naturally occurring materials, but a common technique is to alternately layer cationic and anionic polyelectrolytes, such as PAH and PAA,[39] onto a support that is ultimately removed to create a concavity within the capsule. These capsules have been used for drug delivery, sensing, catalysis and microreactors.[40]

1.4.3 Poly(sodium 4-styrenesulfonate) (PSS)

Poly(sodium 4-styrenesulfonate) (PSS) is a water-soluble, synthetic strong polyelectrolyte prepared via free radical polymerization.[41,42,43] As a polyanion, PSS always

possesses a negative charge due to the dissociation of the sodium counterion that leaves behind negative sulfate groups on the polymer (repeat unit shown in **Figure 6**). Despite this electrostatic charge, PSS is amphiphilic due to its hydrophobic carbon backbone and aromatic rings. PSS is amorphous and atactic like PAA and PAH.

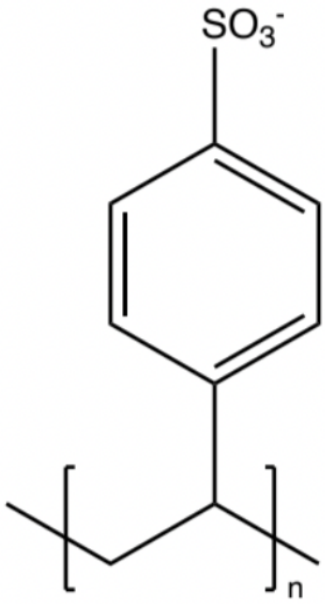

Figure 6. The structure of the repeat unit of poly(4-styrenesulfonate)

Much of its potential for biomedical use stems from the permanent electrostatic charge on PSS, which makes it a conducting polymer. There are a number of tissue types that respond to electrical fields, so the incorporation of conducting polymers such as PSS into biomaterials combined with the application of an external electric field allows for localized electric stimulation that can support naturally occurring processes. A form of PSS in which it is combined with a polycation called poly(3,4-ethylenedioxythiophene) (PEDOT) to form the copolymer PEDOT:PSS has received significant attention from the biomedical field due to its electrochemical, thermal, and oxidative stability.[44] PEDOT:PSS has been used for its conducting

properties in various tissue engineering applications such as bone healing[45,46] and neuronal differentiation.[47] PSS has also been incorporated into LBL assemblies, as described above, with cationic polyelectrolytes such as PAH.[48] Additionally, PSS acts as a cation exchange resin (the sodium counterion can be exchanged with another available cation), a property that has been exploited for the treatment of hyperkalemia[49] (elevated levels of potassium) and lithium toxicity.[50]

1.4.4 Poly(vinyl pyrrolidone)

Poly(vinyl pyrrolidone) (PVP) is an amphiphilic, water-soluble, synthetic polymer prepared via the free radical polymerization of vinylpyrrolidone (**Figure 7**)[51]. Each repeat unit possess a pyrrolidone group, whose ketone and tertiary amine endow it with some hydrophilicity while the carbon backbone is responsible for its hydrophobicity, resulting in an overall amphiphilic polymer that is soluble in both aqueous and organic solvents.[51] PVP is amorphous and can be comprised of a range of tacticities depending on the preparation conditions.[52] Unlike PAA and PAH, PVP is not a weak polyelectrolyte, so it is not ionizable, and unlike PSS, it does not bear a permanent charge. Of the comparison polymers, it is most like PVOH due to its amphiphilicity, water-solubility, and neutrality; it differs only in its lack of crystallinity, offering the opportunity to isolate crystallinity as a variable in thin film deposition and stability.

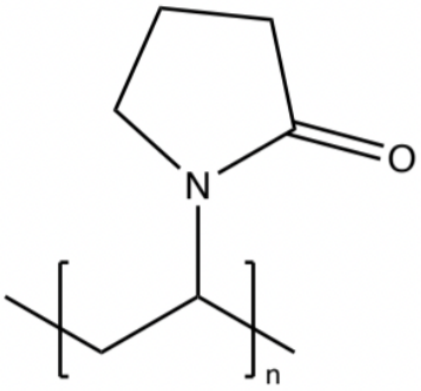

Figure 7. The structure of the repeat unit of poly(vinyl pyrrolidone)

It has been well-established that PVP adsorbs to silica, with both hydrogen bonding and the hydrophobic effect driving adsorption.[53,54,55,56,57]. The proposed mechanism for hydrogen bonding is shown schematically in **Figure 8**.[54] Additionally, PVP is non-toxic, pH-stable, biocompatible, and biodegradable, which has earned it a role in many industries primarily pharmaceuticals and cosmetics. For example, the ability of PVP to inhibit the crystallization of polymers and act as a complexing agent allows it to increase the solubility of poorly soluble and high-dose drugs, thus increasing bioavailability.[58,59] PVP has also been used for gene delivery,[60] in hairsprays,[61] and as an antiseptic when complexed with iodine.[62,63]

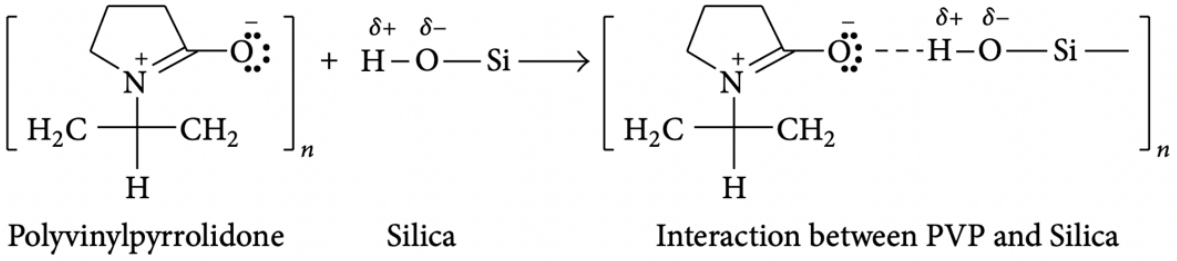

Figure 8. The lone pair of electrons on the pyrrolidone nitrogen shift to form a pi bond with the carbonyl carbon, placing a formal negative charge on the carbonyl oxygen that allows it to hydrogen bond with the silanol groups on the silicon substrate.

Table I. Repeat unit structure, crystallinity (tacticity), glass transition temperature (T_g), and pKa of PVOH and the four comparison polymers used in this work.

Polymer Name	Repeat Unit	Crystallinity (Tacticity)	T_g	pKa
PVOH	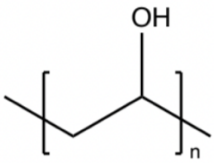	Semicrystalline (Atactic)	95 °C[64]	N/A
PAA	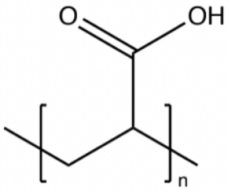	Amorphous	103 °C[64]	4.5-6.5[28,29,30]
PAH	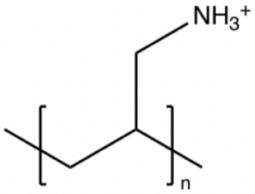	Amorphous	225 °C[65]	8.7[30,38]
PSS	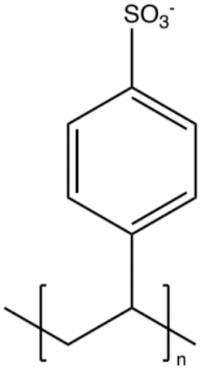	Amorphous	230 °C[66]	N/A
PVP	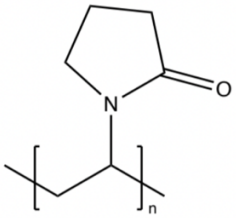	Amorphous	175 °C[67]	N/A

1.5 Spin Coating

1.5.1 Introduction

There exists a variety of methods for preparing thin films which can be classified broadly as either physical or chemical deposition techniques. Within the former is a family of methods termed sol-gel techniques, which use gravitational or centrifugal force to spread a solution over a substrate and evaporation to remove excess solvent.[68] Two of the most common sol-gel techniques are dip coating and spin coating, the second of which is the focus of the work described here.

Spin coating takes place in four steps,[69] depicted in **Figure 9:**

1. Deposition: polymer solution is introduced to the surface of the substrate, which is mounted on a stage.
2. Spin up: the stage on which the substrate is mounted begins to spin, and under the centrifugal force of the spinning stage, the polymer solution spreads to cover the entire surface of the substrate.
3. Spin off: as polymer solution flows radially outward, excess solution is spun off the substrate. In the case of non-volatile, Newtonian solutions, the liquid film becomes nearly uniform in thickness as it thins due to spin-off of excess polymer solution.
4. Evaporation: solvent evaporates, leaving behind concentrated polymer chains that form the solid thin film. Solvent evaporation overlaps with the three previous steps, but its effect becomes most pronounced towards the end of spin-off, when the film is thin enough for evaporation to significantly impact the local concentration of polymer.

In the event of favorable chemical interactions between the polymer chains and substrate, polymer will spontaneously deposit onto the surface of the substrate before spin is initiated, forming what has been termed the h_1 component of the total thin film thickness.[70] This process is referred to as spontaneous deposition. The rest of the film, the h_2 component, forms via spin deposition as the liquid layer of polymer solution thins due to spin-off and solvent departs via evaporation.[70] Because the h_1 layer contributes to the total thickness of the resulting film and depends on the amount of time allowed for spontaneous deposition to occur, the amount of time between deposition and spin-up is maintained constant across all trials so that any contribution to total film thickness from the spontaneously deposited layer is consistent across samples. To note this modification of the traditional spin coating procedure, the process involving the time-sensitive spontaneous deposition step has been termed "adsorptive spin coating." All mentions of spin coating experiments henceforth refer to adsorptive spin coating.

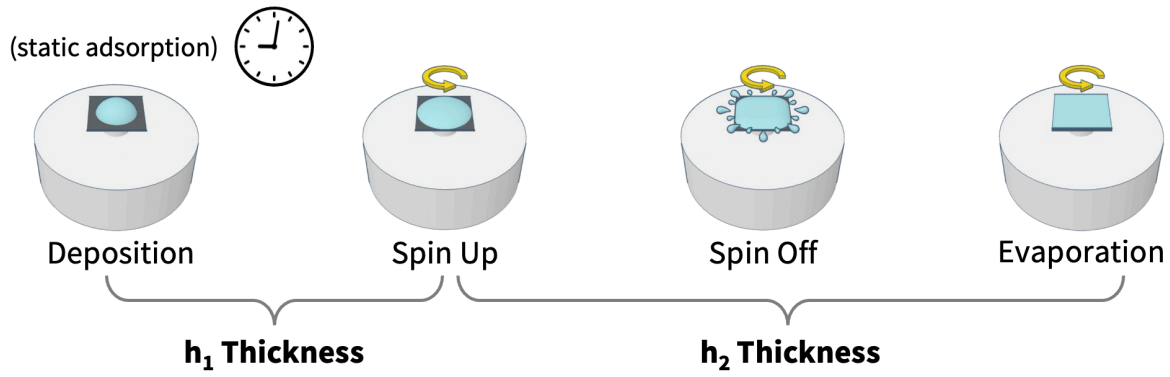

Figure 9. Spin coating takes place in four stages: deposition, spin up, spin off, and evaporation. Spontaneous deposition of polymer occurs immediately after deposition, forming an h_1 layer whose thickness is independent of spin rate but depends on polymer-substrate interactions and time allowed for deposition. Spin deposition occurs while solution is spun off and solvent is

evaporated, forcing remaining polymer chains to deposit. This forms the h_2 layer that is dependent on spin rate and polymer-polymer interactions.

1.5.2 Theory

The thickness of thin films is of critical importance for most applications; therefore, the past several decades have seen significant attention dedicated to the development of mathematical models to describe the spin coating process with the goal of achieving tunable thickness. One of the most prevalent models used to predict the thickness of spin coated polymer thin films is the Meyerhofer Model (Eq. 1)[71]:

$$h_f \propto k\omega^{-\frac{1}{2}} \qquad \text{Eq. 1}$$

where k is a proportionality constant related to the viscosity of the polymer solution. However, a range of exponents deviating from the $-\frac{1}{2}$ proposed by Meyerhofer have been reported,[72,73] and such deviations may be partially explained by the assumptions made during the derivation of this model:

(1) It is assumed that the evaporation and spin off (outflow) stages occur independently and do not overlap.

(2) The model does not account for the polymer-substrate interactions that drive spontaneous deposition and the formation of the h_1 layer.

(3) The model assumes that there is no slip at the substrate-solution interface, which is not accurate for scenarios where dewetting occurs.

1.6 Dewetting

1.6.1 Contact Angle

In the bulk of a material, molecules are able to form favorable cohesive interactions with neighboring molecules of the same material, but for a molecule to exist at the surface of the material, it must break half the bonds it had with neighboring molecules and therefore reduce the number of favorable cohesive interactions it participates in. This breaking of bonds results in two forces associated with the surface of a material: an inward force of attraction experienced by surface molecules that are attracted to bulk molecules and a force parallel to the surface that arises from the attractive intermolecular forces between molecules of the same material at the surface.[74,75] The former is surface tension, and the stronger the intermolecular forces between molecules of the material, the greater the surface tension. Because it requires energy to disrupt intermolecular interactions and create a surface, liquids tend to occupy a three-dimensional shape that minimizes their surface area, most commonly a spherical droplet.

In the case of a liquid thin film on a solid substrate, there are three surfaces, or interfaces: the solid/liquid interface, the solid/gas interface, and the liquid/gas interface. These three parameters combine to express the spreading coefficient according to the equation below:[75,76]

$$S = \gamma_{SG} - (\gamma_{SL} + \gamma_{LG}) \qquad \text{Eq. 2}$$

where γ_{SG}, γ_{SL}, and γ_{LG} are the surface tensions of the solid/gas, solid/liquid, and liquid/gas interfaces, respectively. The spreading coefficient, S, dictates the wetting regime of the system (**Figure 10**):

(1) Total wetting: When $S > 0$, the liquid spreads across the entire solid surface and forms a continuous liquid layer. If $S > 0$, γ_{SG} must be greater than γ_{SL} and γ_{LG}

combined, so it is more energetically costly to have an exposed solid/gas interface than solid/liquid and liquid/gas interfaces. Therefore, the system can reduce its energy if the liquid spreads to cover the substrate and minimize the solid/gas surface energy.

(2) Partial wetting (dewetting): When $S < 0$, the liquid retracts from the surface and beads up, resulting in areas of exposed solid/gas interface. If $S < 0$, γ_{SG} must be less than γ_{SL} and γ_{LG} combined, so it is more energetically costly to have solid/liquid and liquid/gas interfaces. Therefore, the system can reduce its energy if the liquid retracts from the solid surface (to minimize solid/liquid surface energy) and forms hemispherical droplets (to minimize liquid/gas surface energy).

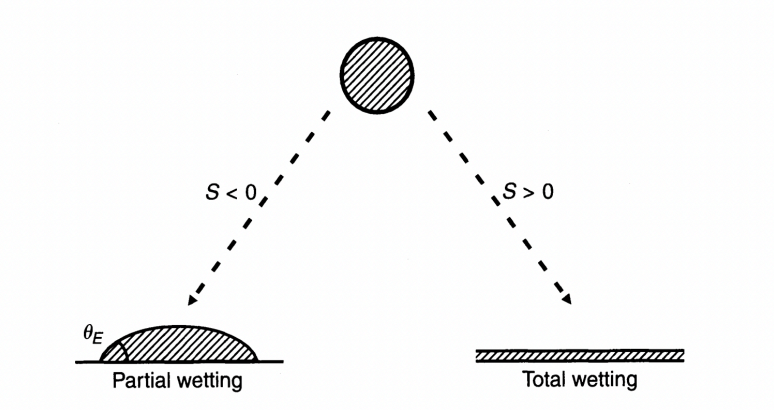

Figure 10. Partially wetting fluids retract from their solid substrates and form hemispherical droplets, while totally wetting fluids spread across their solid substrates and form continuous liquid films.

At equilibrium, that is when the drop is not moving and its volume is constant, the horizontal components of the forces created by the three surface tensions are in equilibrium (**Figure 11**):

$$\gamma_{SG} = \gamma_{SL} + \gamma_{LG}\cos(\theta) \qquad \text{Eq. 3}$$

This equation can be rearranged to give Young's equation for determining the contact angle of a liquid layer on a substrate:[76]

$$\gamma_{LG}\cos(\theta) = \gamma_{SG} - \gamma_{SL} \qquad \text{Eq. 4}$$

Solving Eq. 2 for γ_{SG} and plugging it into the above equation makes it possible to estimate the contact angle based on the wetting regime of the film:

$$S = \gamma_{LG}[\cos(\theta) - 1] \qquad \text{Eq. 5}$$

From Eq. 5 it can be seen that for there to be a contact angle (i.e. for partial wetting to occur) the spreading coefficient, S, must be negative because $\cos(\theta)$ is undefined for values greater than 1 and less than -1 (and γ_{LG} is always greater than or equal to zero, so $\frac{S}{\gamma_{SG}}$ will have the same sign as S).

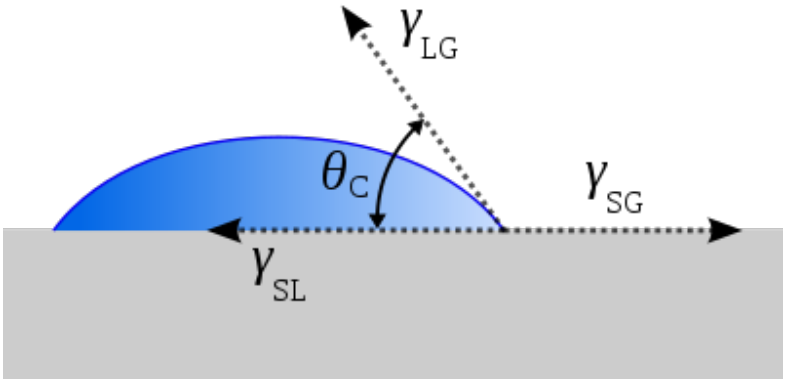

Figure 11. The contact angle of a fluid on a solid substrate is a product of the balance between the forces created by the solid/gas, solid/liquid, and liquid/gas surface tensions.

1.6.2 Mechanisms of Dewetting

As described in the previous section, dewetting (i.e. partial wetting) refers to the process by which a material coated on a surface retracts from the surface and beads up. The opposite process, wetting or spreading, results in the uniform coating of a surface and production of a stable thin film. The balance between cohesive (polymer-polymer) and adhesive (polymer-substrate) forces dictates whether a polymer solution will wet or dewet a given substrate. If the cohesive forces dominate, the film will dewet the surface; if the adhesive forces dominate, the film will wet the surface. In many applications, dewetting is an obstacle to be avoided because most applications of thin films depend on their stability and continuous coverage of the underlying substrate. However, there has more recently emerged an interest in harnessing controlled dewetting to produce patterned thin films for applications such as magnetic recording, organic semiconductors, and biosensors.[77]

Dewetting occurs in three stages:[78]

(1) Rupture of the liquid layer: A liquid film can rupture by any combination of three mechanisms: nucleation of defects on the substrate surface (heterogeneous nucleation), amplification of thermal fluctuations at the surface of the film until the point of contact with the underlying substrate (spinodal dewetting), or nucleation caused by thermal energy that increases polymer chain mobility sufficiently to allow films to overcome an energy barrier to film thinning (thermal nucleation).[75] Thermal fluctuations at the surface of the liquid film are driven by the disjoining pressure that allows the film to reduce its free energy by altering the distance between the liquid-air and solid-liquid interface (i.e. altering the film thickness). During spinodal

decomposition, the thermal fluctuation with the fastest growing amplitude is responsible for the rupture of the film because it makes contact with the substrate before fluctuations of slower-growing amplitude can reach the substrate. The spacing between the holes is proportional to the wavelength of the fluctuation with the fastest-growing amplitude, which has been shown to be proportional to the thickness of the film squared.[78] Each of the three dewetting mechanisms produces films with distinct final morphologies, which are shown in **Figure 12**.

(2) Hole growth and convergence: Once a hole has formed, the liquid-air and solid-liquid interfaces are in contact, resulting in a contact angle formed by the edge of the receding liquid layer and the substrate (as depicted in **Figures 11**). The velocity of hole growth, which is constant with time, is proportional to the cube of the contact angle.[78] As the holes grow in size, they impinge on neighboring holes, and the rims forming the boundaries between holes drain to form larger holes out of the converged smaller holes. Finally, the larger holes converge with each other and form a polygonal pattern outlined by ribbons of polymer solution (**Figure 13**).

(3) Formation of droplets: Finally, the ribbons of solution decay into droplets according to one of two mechanisms depending on the contact angle of the polymer solution on the substrate (**Figure 13**). For large contact angles, fingering instabilities drive the decay of ribbons into droplets; whereas for small contact angles, Rayleigh instabilities are responsible for the decay of the ribbons into droplets.[78] Once the droplets have formed, exchange of material between them is not possible, so the film ceases to change in morphology.

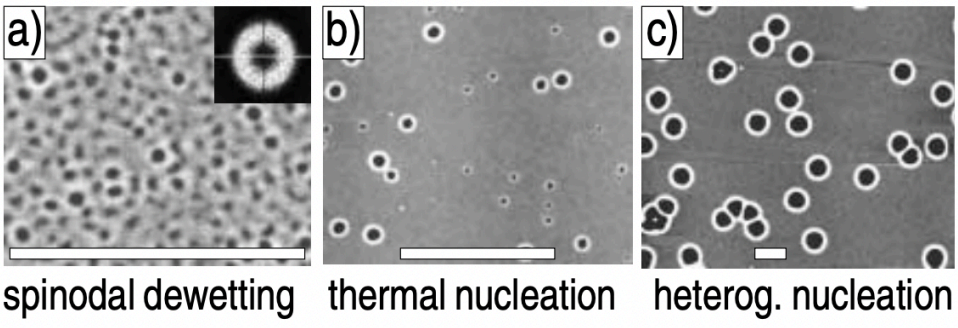

Figure 12. There are three mechanisms by which a liquid thin film can rupture. Spinodal dewetting (a) produces small holes of uniform size separated by a distance proportional to film thickness squared. Thermal nucleation (b) produces randomly spaced holes of various sizes because it occurs continuously over a long time frame. Heterogeneous nucleation (c) produces large holes with a random distribution and spaced far apart.[79]

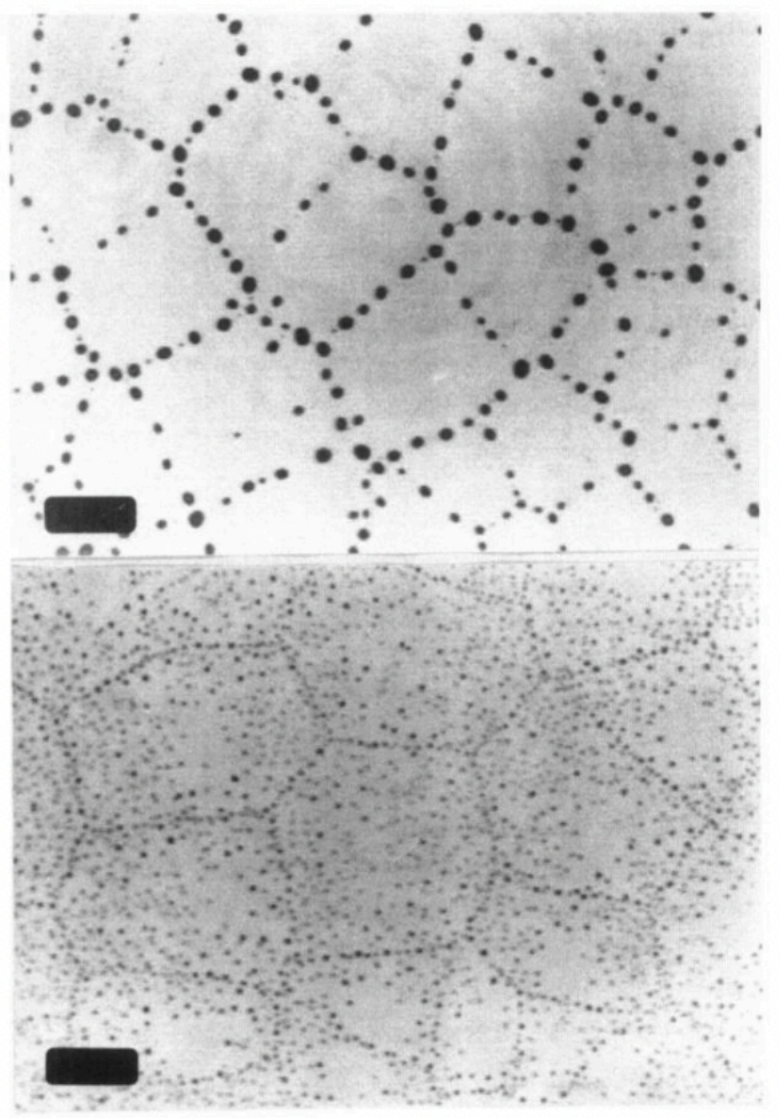

Figure 13. The final stage of dewetting is characterized by ribbons of polymer that have decayed into droplets.[78]

1.6.3 Theory of Dewetting

The total free energy of a liquid thin film per unit area depends on the interactions between the solid, liquid, and gas phases and can be expressed as the sum of the apolar and polar components of these energies of interaction:[80]

$$\Delta G_{total} = \Delta G_{SLG}^{AP} + \Delta G_{SLG}^{P} \quad \text{Eq. 6}$$

The apolar contribution to total free energy is given by the equation below:[80]

$$\Delta G_{SLG}^{AP} = S_{AP} \frac{{d_0}^2}{h^2} \quad \text{Eq. 7}$$

where S_{AP} is the apolar component of the total spreading coefficient, S, d_0 is the equilibrium distance for film thickness due to short-range Born repulsion (i.e. the minimum thickness for a film of 1 polymer chain, below which repulsive forces dominate), and h is the film thickness.

The polar contribution to total free energy is given by the equation below:[80]

$$\Delta G_{SLG}^{P} = S_P e^{\frac{d_0 - h}{l}} \quad \text{Eq. 8}$$

where S_P is the polar component of the total spreading coefficient, S, and l is the correlational length (distance below which molecules interact) of the polar fluid, water.

Note that for both Eq. 7 and Eq. 8, when the film thickness equals the minimum thickness ($h = d_0$), the free energy of both the apolar and polar components of the total free energy are equal to the corresponding component of the spreading coefficient.

The spreading coefficient is equal to the sum of the apolar and polar components of spreading and related to the contact angle (θ) of the fluid on the solid substrate as follows[81]:

$$S = S_{AP} + S_P = \gamma_{LG}(cos\theta - 1) \quad \text{Eq. 9}$$

Differentiating the total free energy of the film per unit area gives the total free energy per unit volume, otherwise referred to as the effective interface potential per unit volume. Because the negative derivative of energy is force, differentiating the total free energy per unit

area also gives the negative force per unit area, or the negative of the disjoining pressure (this is related to the intermolecular forces per unit area):[80,81]

$$\Delta G_{total} = \Delta G_{SLG}^{AP} + \Delta G_{SLG}^{P} \quad \text{Eq. 10}$$

$$\Delta G_{total} = S_{AP}\frac{{d_0}^2}{h^2} + S_P e^{\frac{d_0 - h}{l}}$$

$$\Delta G'_{total} = -2S_{AP}\frac{{d_0}^2}{h^3} - \frac{S_P}{l}e^{\frac{d_0 - h}{l}} = -P = -\frac{F}{A} \quad \text{Eq. 11}$$

The negative derivative of the potential energy of the system per unit volume, Eq. 11, is given by Eq. 12

$$\Delta G''_{total} = 6S_{AP}\frac{{d_0}^2}{h^4} + \frac{S_P}{l^2}e^{\frac{d_0 - h}{l}} \quad \text{Eq. 12}$$

Spinodal dewetting occurs when thermal fluctuations at the surface of the film grow spontaneously until they make contact with the substrate and cause the film to rupture. The wavelength of the fastest growing fluctuation, which has been shown to correlate to the spacing between holes, is related to Eq. 12:[79,81]

$$\lambda = \sqrt{-\frac{8\pi\sigma}{\Delta G''_{total}}} \quad \text{Eq. 13}$$

where σ is surface tension of the film. There is only a real solution to Eq. 13 when $\Delta G''_{total}$ is negative. Therefore, spinodal dewetting is only observed in situations where the second derivative of the total free energy of the system is negative.

1.6.4 Stability of Thin Films

Seeman et. al. has shown that it is possible to reconstruct the effective interface potential per unit area, ϕ, from observed dewetting morphologies of polystyrene thin films spin coated on silicon from toluene solution. In this study, they presented three scenarios of dewetting distinguished by ϕ of the film as a function of initial film thickness, h (**Figure 14**). These three scenarios are:

(1) Stable (curve 1): When $\phi(h) > 0$ and $\phi''(h) > 0$ for all film thicknesses, there is a global minimum at infinite film thickness, and free energy increases exponentially as film thickness decreases. This means that it is energetically costly for the film to thin and dewet via spinodal dewetting, so it is stable at all film thicknesses. Films in the stable scenario can only dewet via heterogeneous nucleation (i.e. a defect or dry spot on the substrate, see section **1.6.2**).

(2) Unstable (curve 2): When there is a global minimum in $\phi(h)$ at some film thickness $h = h^*$, the system can decrease energy by reducing its thickness to h^* (assuming the initial film thickness is greater than h^*), which is accomplished via spinodal dewetting. In this scenario, $\phi''(h) < 0$ for most film thicknesses greater than h^*. In section **1.6.3** it is shown that there is only a real solution to Eq. 13 when $\Delta G''_{total}$ (i.e. $\phi''(h)$) is negative. This is in agreement with the reconstructed free energy curves obtained by Seeman et al. (**Figure 14**).

(3) Metastable (curve 3): metastable films behave like unstable films at lower film thicknesses, when $\phi''(h) < 0$ and the film can spinodally dewet to the thickness, h^*, corresponding to the global minimum. However, at greater film thicknesses, $\phi''(h) > 0$, and there is an energy barrier to reducing the film thickness. For values of h greater than the local maximum, metastable films behave like stable films. Near the sign change of $\phi''(h)$, it is possible for the film to overcome the energy barrier to film thinning if sufficient thermal energy is applied to the system. This dewetting mechanism is thermal nucleation, and annealing thin films is a common method used to distinguish between stable and metastable films.

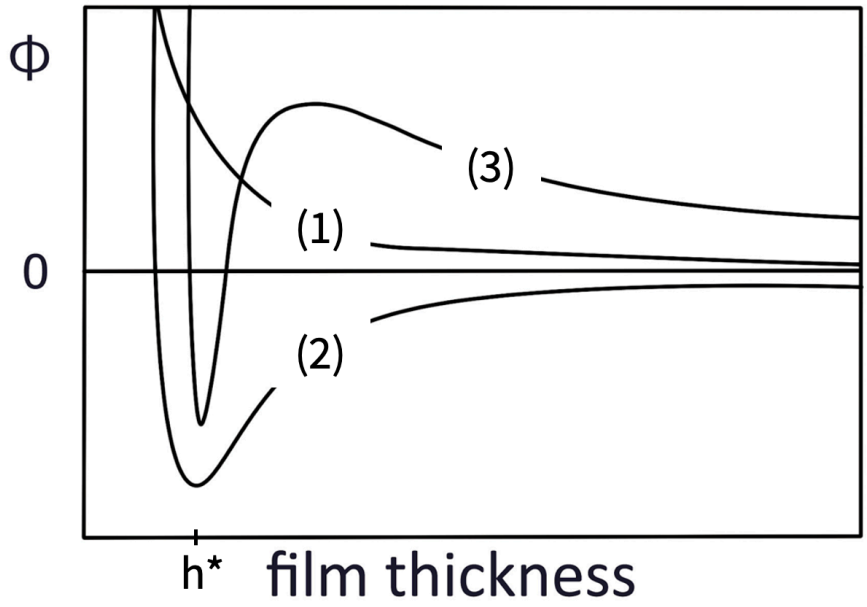

Figure 14. There are three scenarios for film stability based on how a film's effective interface potential per unit area, ϕ, changes with film thickness. Curve 1 represents a stable system, curve 2 represents an unstable system, and curve 3 represents a metastable system. There is a global

minimum in the free energy functions of unstable and metastable films at film thickness h* that allows these films to dewet spinodally.

2. MATERIALS AND METHODS

Materials

Silicon wafers (100 orientation, P/B doped, resistivity 1-10 Ω·cm, thickness 475-575 μm) were purchased from International Wafer Service. Poly(vinyl alcohol) (PVOH 99%H, MW = 89-98 kDa and >99% hydrolyzed; PVOH 88%H, MW = 85-124 kDa and 88% hydrolyzed), Poly(allylamine hydrochloride) (PAH, MW = 50,000), Poly(sodium 4-styrenesulfonate) (PSS, MW = 70,000), and Poly(vinyl pyrrolidone) (PVP, MW = 40,000) were purchased from Sigma-Aldrich. Poly(acrylic acid) (PAA, 25 wt% solution, MW = 50,000) was purchased from Polysciences. Oxygen gas (99.999%) was purchased from Middlesex Gases Technologies. Water was purified using a Millipore Milli-Q Biocel System (Millipore Corp., resistivity ≥ 18.2 MΩ/cm). All reagents were used without further purification. Glassware was cleaned in a base bath (potassium hydroxide in isopropyl alcohol and water), rinsed with distilled water, and stored at 110 °C.

Instrumentation

Silicon wafers and glassware were dried in a Precision 51221126 Gravity Convection Lab Oven (Thermo Fisher Scientific, Inc., USA). The silicon wafers were cleaned using an O_2 plasma treatment in a PDC-001 Harrick plasma cleaner. Spin coating was done using a Laurell WS-650MZ-23NPPB single wafer spin processor. Annealing of the thin films was done using a 150/Timer heater (J-KEM Scientific, Inc.). The size and dispersity of prepared polymer solutions were measured using a Zetasizer Nano-S (DLS) from Malvern. Thin film thickness and silicon wafer native oxide layer thickness were measured using a Gaertner Scientific LSE Stokes ellipsometer with a He-Ne laser light source (λ=632.8 nm) at a 70° incident angle (from the

normal to the plane of incidence). The following refractive indices were used to calculate the surface layer thicknesses: air, $n_0 = 1$; silicon oxide and polymer layers, $n_1 = 1.46$; silicon substrate, $n_s = 3.85$, and $k_s = -0.02$. Dynamic contact angle measurements were obtained using a Rame-Hart telescopic goniometer with a Gilmont syringe and a 24-gauge flat-tipped needle. Dynamic advancing and receding contact angles were captured with a camera and analyzed digitally. The nanoscopic surface morphology of the silicon wafers and polymer thin films was characterized using a Veeco Metrology Dimension 3100 atomic force microscope (AFM) with a silicon tip operating in tapping mode. Microscopic features of the thin films were characterized using an Olympus BX51 optical microscope in reflective dark field. The pH of polymer solutions was measured using an AB150 pH meter from Fisher Scientific.

Substrate Preparation

Silicon wafers were cut into 1.4 cm x 1.4 cm squares (2.0 cm x 2.0 cm were used for drop casting experiments and spin coating PSS, PAA^-, and PAH at 900 rpm). Wafers were cleaned by rinsing under distilled water, drying with compressed air, and storing for 30 minutes in a glass petri dish in an oven at 110 °C. Next, wafers underwent a 15-minute oxygen plasma treatment at 300 mTorr in a 30 W plasma cleaner. Finally, wafers were allowed to equilibrate for an additional 15 minutes in a closed petri dish inside the plasma cleaner prior to removal to minimize the accumulation of dust and other impurities on the highly reactive and energetic surface.

Polymer Preparation

PVOH solutions were prepared by dissolving the desired amount of PVOH powder in Milli-Q water in a clean polypropylene bottle and heating at 88-94 °C for 3 hours while stirring. The PVOH solutions were allowed to equilibrate for at least 3 days prior to characterization of dispersity using DLS and subsequent use.

PAA solutions of 0.1 wt% were prepared by adding 200 µL 25 wt% PAA stock solution to 49.80 mL Milli-Q water with continuous stirring on a stir plate. The dispersity of the PAA solutions was characterized immediately following preparation. Charged PAA^- solutions were prepared by adding approximately 700-800 µL of 1.0 M NaOH to 50 mL 0.1 wt% PAA solutions prepared using the aforementioned protocol. The 700-800 µL of NaOH were added in 100 µL increments at least 2 minutes apart to allow for maximum dispersion of the NaOH and deprotonation of the PAA. PAA^- solutions were titrated to pH values ranging from 8-11 in order to probe the effects of pH on PAA aggregation. The dispersity of the PAA^- solutions was characterized immediately following preparation. In order to investigate the effects of heating on PAA^- aggregation, PAA^- solutions were boiled at 90 °C for 1 hour in a water bath on a heating plate. The dispersity of the boiled PAA^- solutions was characterized immediately following boiling (after allowing solutions to cool for several minutes).

To prepare diluted solutions of PAA^- for drop casting experiments, 5 mL of 0.1 wt% PAA^- was dissolved in 45 mL Milli-Q water to produce 0.01 wt% PAA^-. Next, 5 mL of 0.01 wt% PAA^- was dissolved in 45 mL Milli-Q water to produce 0.001 wt% PAA^-. The pH of each solution was measured after each dilution step.

PAH solutions of 0.1 wt% were prepared by adding 0.050 g PAH powder to 49.950 g Milli-Q water with continuous stirring on a stir plate for several days to completely dissolve the powder. Following several days of equilibration, the hydrodynamic size and dispersity of PAH solutions was characterized using DLS. A series of PAH_{SiO^-} solutions were prepared by adding 0, 30, 60, 90, 120, 150, and 170 μL 1.0 M NaOH each to a 50 mL batch of 0.1 wt% PAH. Each amount of NaOH was added in 30 μL increments under constant stirring. The pH of each solution was measured, and DLS was used to measure the hydrodynamic size and dispersity of each solution. 0.1 wt% PAH titrated to a pH of 6.5 was used for spin coating experiments because this was anticipated to be sufficient to deprotonate the silicon wafer (pKa ~5.6) but not the polymer (pKa ~8.8).

PSS solutions of 0.1 wt% were prepared by dissolving 0.050 g of PSS powder in 49.950 g of Milli-Q water and stirring. The hydrodynamic size and dispersity of PSS solutions were characterized using DLS immediately following preparation.

PVP solutions of 0.1 wt% were prepared by dissolving 0.050 g PVP powder in 49.950 g of Milli-Q water and stirring. The hydrodynamic size and dispersity of PVP solutions were characterized using DLS immediately following preparation.

The solution pH, polymer charge, and substrate charge for each polymer system are displayed in **Table II**.

Table II. Structure, pKa, solution pH, polymer charge, and substrate charge for each polymer system.

Polymer Name	Polymer Structure	Polymer pKa	Solution pH	Polymer Charge	Substrate Charge (pKa ~5.6)
PVOH 99%H	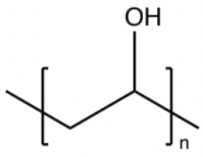	--	6-7	Neutral	Negative
PVOH 88%H	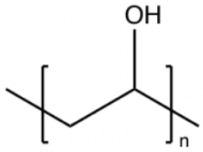	--	6-7	Neutral	Negative
PAA	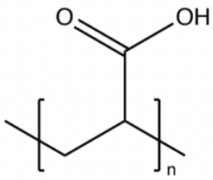	4.5-6.5	3.27	Neutral	Neutral
PAH	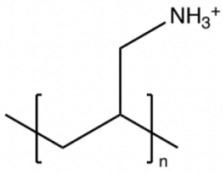	8.7	3.21	Positive	Neutral

PSS	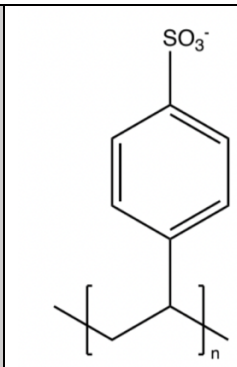	--	5.89	Negative	Neutral/Negative
PAA^-	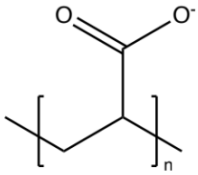	4.5-6.5	8-11	Negative	Negative
PAH_{SiO-}	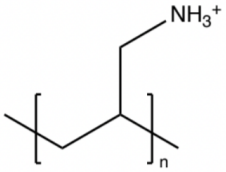	8.7	7	Positive	Negative

Adsorptive Spin Coating

For spin coating experiments, 100 µL (for the 1.4 x 1.4 cm^2 wafers) or 200 µL (for the 2.0 x 2.0 cm^2 wafers, used for 900 rpm) of the polymer solution was pipetted onto the substrate mounted on the spin coater stage and allowed to spontaneously adsorb for 1 minute. Then the sample was spun at a desired spin rate (spin rates of 900, 1400, 2200, 3500, 4800, and 6000 rpm were used to produce films with a range of thicknesses and generate spin curves for each polymer). Following spin, the thicker samples (900 and 1400 rpm) were placed flat on a

benchtop and allowed to air dry for several minutes. Once all samples were dry, they were stored in a well plate in a desiccator overnight before characterization.

Static Adsorption

Static adsorption experiments were conducted for 1 and 10 minutes; it was determined that both 1-minute and 10-minute static adsorption produced films of comparable thickness. Results reported in Section 3.4 were obtained using the 10-minute static adsorption protocol. Results reported in Section 3.5 were obtained using the 1-minute static adsorption protocol.

For 1-minute static adsorption, wafers were placed on a cap inside a petri dish, and 100 μL of the desired polymer solution was pipetted onto the wafer. After 1 minute, the polymer solution droplet was diluted with 1 mL Milli-Q water, then the wafer was rinsed three times using Milli-Q water and dried using N_2 gas. For 10-minute static adsorption, wafers were placed in well plates, and the wells were filled with polymer solution until the wafers were completely submerged. After 10 minutes, the air-solution interface was disturbed by a pair of tweezers, the wafers were removed from the solutions, rinsed three times with Milli-Q water, and dried with N_2 gas. All samples were stored in a desiccator overnight prior to characterization. As a control experiment, static adsorption with Milli-Q water was done using the 10-minute static adsorption setup.

Experiments done to investigate the loosely bound layer theory (Section 3.5) were performed using the protocol for 1-minute static adsorption. However, the number of rinse steps was varied: no rinse, 1 rinse, and 3 rinse steps were all tested. For the no rinse samples, wafers

were tapped dry, and for the 1x rinse and 3x rinse samples, one rinse step consisted of diluting the polymer solution on the wafer with 1 mL Milli-Q water (this was done once for 1x rinse and three times for 3x rinse). The N_2 gas drying step remained the same for all samples regardless of the number of rinse steps.

Drop Casting

Drop casting was performed with 0.1 wt%, 0.01 wt%, and 0.001 wt% PAA and PAA^-. 200 µL polymer solution was pipetted onto 2.0 x 2.0 cm^2 wafers in a petri dish, which were allowed to air dry overnight with the lid of the dish partially removed. The next day, samples were stored in a desiccator until characterization.

Annealing

To test the stability of spin cast PVOH 99%H, PVOH 88%H, and PVP films, samples were placed in glass scintillation vials, which were placed in a heater at 100 °C for 30 minutes (thermal annealing was performed for 15, 30 and 60 minutes initially, but no difference in thickness, morphology, or contact angle was observed past 30 minutes of heating, so all subsequent annealing experiments were performed for 30 minutes). Following 30 minutes of thermal annealing, samples were returned to a well plate and stored in a desiccator until characterization.

To test the stability of statically adsorbed PAA and PAA^- (Section 3.5), samples were placed in glass scintillation vials, and 20 µL of Milli-Q water was added to the bottom of the scintillation vial such that it was not in contact with the wafer. The scintillation vials were placed

in a heater at 100 °C for 30 minutes. Following 30 minutes of thermal annealing, the caps of the vials were removed while the vials were still on the heating plate to release the water vapor so that it did not condense onto the samples upon removal from the heater. After venting the vials, they were removed from the heater, and the samples were returned to a well plate and stored in a desiccator until characterization. (The difference between the two annealing protocols described is not due to a difference in the polymers, but simply reflects an updated version of the thermal annealing protocol.)

3. RESULTS AND DISCUSSION

The work described here aims to contribute to the ongoing effort to propose and validate a new model for predicting the thickness of spin coated polymer thin films. The existing Meyerhofer model establishes a correlation between the spin coated thickness and the spin rate raised to the power of -0.5; however, experimental results often do not agree with this model. One of the oversights of the Meyerhofer model is that it does not consider the two deposition mechanisms involved in spin coating: spontaneous deposition forms an h_1 layer independent of spin rate and reflective of polymer-substrate interactions, and spin deposition forms an h_2 layer dependent on spin rate and reflective of polymer-polymer interactions.

In order to validate this decoupled thickness model and probe the effects of polymer crystallinity, hydrophobicity, and charge on the stability of polymer thin films, each polymer system was first characterized as either stable, metastable, or unstable, and spin curves were generated for each system. In order to obtain an h_2 spin curve for each system, static adsorption experiments were used to produce h_1 layer thickness values for each system. These h_1 thickness values were then subtract from the corresponding polymer's spin curve at all spin rates to produce an h_2 spin curve that is anticipated to better match the Meyerhofer model.

Thickness values were obtained using ellipsometry. Film morphologies were visualized at the nanoscopic scale using atomic force microscopy (AFM) and at the microscopic scale using optical microscopy. Contact angle goniometry was used to determine the advancing and receding contact angles of water on the polymer films, which give an indication of the degrees of hydrophobicity and hydrophilicity of the films, respectively.

h_1 layer thicknesses obtained from static adsorption did not match expectations based on the properties of each polymer system and what was projected by spin coated film thicknesses at

the highest spin rate (which is typically an indicator of h_1 layer thickness). This discrepancy was attributed to the fact that part of the h_1 layer is more loosely bound than the initial layer of polymer deposited, and this loosely bound layer is easily removed by the rinse steps involved in the static adsorption process. Therefore, the final section of the results details the results of the preliminary experiments performed to test the loosely bound layer hypothesis. Uncovering the existence of the loosely bound layer offers a more nuanced understanding of the polymer deposition process that will allow future work to determine the best experimental methods for obtaining the reliable h_1 thickness values needed to validate the decoupled thickness model.

3.1 Stable Systems

AFM images of PVOH 99%H, PVOH 88%H, and PVP show that all three polymers form continuous thin films on silicon wafers across all spin rates (**Table III**). The absence of dewetting, particularly at the higher spin rates that correspond to lower film thicknesses, suggests that these three polymers are stable when prepared on a silicon substrate.

Table III. AFM images (data scale 5 nm, aspect ratio 5 μm x 1.25 μm), section analysis, and RMS roughness (in nm) of 0.1 wt% PVOH 99%H, PVOH 88%H, and PVP thin films prepared by spin coating on silicon wafer at various spin rates.

Spin Rate (rpm)	PVOH 99%H	PVOH 88%H	PVP

900	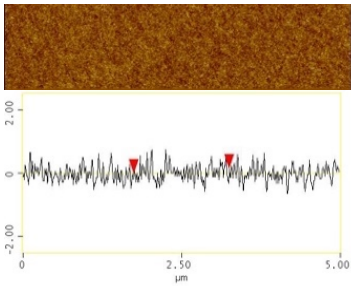 RMS = 0.242	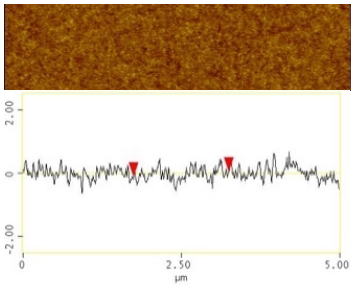 RMS = 0.201	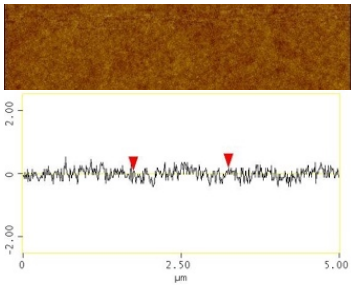 RMS = 0.191
1400	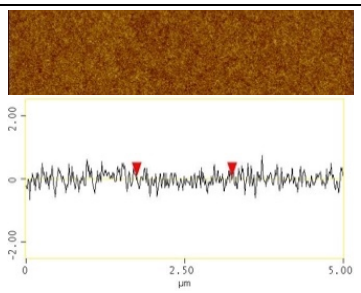 RMS = 0.216	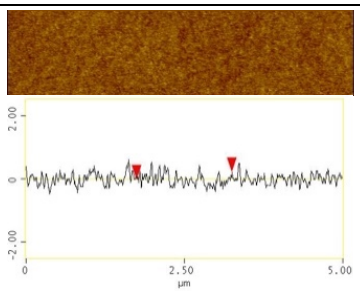 RMS = 0.183	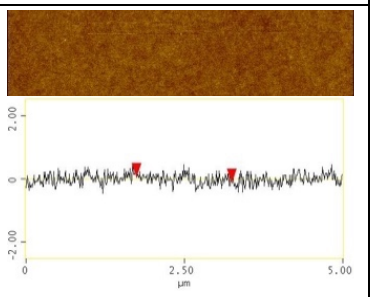 RMS = 0.168
2200	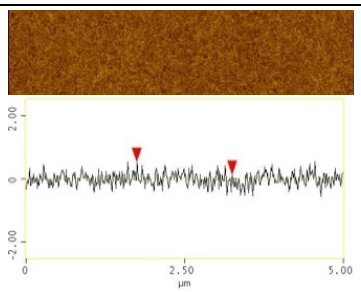 RMS = 0.204	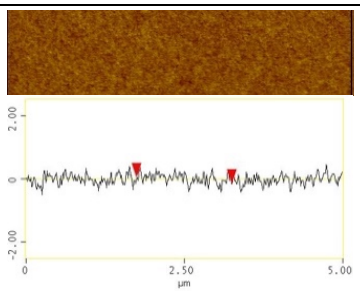 RMS = 0.170	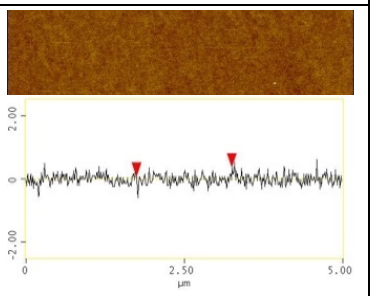 RMS = 0.165
3500	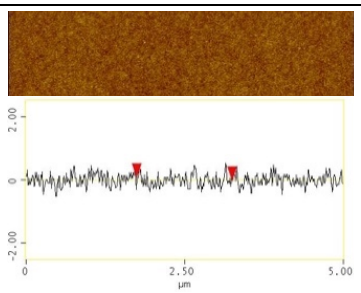 RMS = 0.195	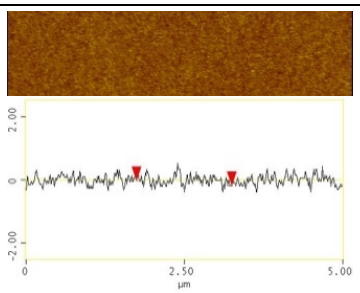 RMS = 0.156	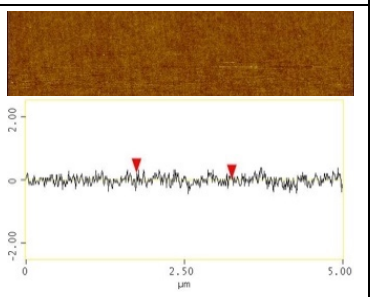 RMS = 0.165
4800	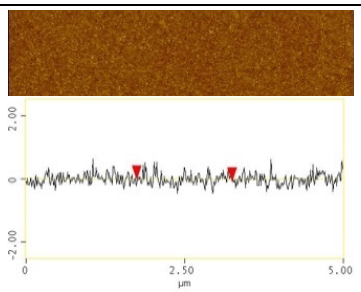 RMS = 0.185	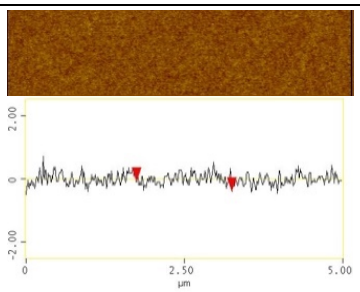 RMS = 0.162	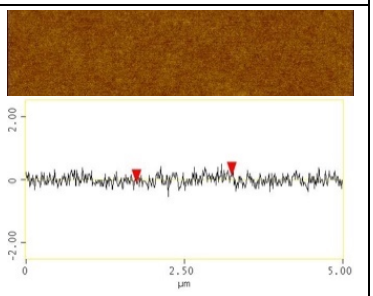 RMS = 0.166

6000	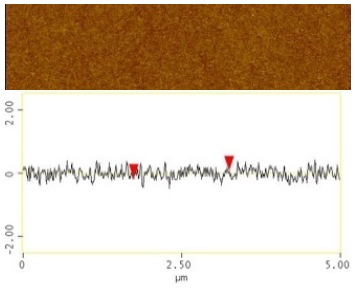 RMS = 0.168	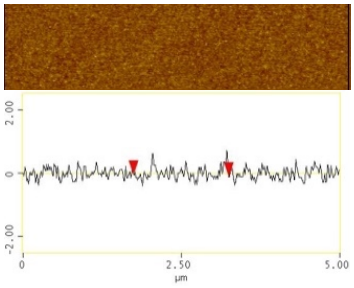 RMS = 0.175	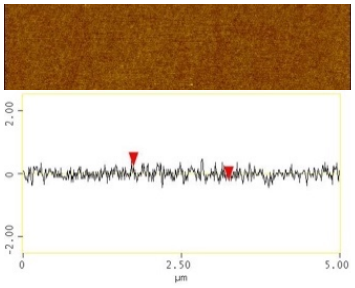 RMS = 0.174

Spin curves for all three systems are shown in **Figure 15.** The PVOH 99%H and PVOH 88%H spin curves indicate a strong h_2 thickness dependence on spin rate evidenced by the spin curve exponents of -1.21 and -0.833, respectively. On the other hand, PVP has a spin curve exponent of -0.382 and visually appears much shallower than the other two spin curves. Exponents closer to zero typically correspond to a weak dependence of the h_2 thickness on spin rate and are considered indicative of dewetting due to solution slipping across the substrate in the presence of centrifugal force. However, PVP films were the thickest of the three polymers at the highest spin rate. At high spin rates, most of the polymer solution is spun off the substrate, and the h_2 thickness is assumed to be negligible. Therefore, the relatively large thickness values of the PVP spin curves at higher spin rates suggests the presence of an h_1 layer. This also appears to be the case for the PVOH 88%H films. One feature that both PVOH 88%H and PVP share is their relative hydrophobicity compared to PVOH 99%H, which suggests that hydrophobic interactions may be a driving force for spontaneous adsorption and formation of an h_1 layer on silicon wafers.

Stability, as indicated by the AFM images in **Table III**, arises when polymer-substrate interactions are stronger than polymer-polymer interactions, resulting in polymer spreading. Therefore, it can be concluded that all three of the stable polymers have stronger polymer-substrate interactions than polymer-polymer interactions. However, this conclusion is at odds

with other pieces of evidence obtained from the spin curves and from a knowledge of the nature of each system:

(1) If polymer-substrate interactions are stronger than polymer-polymer interactions for all three polymers, why does PVOH 99%H appear to have a negligible h_1 thickness unlike the significant h_1 thicknesses observed for PVOH 88%H and PVP at high spin rates?

(2) Why do the more hydrophobic polymers adsorb to the superhydrophilic silicon substrate, when it would be expected that the more hydrophilic PVOH 99%H would be better suited for hydrogen bonding with the silanol and silanolate groups on the substrate?

More information about the polymer-polymer and polymer-substrate interactions in each system can be obtained by decoupling the spin curves into their h_1 and h_2 components. In order to do so, static adsorption experiments with each polymer on silicon wafer were performed to generate h_1 thicknesses that could be subtracted from the total spin curve to yield spin curves representative of only h_2 thicknesses and therefore polymer-polymer interactions. These results are discussed in Section 3.4.

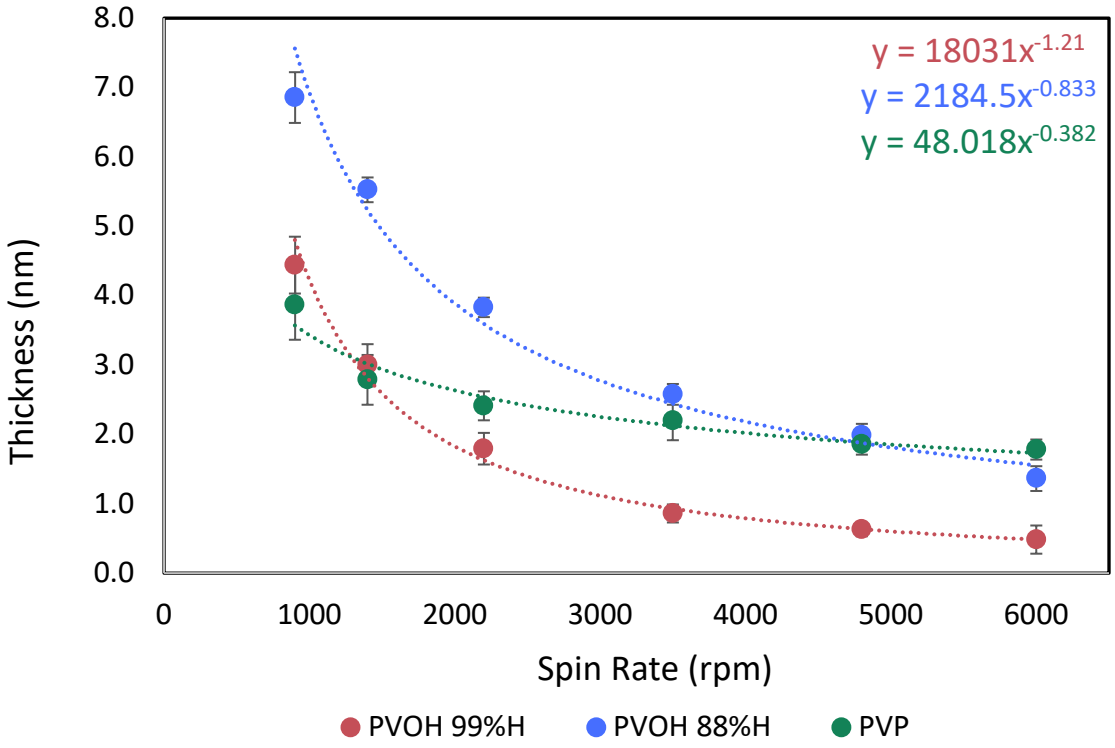

Figure 15: Spin curves of 0.1 wt% PVOH 99%H, PVOH 88%H, and PVP thin films prepared via spin coating on silicon wafer at various spin rates.

The dynamic water contact angles of 0.1 wt% PVOH 99%H, PVOH 88%H, and PVP are plotted as a function of spin rate in **Figure 16**. All three polymers display low receding contact angles that do not vary significantly with spin rate. However, each polymer has a unique trend in advancing contact angle as a function of spin rate.

Both PVOH 99%H and PVOH 88%H have relatively large advancing contact angles at the lower spin rates that correspond to thicker films. Because PVOH is semicrystalline, its hydroxyl groups engage in the inter- and intramolecular hydrogen bonding responsible for crystallization, which has been reported as a driving force for PVOH adsorption to hydrophilic substrates.[4,5] Therefore, the hydroxyl groups are not available to hydrogen bond with water, so the water interacts primarily with the hydrophobic backbone of the polymers or the available

acetate groups (in the case of PVOH 88%H). As spin rate increases, there is a decrease, to different extents, in the advancing contact angles of both PVOH 99%H and PVOH 88%H. This is likely due to the thinning of the films as spin rate increases, resulting in a reduced ability for polymer chains to crystallize. Because the polymer chains cannot crystallize to the same degree in thinner films, more hydroxyl groups are available to interact with the water at the surface and make the films more hydrophilic, reducing their advancing contact angles. However, the PVOH 88%H films do not decrease in thickness as much as the PVOH 99%H films, so they retain some of their crystallinity and therefore not as many hydroxyl groups become freed up to interact with the water droplet at the surface of the film. The greater percentage of hydrophobic acetate groups in PVOH 88%H may also contribute to the higher advancing contact angle on PVOH 88%H films at greater spin rates. Additionally, as the films become thinner at higher spin rates, the hydrophilic silicon substrate may be detectable by the probe fluid, which contributes to the decrease in advancing contact angle for both PVOH 99%H and PVOH 88%H. This effect likely plays a larger role in PVOH 99%H films, which are thinner at the higher spin rates than the PVOH 88%H films.

PVP advancing contact angles are low, approximately 10°, across all spin rates. This result seems counterintuitive given the relative hydrophobicity of PVP compared to PVOH, however, PVP is not crystalline, so the aforementioned process by which increased crystallization increases advancing contact angle does not apply to PVP. Additionally, the advancing contact angle of water on statically adsorbed PVP films is approximately 40°. This discrepancy is attributed to the fact that during the spin deposition step of adsorptive spin coating, polymers are forced to deposit in a random and thermodynamically unfavorable conformation in which some of the hydrophilic regions of the polymer are pointed upward. This

creates a hydrophilic surface with a somewhat high surface energy. In the case of static adsorption, however, there is more time for the PVP chains to deposit in a thermodynamically favorable conformation characterized by the inward orientation of hydrophilic regions of the polymer and outward orientation of hydrophobic regions of the polymer due to the hydrophobicity of air. This increases the advancing contact angle of water on statically adsorbed PVP films relative to their spin coated counterparts and also offers an explanation for why the spin coated PVP films have such a low advancing contact angle given their hydrophobicity.

In order to confirm the stability of these systems and rule out the possibility of metastability, PVOH 99%H, PVOH 88%H, and PVP thin films prepared at 6000 rpm (the thinnest of the spin coated films) were thermally annealed. Spin coating offers a relatively short amount of time for polymers to adsorb to the substrate before solvent is completely evaporated. This results in films that are most likely in kinetically trapped states. Thermally annealing spin coated films increases polymer mobility and allows thin films to achieve a thermodynamically favorable conformation that is more representative of their true stability or lack thereof.

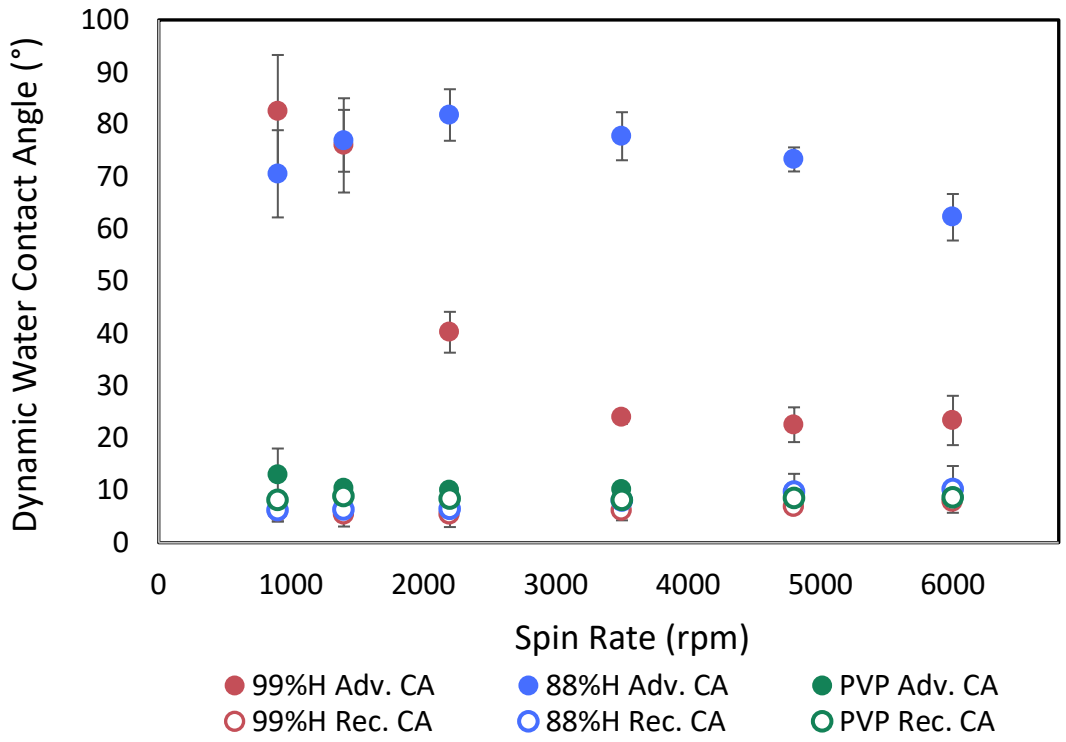

Figure 16. Dynamic water contact angles on 0.1 wt% PVOH 99%H, PVOH 88%H, and PVP thin films prepared via spin coating on silicon wafer at various spin rates.

The AFM images of thermally annealed PVOH 99%H, PVOH 88%H, and PVP films in **Table IV** show that after thermal annealing, the films are still continuous. This is strong evidence that these three systems are stable.

The thickness of PVOH 99%H, PVOH 88%H, and PVP thin films before and after thermal annealing are shown in **Figure 17.** There was negligible change in thickness following annealing, which confirms that the pre-annealing films did not contain a significant amount of water that could have contributed to swelling of the films. The consistency in thickness before and after annealing also confirms that there was no degradation of the films upon heating.

Table IV. AFM images (data scale 5 nm, aspect ratio 5 µm x 1.25 µm), section analysis, and RMS roughness (in nm) of 0.1 wt% PVOH 99%H, PVOH 88%H, and PVP thin films prepared at 6000 rpm and thermally annealed for 30 minutes at 100 °C.

Polymer	AFM Image	Section Analysis	RMS Roughness
PVOH 99%H	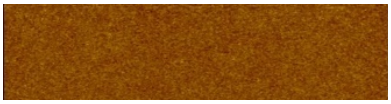	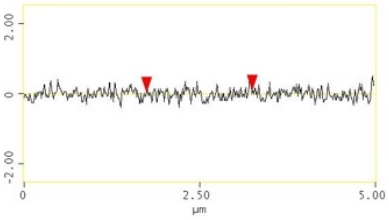	0.149
PVOH 88%H		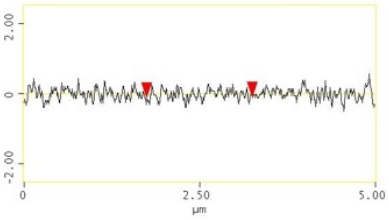	0.176
PVP		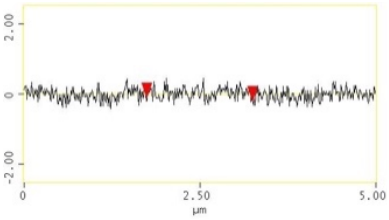	0.166

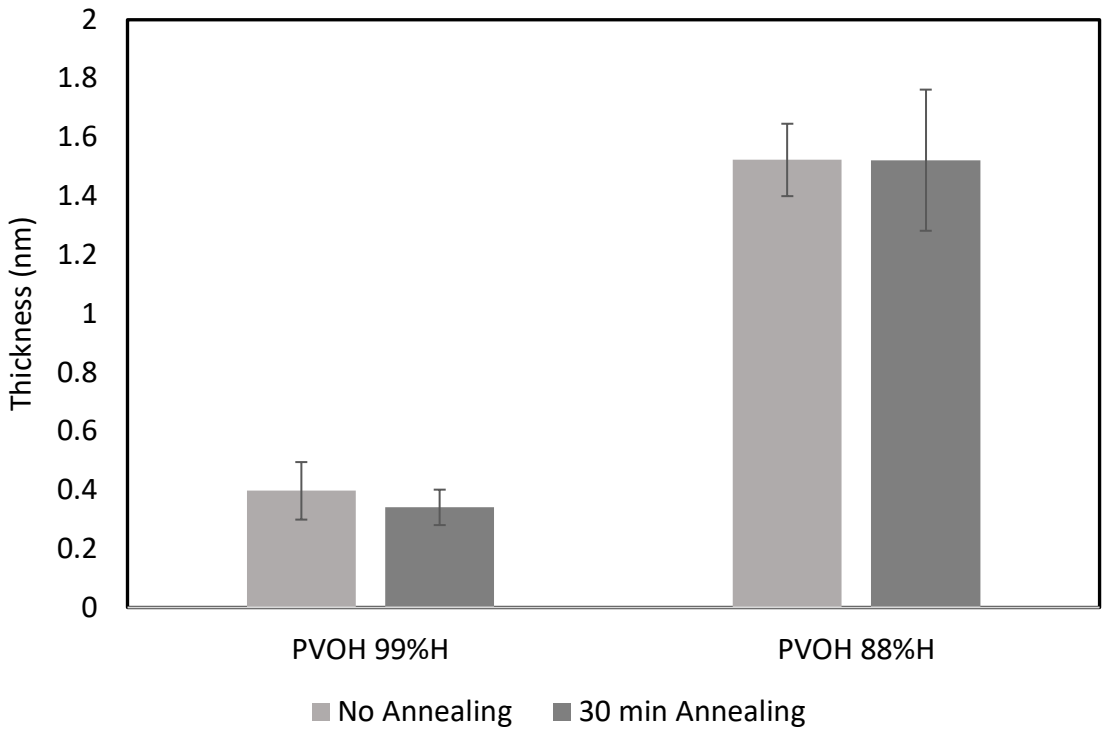

Figure 17. Thickness (nm) of PVOH 99%H and PVOH 88%H thin films prepared by spin coating at 6000 rpm before and after thermally annealing at 100 °C for 30 minutes.

Figure 18. shows the change in dynamic water contact angles on PVOH 99%H, PVOH 88%H, and PVP thin films before and after thermally annealing at 100 °C for 30 minutes. Early annealing experiments were conducted for 15, 30 and 60 minutes of annealing at 100 °C; however, it was determined that 30 minutes of annealing was sufficient to produce the observed changes in contact angle and that beyond 30 minutes, no further changes in contact angle occurred.

Both advancing and receding contact angles on PVP thin films appeared not to change significantly after annealing. However, PVOH 99%H and PVOH 88%H thin films displayed opposing trends in advancing contact angle change. While advancing contact angles on PVOH 99%H films appear to increase after annealing, advancing contact angles on PVOH 88%H films

appear to decrease. The increase observed for PVOH 99%H may be attributable to surface reconstruction made possible by increased polymer mobility at higher temperature. Hydrophilic surfaces have higher surface tensions than hydrophobic surfaces due to the hydrophobic nature of air. Therefore, the PVOH 99%H thin films could reduce their surface energy by orienting their hydroxyl groups towards the bulk of the film and their carbon backbones towards the surface, thus increasing the advancing contact angle. Additionally, higher polymer mobility allows PVOH to increase its extent of crystallinity by forming more inter- and intramolecular hydrogen bonds.[11,12,16] This renders hydroxyl groups in the film unavailable to hydrogen bond with water at the surface and increases the advancing contact angle. Because PVOH 99%H is more crystalline than PVOH 88%H, this crystallization process is expected to occur to a greater degree in PVOH 99%H films, resulting in a more drastic increase in contact angle for PVOH 99%H. The decrease in the contact angles on PVOH 88%H thin films after annealing may be due to increased hydrophobic interactions within the bulk of the film. The acetate groups, which exist in a greater number in PVOH 88%H, can form hydrophobic interactions in the bulk of the film, which drives the PVOH 88%H films to orient the carbon backbone and acetate groups inward and the hydroxyl groups outwards towards the surface of the film. This makes the film surface more hydrophilic and reduces the contact angle on PVOH 88%H.

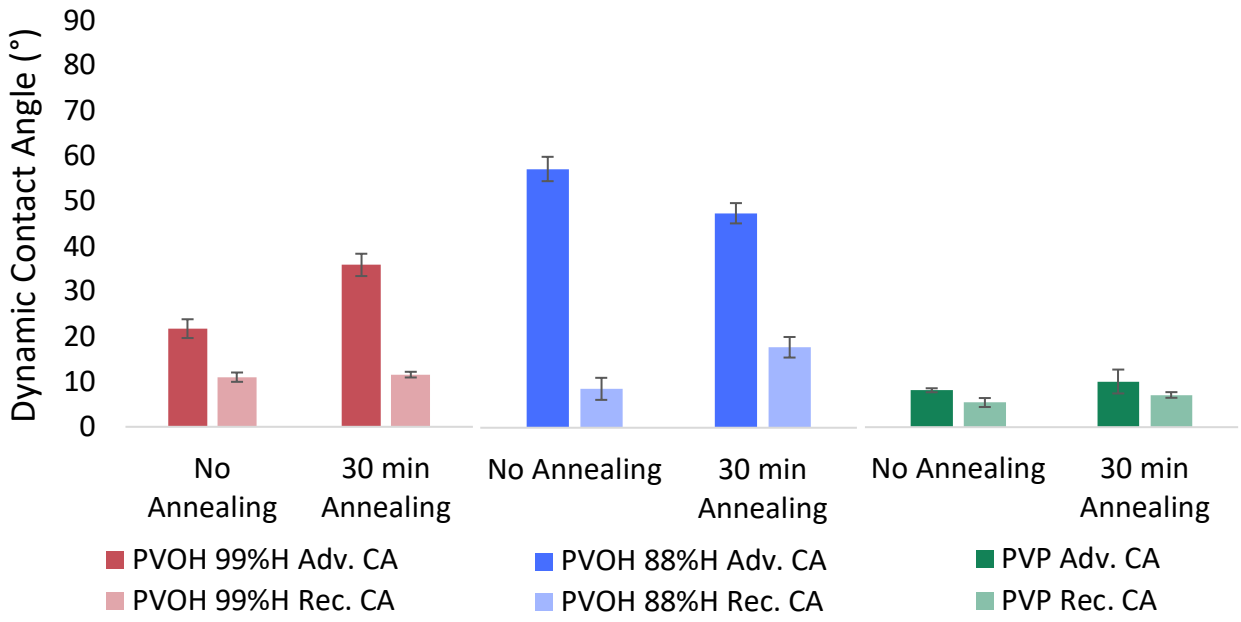

Figure 18. Dynamic water contact angles of 0.1 wt% PVOH 99%H, PVOH 88%H, and PVP thin films prepared via spin coating at 6000 rpm on silicon wafer followed by thermal annealing at 100 °C for 30 minutes.

3.2 Metastable Systems

In order to probe the effects of crystallinity and polymer charge on the stability of polymer thin films, spin coating experiments were conducted with a number of comparison polymers, described in the introduction section. PAA, PAH, and PSS were spin coated on silicon wafers at the same six spin rates used for the stable polymers. AFM images of these three systems as a function of spin rate are shown in **Table V**. All three systems display dewetting that intensifies as spin rate increases and film thickness decreases.

Dewetting occurs when the spreading coefficient is negative because the solid-gas surface tension is less than the liquid-gas and solid-liquid surface tensions combined such that the energy of the system can be minimized by the formation of droplets and maximization of exposed substrate. This corresponds to greater cohesive forces than adhesive forces. Therefore, the dewetting displayed in the AFM images suggest that the cohesive forces of PAA, PAH, and PSS all outweigh their respective adhesion to the silicon substrate.

PAA represents a neutral polymer-neutral substrate system. It is anticipated that hydrogen bonding between the carboxylic acids in PAA and the silanol and silanolate groups would contribute to strong adhesive forces. However, the dewetting observed under AFM indicates that the cohesive forces between polymers are stronger than the adhesive forces driving adsorption. This suggests that the hydrogen bonding between the polymer chains is more favorable than the hydrogen bonding between the polymer and the substrate, such that hydrogen bonding is insufficient to promote spreading.

A similar situation is observed for PAH, which represents a positive polymer-neutral substrate system. In this case, cohesive forces were anticipated to be low due to electrostatic repulsion, while adhesive forces were anticipated to be driven by hydrogen bonding between the

amine and silanol groups on the substrate. The fact that dewetting was observed suggests again that hydrogen bonding and ionic interactions with the substrate are insufficient to promote spreading and that the cohesive forces remain strong enough that like charge repulsions do not dominate.

PSS represents a negative polymer-negative substrate system. Therefore, the polymer-substrate and polymer-polymer interactions are likely both characterized by electrostatic repulsion. Of the three systems shown in **Table V**, PSS dewets most extensively even at lower spin rates, which is likely a product of the like-charge repulsion both between the polymer and the substrate as well as between polymer chains.

Table V. AFM images (data scale 5 nm, aspect ratio 5 µm x 1.25 µm), section analysis, and RMS roughness (in nm) of 0.1 wt% PAA, PAH, and PSS thin films prepared by spin coating on silicon wafer at various spin rates.

Spin Rate (rpm)	PAA	PAH	PSS
900	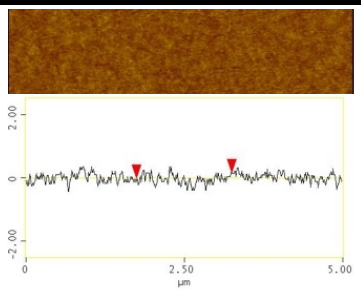 RMS = 0.145	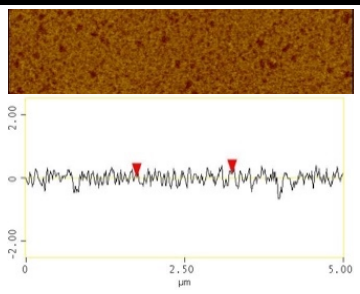 RMS = 0.194	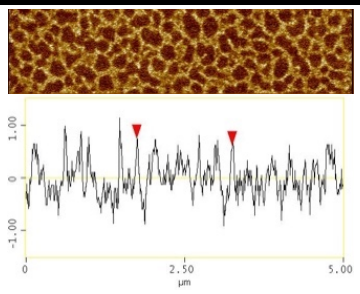 RMS = 0. 0.334

1400	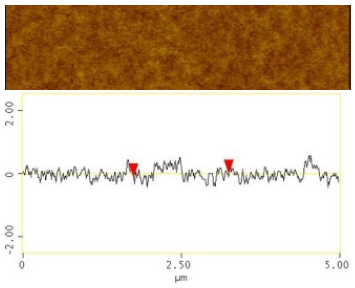 RMS = 0.154	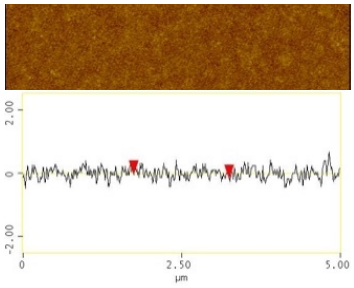 RMS = 0.156	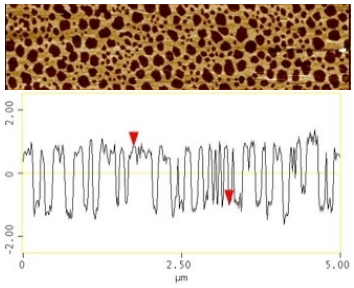 RMS = 0.835
2200	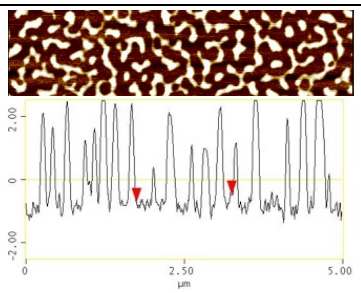 RMS = 1.185	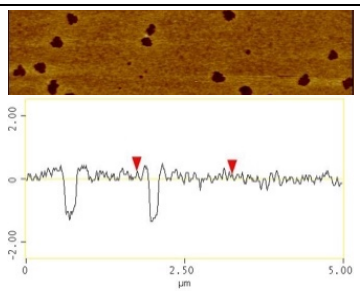 RMS = 0.253	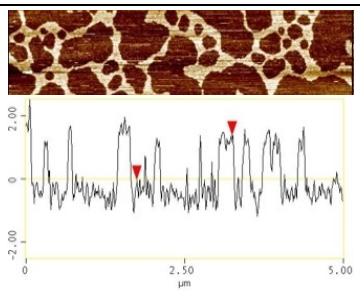 RMS = 0.857
3500	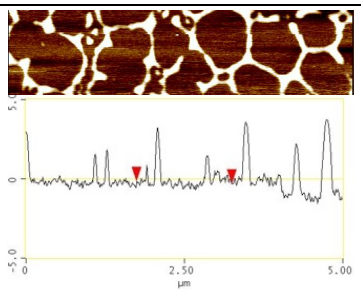 RMS = 1.197	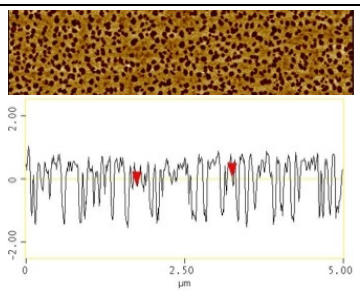 RMS = 0.668	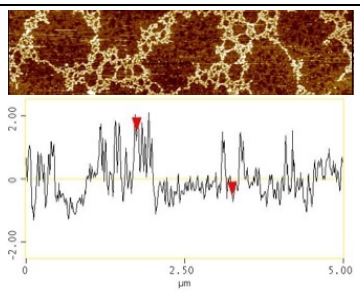 RMS = 0.702
4800	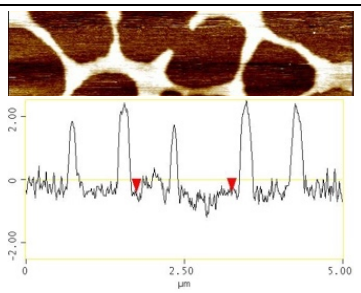 RMS = 1.118	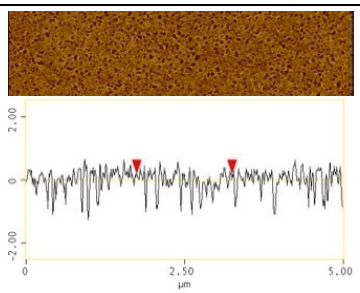 RMS = 0.315	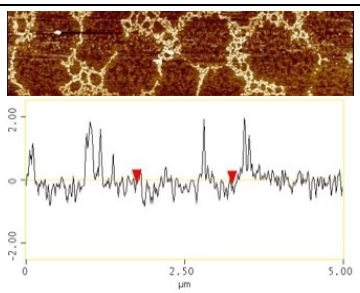 RMS = 1.236
6000	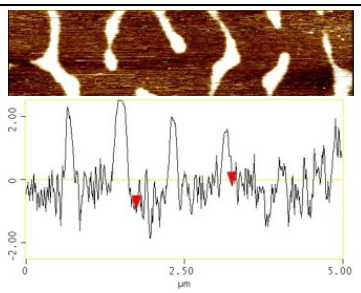 RMS = 1.094	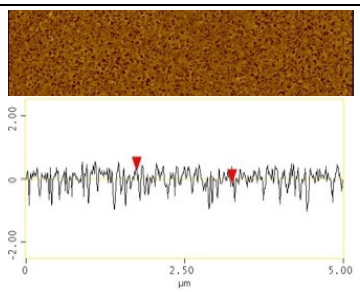 RMS = 0.292	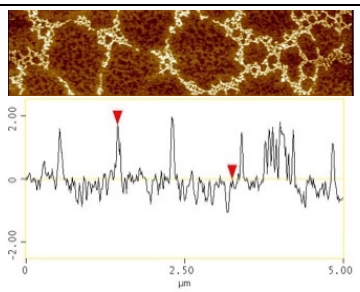 RMS = 0.583

PAA, PAH, and PSS spin coated films show a very similar thickness dependence on spin rate, with all three polymers producing thinner films across all spin rates compared to the stable polymers (**Figure 19**). There are several noteworthy comparisons between the stable and metastable spin curves that shed some light on the relative contributions of adhesive and cohesive forces.

At the highest spin rate, PAA, PAH, and PSS thin films are comparable in thickness to PVOH 99%H. Of the stable polymers, PVOH 99%H is the most hydrophilic, a property that it shares with PAA, PAH, and PSS. This supports the theory that the greater thickness of the PVOH 88%H and PVP films at 6000 rpm is likely due to hydrophobic interactions. Furthermore, because the contribution of the h_1 layer is much more significant than that of the h_2 layer at high spin rates, it would follow that hydrophobic interactions are the driving force for the formation of the h_1 layer of the PVOH 88%H and PVP films. This is contrary to expectation because of the extremely hydrophilic nature of the silicon wafer and the previous research that indicates that hydrogen bonding is the driving force for PVOH adsorption to silicon substrates.[17,18,19,20]

At low spin rates, the PAA, PAH, and PSS thin films are much thinner than all three stable polymer films. At low spin rates, the h_2 layer is the dominant contributor to total film thickness. PVOH is semicrystalline, which is likely why it is so much thicker than the polyelectrolytes at low spin rates: crystallinity increases the cohesive forces of the polymer solution during spin and solvent evaporation. Increased cohesion increases the viscosity of the polymer solution, which allows it to resist the centrifugal force of spinning, resulting in less spun off solution and therefore a greater equilibrium thickness. However, while the low thicknesses of PAA, PAH, and PSS at low spin rates suggest weak cohesion between polymer chains, the dewetting observed under AFM suggests that the cohesive forces dominate over the adhesive

forces. It was established previously that PAA, PAH, and PSS all display weak adhesion to the silicon substrate as evidenced by low film thicknesses at high spin rates. Therefore, the most likely reconciliation of the contradictory pieces of evidence obtained from the spin curves and AFM images is that PAA, PAH, and PSS have both weak cohesion (compared to PVOH) and weak adhesion, but cohesion is slightly stronger than the adhesion, leading to dewetting. The weak cohesion for PAH and PSS is likely due to the electrostatic repulsion. However, the two primary questions that remain unanswered are (1) why the electrostatic repulsion between polymer chains is favorable enough to produce cohesive forces stronger than the adhesive forces, and (2) why hydrogen bonding is not a stronger driving force for adhesion and spreading.

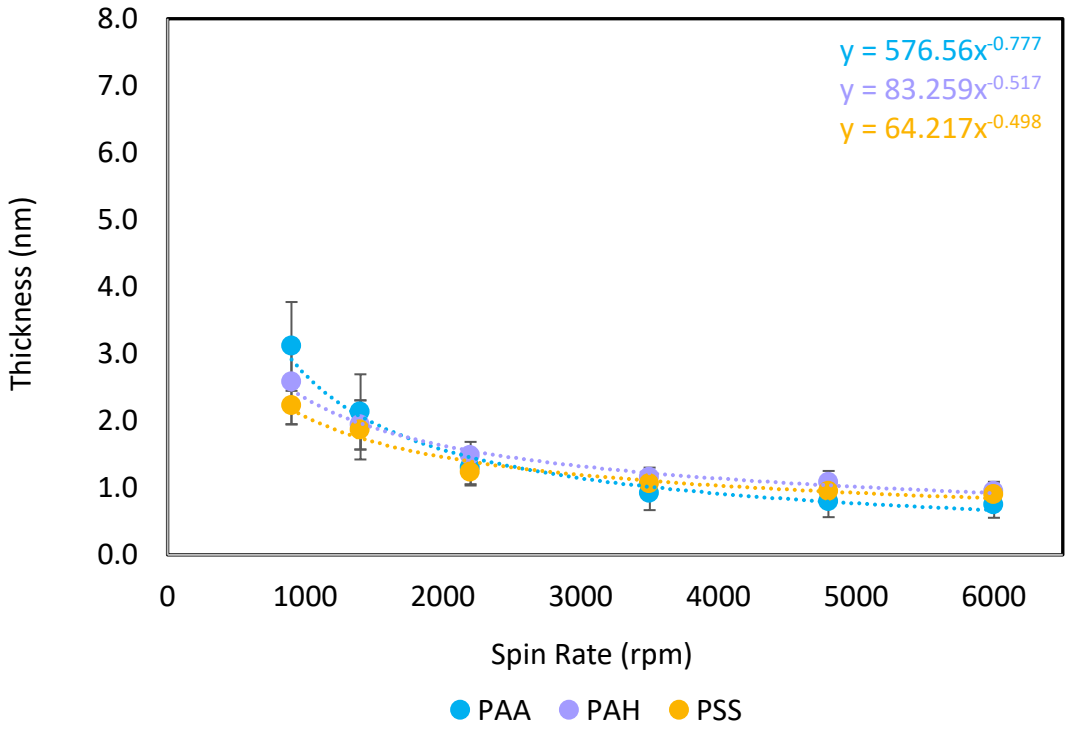

Figure 19: Spin curves of 0.1 wt% PAA, PAH, and PSS thin films prepared via spin coating on silicon wafer at various spin rates.

While discussing the trend in thickness at low spin rates, it is also worth noting that the PVP films are thinner than the two PVOH films at 900 rpm, but still thicker than all three polyelectrolyte films at 900 rpm. This agrees well with the expectation for the PVP system. The lack of crystallinity suggests that its cohesive forces are weaker than those of PVOH leading to a thinner h_2 layer, while the fact that it is thicker than PAA, PAH, and PSS at higher spin rates can be attributed to its thicker h_1 layer and the lack of electrostatic repulsion between polymer chains. Subtracting the 6000 rpm thickness of a spin curve from the 900 rpm thickness offers a rough estimate of the h_2 contribution to total film thickness at 900 rpm. When this is done for all polymers (**Figure 20**), it can be seen that PVOH 99%H and PVOH 88%H have the highest h_2 contribution at the lowest spin rate, which suggests that crystallinity is the most influential factor that drives cohesion. In addition to crystallinity, hydrophobic interactions between polymer chains also promotes strong cohesion, evidenced by the fact that the PVOH 88%H h_2 layer is thicker than the PVOH 99%H h_2 layer. PVP, PAA, PAH, and PSS all have significantly lower h_2 thicknesses at the lowest spin rates due to their lack of crystallinity; however, PVP and PAA form slightly thicker h_2 layers than PAH and PSS. This is likely due to the neutrality of PVP and PAA compared to the electrostatic charge present on PAH and PSS, which results in like-charge repulsion and reduces the cohesive forces in those systems.

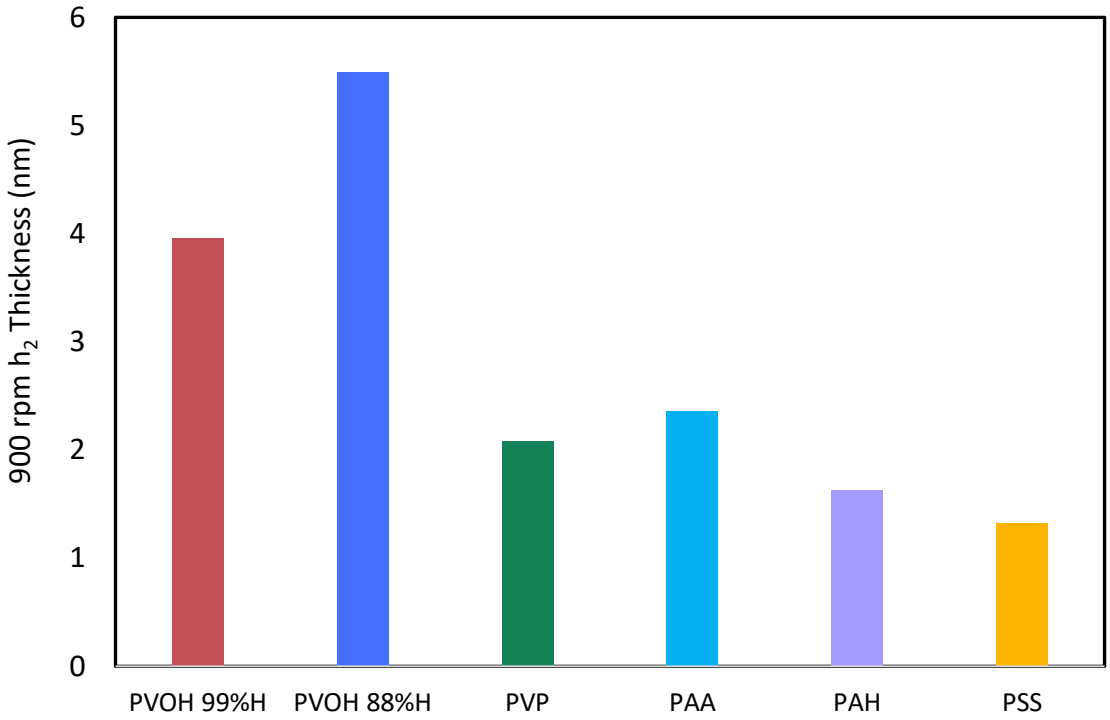

Figure 20: Spin deposited thickness (nm) at 900 rpm for PVOH 99%H, PVOH 88%H, PVP, PAA, PAH, and PSS thin films prepared by spin coating on silicon wafers (spin deposited thickness was determined by subtracting total thickness at 6000 rpm from the total thickness at 900 rpm for each polymer)

To gauge the effect of crystallinity, hydrophobicity, and polymer charge on spontaneous adsorption, the thickness of each polymer at 6000 rpm (assumed to be representative of h_1 layer thickness) was plotted and is displayed in **Figure 20**. PVOH 88%H and PVP have the highest 6000 rpm thickness, suggesting that polymer hydrophobicity is the primary contributor to spontaneous deposition.

Based on the significant difference in the 6000 rpm thickness values for PVOH 99%H and PVOH 88%H, crystallinity plays less of a role in driving spontaneous deposition. This implies that crystallinity is more significant when the polymer is in solution and it increases the

viscous forces, thus increasing the h_2 layer thickness. However, because spontaneous deposition is determined by the interaction between the polymer and the substrate, crystallinity is less influential in determining the thickness of the spontaneously deposited layer. However, it is interesting to note that while crystallinity cannot promote polymer-substrate affinity when the polymer is in solution, it likely plays an influential role in the adhesive forces following evaporation of the solvent because both PVOH 99%H and 88%H form stable films at all spin rates, meaning their adhesion to the substrate must outweigh their respective cohesive forces. That is, crystallinity is more relevant to the cohesive forces when the polymer is in solution and to the adhesive forces once the films have dried.

Finally, it is difficult to comment on the role of polymer charge on spontaneous deposition based on the results shown in **Figure 21**. PAA, PAH, and PSS all have a similar thickness at 6000 rpm, which is slightly thicker than that of PVOH 99%H. Each of the three systems has a different polymer-substrate charge relationship. PAA is a neutral polymer on a neutral substrate, and PAH is a positive polymer on a neutral substrate, so in both systems there is no electrostatic attraction or repulsion driving or impeding spontaneous adsorption. PSS is a negative polymer on a negative substrate, so electrostatic repulsion is expected to impede spontaneous deposition. However, PSS displays a similar h_1 thickness to PAA and PAH.

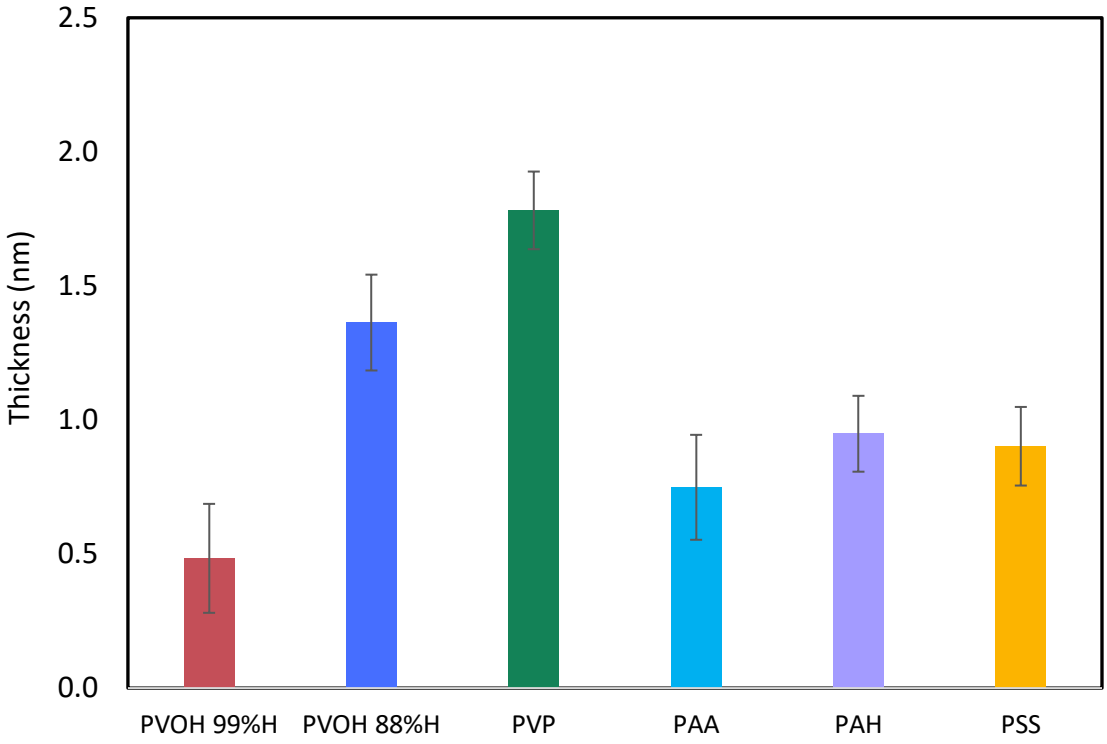

Figure 21: Spontaneously deposited thickness (nm) for PVOH 99%H, PVOH 88%H, PVP, PAA, PAH, and PSS thin films prepared by spin coating on silicon wafers (reported values are the thickness of each polymer at 6000 rpm because thickness at the highest spin rate is assumed to be representative of spontaneously deposited thickness).

Another point of comparison between the different polymer systems is their spin curve exponents. The Meyerhofer model predicts a spin curve exponent of -0.5 for all polymers,[66] but as mentioned previously, this prediction often fails to agree with experimental results. The spin curve exponents for each polymer are shown in **Figures 15** and **19.** There is a range of exponents, with only PAH and PSS being near the predicted -0.5 value. The spread of values for spin curve exponents raises the question of what system properties cause each to deviate not only from -0.5, but also from each other.

The spin curve exponent is affected both by the vertical shift of the spin curve and the rate of decay or steepness of the spin curve. In the context of spin coating, the vertical shift corresponds to the h_1 layer thickness, while the steepness or the rate of decay corresponds to the dependence of the h_2 layer thickness on spin rate (i.e. a steeper slope implies that h_2 thickness is very sensitive to changes in spin rate while a shallower slope implies that h_2 thickness is not very sensitive to changes in the spin rate). The sensitivity of the h_2 thickness to spin rate is related to the viscosity of the polymer solution and therefore the polymer-polymer interactions or cohesive forces. In the derivation of his model, Meyerhofer did not consider the presence of a spontaneously deposited h_1 layer, treated viscosity (polymer-polymer interactions) as universal for all polymers, and assumed polymers completely wet the substrate, which is not the case for unstable and metastable scenarios. These are three fundamental reasons why -0.5 is difficult to reproduce experimentally. However, knowing these shortcomings of the Meyerhofer model offers a starting point to answering the question posed above. To probe the relative contributions of spontaneous deposition and spin deposition to the spin curve exponent, the h_1 thickness is subtracted from each point along the spin curve, and the resulting spin curve exponent should reflect only the h_2 layer (i.e. the layer accounted for by the Meyerhofer model). It is hypothesized that the h_2 spin curve exponents should be closer to the -0.5 exponent predicted by Meyerhofer because the h_1 layer has been eliminated.

Both the advancing and receding contact angles of PAA, PAH, and PSS are very low and consistent across all spin rates (**Figure 22**). The low contact angles are suggestive of a hydrophilic surface, which is likely due to the exposed silicon wafer. The slightly higher advancing PAA contact angle at 900 rpm corroborates the continuous film shown under AFM in

Table V. However, this advancing contact angle is still extremely low, which can be attributed to the hydrophilicity of the PAA film.

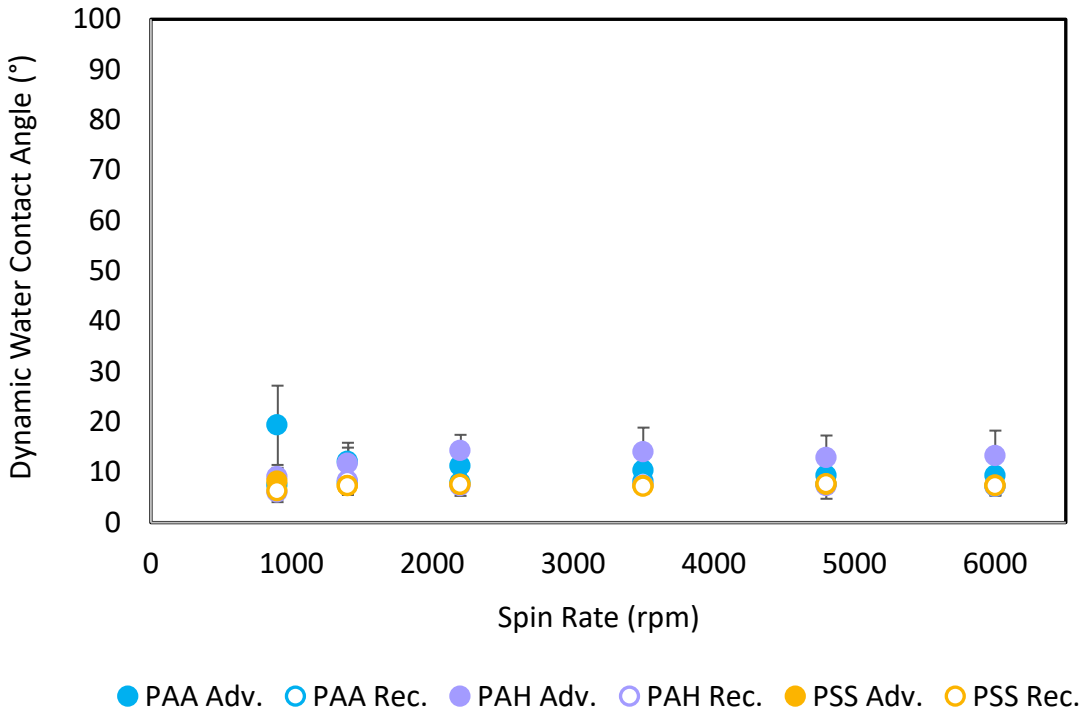

Figure 22: Dynamic water contact angles on 0.1 wt% PAA, PAH, and PSS thin films prepared via spin coating on silicon wafer at various spin rates.

3.3 Probing Polymer Charge by Tuning pH

One of the advantages of working with polyelectrolytes is the ability to alter their charge by tuning the pH of the polymer solution. In order to explore different combinations of polymer and substrate charge, both PAA and PAH solutions were increased in pH (from pH 3.27 to roughly pH 8-9 for PAA and from pH 3.21 to roughly pH 6-7 for PAH) with the goal of creating a negative polymer-negative substrate system for the deprotonated PAA (henceforth referred to as PAA^-) and a positive polymer-negative substrate system for PAH (henceforth referred to as PAH_{SiO^-}). Both systems displayed aggregation upon addition of NaOH; however, despite aggregation, both systems offered evidence in support of the decoupled thickness model as well as raised questions that motivated future directions for the work described.

3.3.1 PAH_{SiO^-}

3.3.1.1 Evidence of PAH Aggregation

While titrating PAH, the solution pH values increase exponentially with every 30 µL of NaOH added, reaching a peak of approximately 7 for 170 µL NaOH (**Figure 23**). DLS measurements show that the hydrodynamic size of PAH starts low (at approximately 2.5 d.nm), peaks around 30 or 60 µL of NaOH added, and gradually decreases until it reaches approximately 85 d.nm (**Figure 23**). Beyond 170 µL NaOH, PAH_{SiO^-} aggregates precipitate out of solution. The two sets of hydrodynamic size data were not averaged to highlight the fact that hydrodynamic size peaked at a different volumes of NaOH for each set (one at 60 µL NaOH and one at 30 µL NaOH) and that the peak hydrodynamic size was significantly different for the two sets (approximately 120 d.nm for one and 290 d.nm for the other) (**Figure 24**).

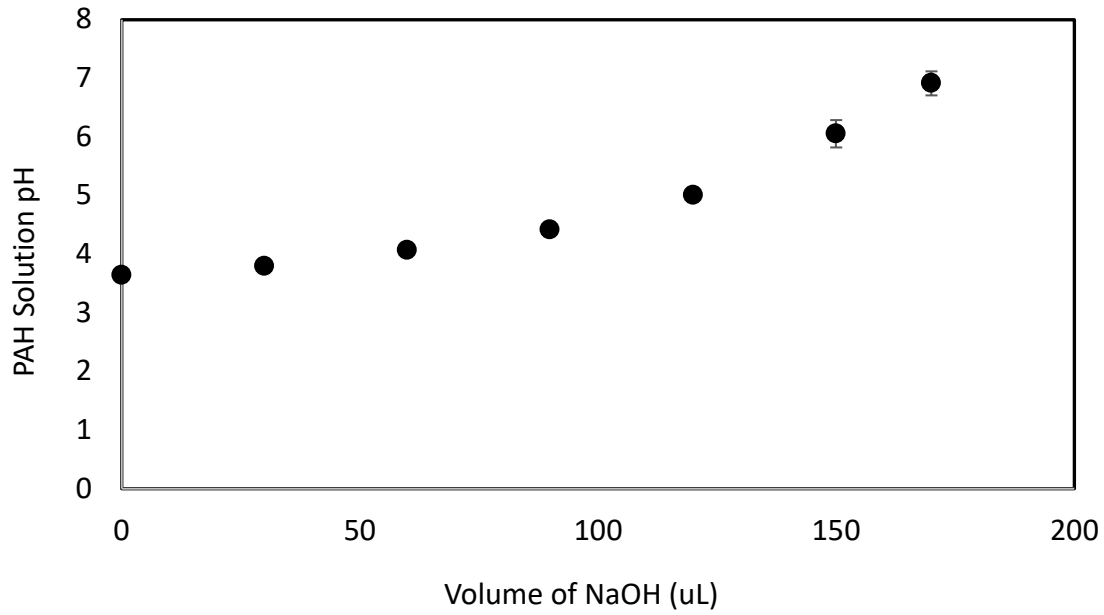

Figure 23. PAH_{SiO^-} solution pH as a function of the volume of 1 M NaOH added to the original PAH solution.

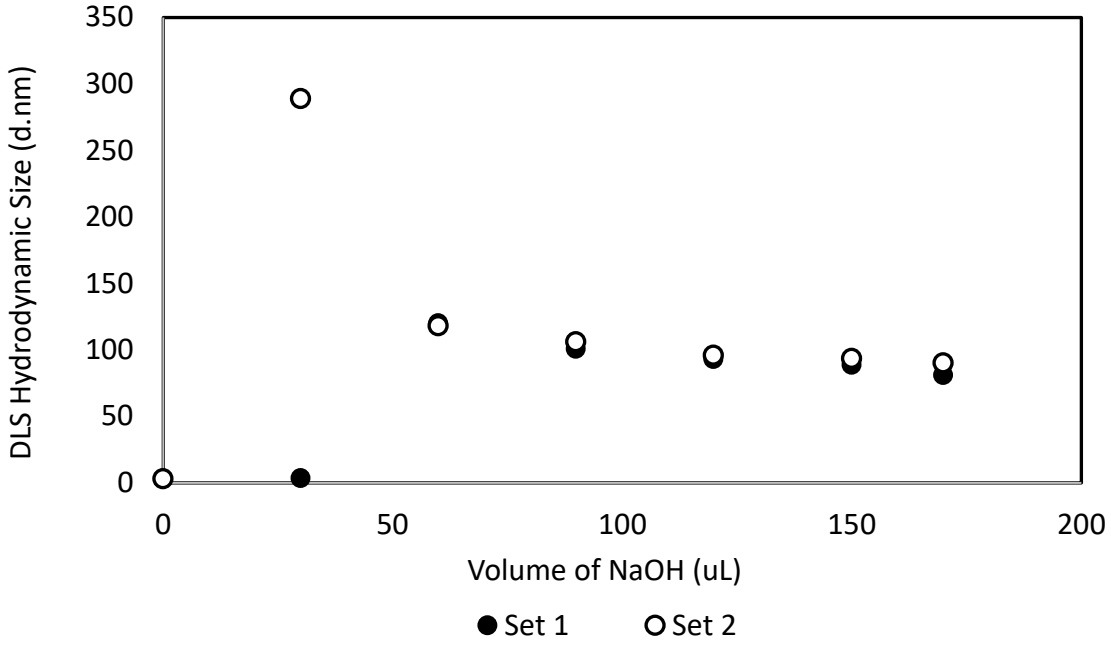

Figure 24. Hydrodynamic sizes (d.nm) of PAH aggregates as a function of the volume of 1 M NaOH added to the PAH solution determined via DLS. Set 1 and Set 2 refer to two experimental replicates following the same experimental design.

3.3.1.2 PAH_{SiO-} Spin Coating

Table VI shows AFM images of PAH_{SiO-} spin coated on silicon wafer at various spin rates. It is apparent from the images that the aggregates in solution adsorb to the substrate during either the spontaneous deposition process or the spin deposition process. Furthermore, the gradual decrease in aggregate size as spin rate increases suggests that larger aggregates are less strongly adsorbed than smaller aggregates and are increasingly spun off the substrate as the centrifugal force gets stronger.

Table VI. AFM images (data scale 5 nm, aspect ratio 5 µm x 1.25 µm), section analysis, and RMS roughness (in nm) of 0.1 wt% PAH_{SiO-} thin films prepared by spin coating on silicon wafer at various spin rates.

Spin Rate (rpm)	AFM Image	Section Analysis	RMS Roughness
900	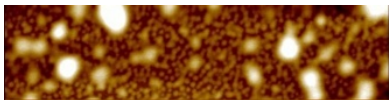	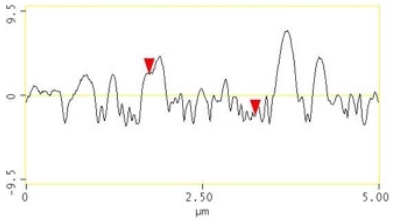	2.683
1400	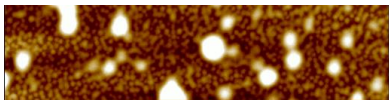	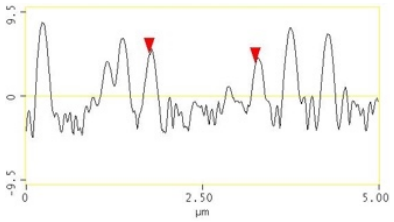	3.064

2200	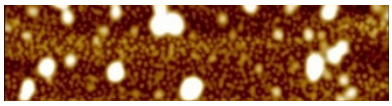	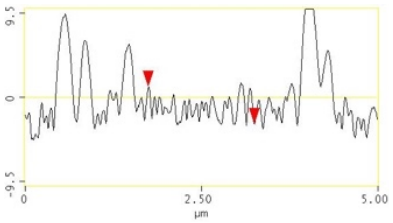	3.185
3500	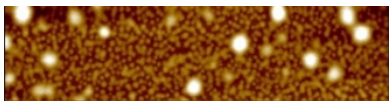	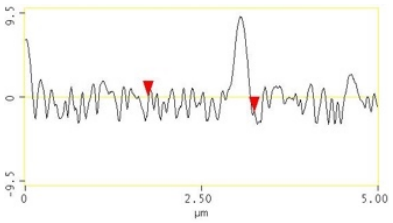	2.009
4800	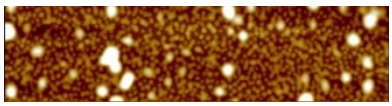	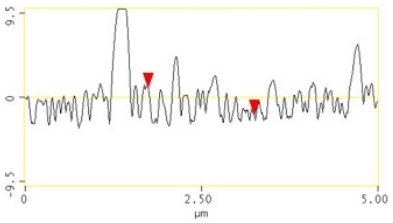	2.330
6000	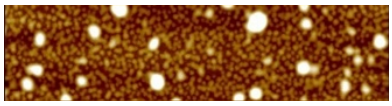	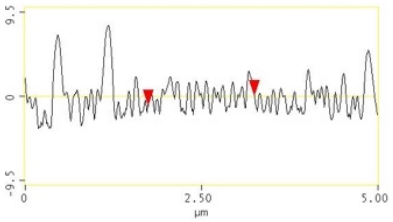	2.461

From **Figure 25**, it can be seen that the PAH_{SiO^-} spin curve is approximately 2.5 nm higher than the PAH spin curve, which is comparable in thickness and exponent to many of the other amorphous polymers' spin curves. This is likely due to the presence of large, positively-charged PAH aggregates that are attracted to the negatively-charged substrate. Additionally, the spin curve exponent for PAH_{SiO^-} (-0.162) is significantly smaller than that of PAH (-0.517), which is close to the -0.5 exponent predicted by the Meyerhofer model. Spin curve exponents close to zero represent systems in which the h_2 dependence on spin rate is low due to weak

cohesive forces between the polymer in solution. In the case of PAH_{SiO-}, this weak cohesion likely arises from the electrostatic repulsion between positively charged PAH aggregates.

Slip is typically a sign of dewetting and associated with spin curve exponents close to zero. However, with the presence of aggregates, adsorption and deposition are significantly different from those of individual polymer chains. The positively charged PAH_{SiO-} aggregates spontaneously deposit onto the negatively charged silicon wafer due to the electrostatic attraction between the two, which forms a significant h_1 layer. However, the electrostatic repulsion between the positively charged PAH_{SiO-} aggregates in solution weakens the cohesive forces, so most of the polymer solution is removed during spin. Therefore, relatively few aggregates are deposited via spin deposition, resulting in a relatively thin h_2 layer that is not strongly dependent on the spin rate. This is likely why the PAH_{SiO-} spin curve is shifted up several nanometers relative to the PAH spin curve but still has a spin curve exponent that is very close to zero.

Figure 26 shows that the advancing contact angles on PAH_{SiO-} are significantly higher (~50°) than the advancing contact angles on PAH. This is easily attributed to the extensive coverage of the substrate by PAH aggregates in the case of the PAH_{SiO-} system (**Table VI**). Meanwhile, the extremely hydrophilic substrate is exposed due to dewetting of PAH in the PAH system, which causes the low advancing contact angles for spin coated PAH.

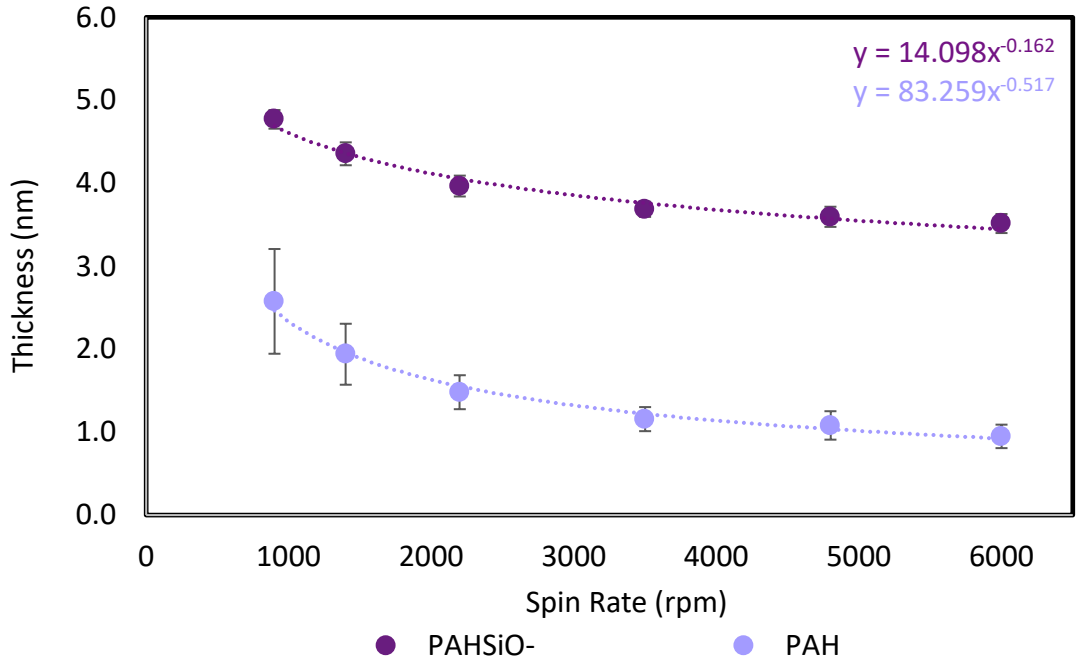

Figure 25. Spin curves of 0.1 wt% PAH_{SiO-} and PAH thin films prepared via spin coating on silicon wafer at various spin rates.

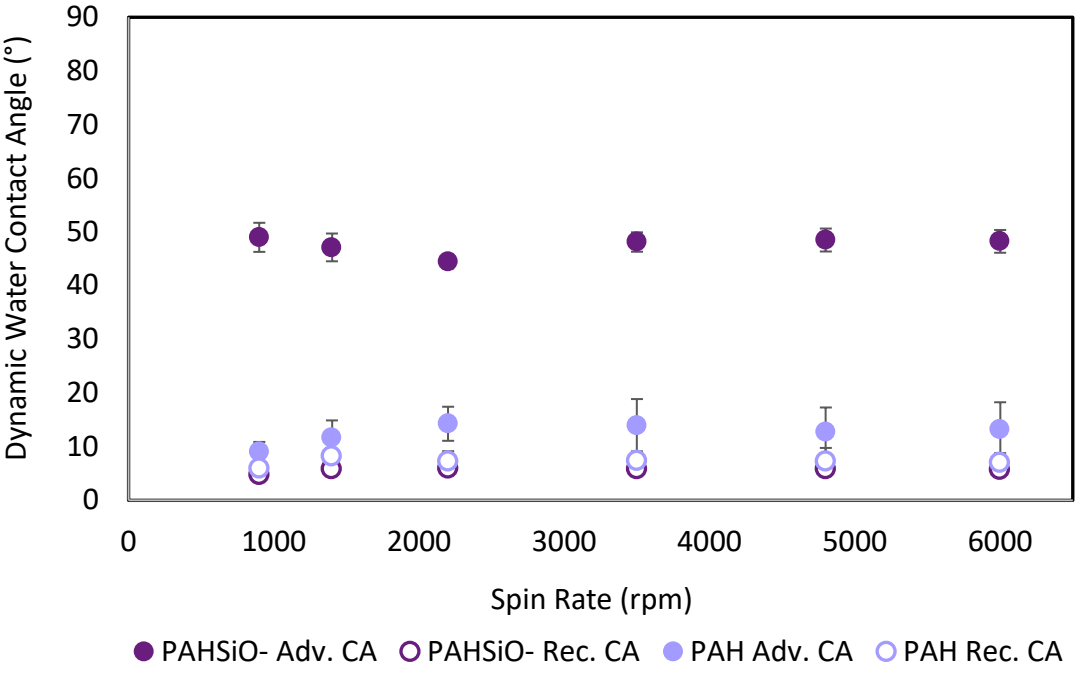

Figure 26. Dynamic water contact angles on 0.1 wt% PAH_{SiO-} and PAH thin films prepared via spin coating on silicon wafer at various spin rates.

3.3.1.3 PAH_{SiO^-} Static Adsorption

As the volume of NaOH added to the PAH_{SiO^-} solution increased, the spontaneously deposited thickness increased exponentially (**Figure 27**). After the first 5 additions (0-120 µL) of NaOH, the adsorbed thickness was at or below 1 nm, and at 150 uL NaOH the thickness begins to increase drastically, reaching a maximum value after adding 170 µL NaOH. This trend displayed in **Figure 27** is unexpected considering **Figure 24** shows that aggregation begins at 30-60 µL NaOH, and aggregates gradually decrease in size with increasing addition of NaOH. There are three possible explanations for this discrepancy.

First, as discussed above, it appears that larger aggregates are more weakly adsorbed than smaller aggregates. At low volumes of NaOH there are no aggregates, at intermediate volumes of NaOH, aggregate size peaks, and at the highest volumes of NaOH the aggregate size is smallest. Therefore, the lack of adsorption at the lowest NaOH volumes is due to a lack of aggregates while the lack aggregates at intermediate NaOH volumes is due to the predominance of large aggregates in solution, which are weakly adsorbed and removed during the rinse step.

Another possible explanation for the contradictory trends in **Figure 24** and **Figure 27** is that beyond the initial peak observed for aggregate size in **Figure 24**, aggregates continue to increase until they precipitate out of solution, and DLS cannot detect the larger aggregates, so only reports the smaller aggregates. If this is the case, then the reason the spontaneously deposited thickness shown in **Figure 27** does not increase significantly until 150 µL NaOH added is because this is the volume of NaOH at which the aggregates are large enough in size to form a sizable layer. This size would be larger than what is shown in **Figure 24** because of the limitations of DLS to detect such large particle sizes.

A third explanation is that significant adsorption doesn't occur until 150 uL NaOH because this is when the silicon substrate becomes sufficiently deprotonated to attract the positively charged PAH aggregates via electrostatic interactions. **Figure 23** shows that the pH of the PAH_{SiO-} solution is approximately 5 at 120 µL NaOH and approximately 6 at 150 µL NaOH. Because the pKa of the silicon wafer is approximately 5.6, it would be expected that it does not become completely deprotonated until 150 uL NaOH, at which point electrostatic interactions between the substrate and aggregates can act as a driving force for adsorption.

A final detail from the static adsorption experiments that is worth noting is that at the highest volume of NaOH added, which is the volume of NaOH added to the solution used for PAH_{SiO-} spin coating experiments, the statically adsorbed thickness is approximately 2.3 nm. This is in good agreement with the 2.5 nm upward shift of the PAH_{SiO-} spin curve relative to the PAH spin curve.

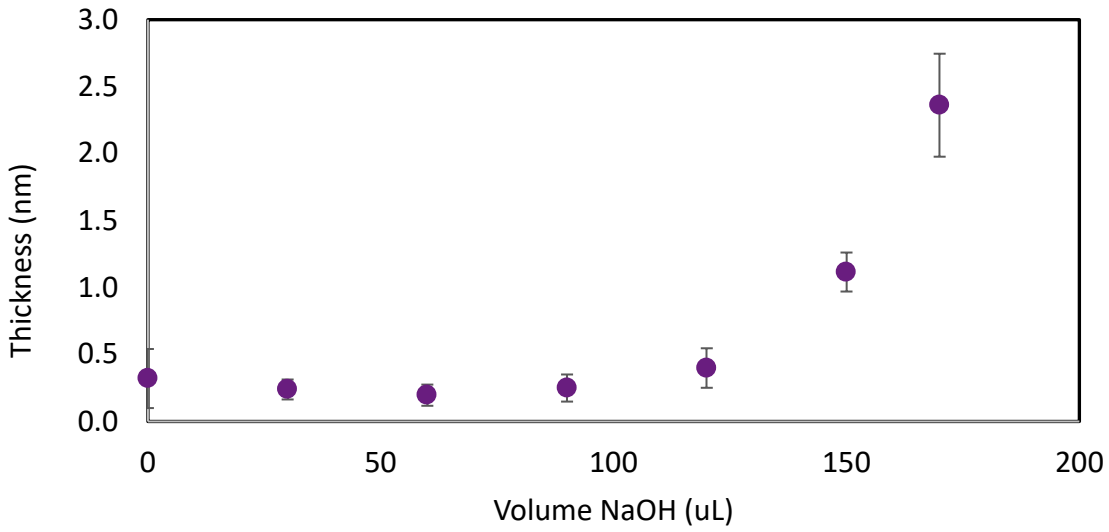

Figure 27. Spontaneously deposited thickness (nm) of PAH_{SiO-} thin films prepared via 10-minute static adsorption experiments on silicon wafer as a function of the volume of 1 M NaOH added to the PAH_{SiO-} solution.

Figure 28 shows a gradual increase in advancing contact angle on PAH_{SiO^-} films as NaOH volume increases. The increase in advancing contact angle follows the increase in spontaneously adsorption thickness (**Figure 27**), which indicates that the increase in advancing contact angle is due to greater coverage of the substrate. The highest advancing contact angle is approximately 55° at 170 uL NaOH. This is the same volume of NaOH used for the spin coating experiments, and the advancing contact angle of water on the spin coated PAH_{SiO^-} samples was around 50° across all spin rates.

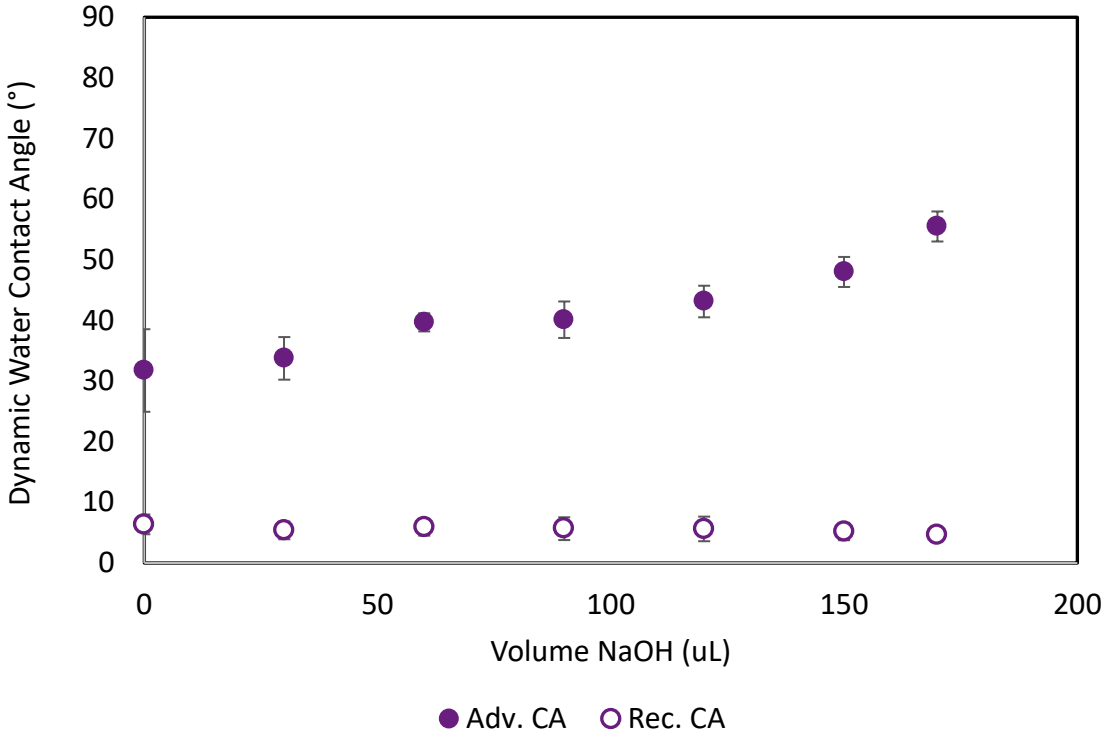

Figure 28. Dynamic water contact angles on 0.1 wt% PAH_{SiO^-} thin films prepared via 10-minute static adsorption on silicon wafer as a function of the volume of 1 M NaOH added to the PAH_{SiO^-} solution.

3.3.2 PAA^-

3.3.2.1 Early Experiments with PAA^-

The AFM images in **Table VII** show signs of dewetting in the PAA^- thin films, although the degree of dewetting does not compare to that of the other polyelectrolytes (**Table V**). This comparison is supported by the RMS roughness values of the PAA^- films, which are significantly lower than those for PAA, PAH, and PSS. However, there was a range of morphologies observed for PAA^- thin films, some of which are included in the Appendix section. Additionally, the AFM images in **Table VII** show no evidence of aggregates. It was mentioned previously that upon addition of NaOH to the PAH and PAA solutions, aggregation was induced. This was primarily deduced from dynamic light scattering (DLS) results and the PAA^- spin curve, and some of the AFM images of PAA^- thin films in the Appendix section display signs of aggregation.

Table VII: AFM images (data scale 5 nm, aspect ratio 5 µm x 1.25 µm), section analysis, and RMS roughness (in nm) of 0.1 wt% PAA^- thin films prepared by spin coating on silicon wafer at various spin rates. (Additional AFM images from different PAA^- spin coating experiments display a range of morphologies and are included in the Appendix)

Spin Rate (rpm)	AFM Image	Section Analysis	RMS Roughness
900		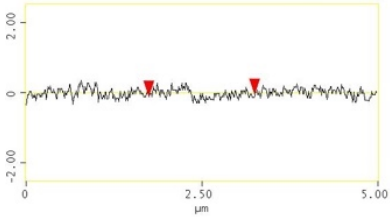	0.127

1400		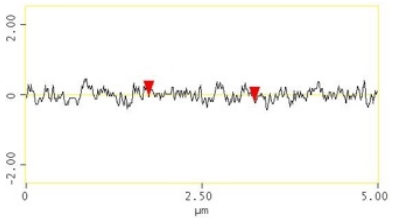	0.169
2200		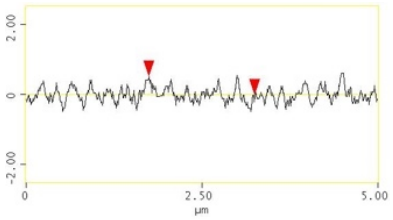	0.191
3500		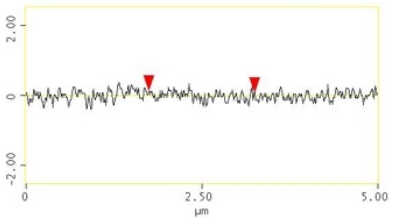	0.139
4800	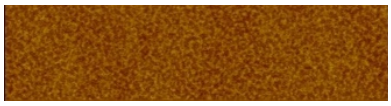	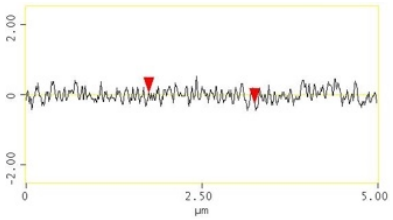	0.175
6000	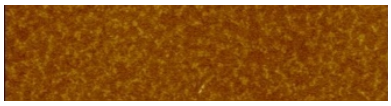	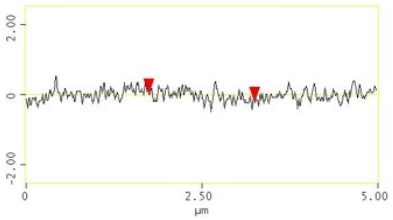	0.158

The PAA^- spin curve is shown in **Figure 29** along with faded spin curves for all other polymer systems included for reference. From the plot, it can be seen that the spin curve for

PAA$^-$ and PVP appear nearly identical, with the PAA$^-$ spin curve being shifted upwards relative to the three polyelectrolyte spin curves by about 1 nm at all spin rates. The similarity between PVP and PAA$^-$ is unanticipated due to the different properties of the two polymers. PVP is stable and is hypothesized to form an h_1 layer due to its hydrophobic interactions with the substrate. Meanwhile, PAA$^-$ is more hydrophilic than PVP, bears a negative charge, and displays signs of dewetting. Furthermore, neutral PAA shows no sign of forming an h_1 layer, which PVP does. Although the AFM images in **Table VII** show no aggregates, the hypothesized source of the upward shift of the PAA$^-$ spin curve relative to the other polyelectrolytes is an h_1 layer comprised of aggregates that adsorbed to the substrate and were not spun off.

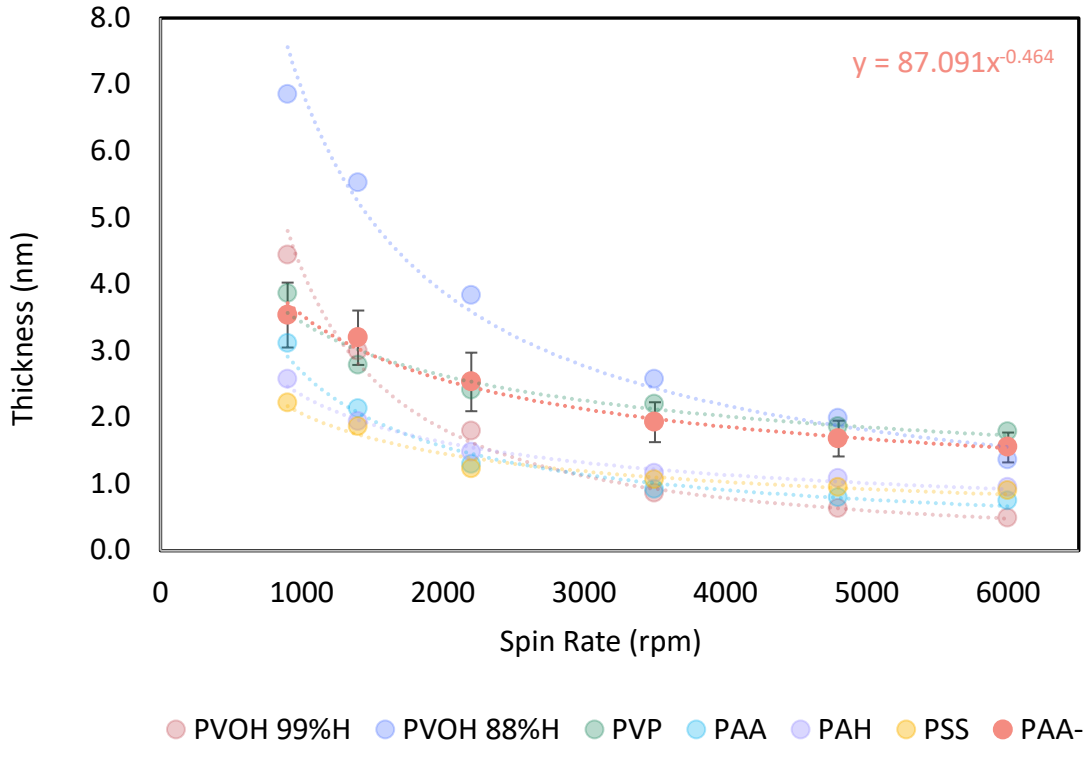

Figure 29: Spin curves of 0.1 wt% PVOH 99%H, PVOH 88%H, PVP, PAA, PAH, and PSS (faded) and PAA$^-$ thin films prepared via spin coating on silicon wafer at various spin rates.

Similar to PAA, PAH, and PSS, the dynamic water contact angles on PAA^- are extremely low and do not vary with spin rate (**Figure 30**). This suggests that the PAA^- films are very hydrophilic, which is anticipated due to its negative electrostatic charge. Furthermore, dewetting of the films exposed patches of silicon substrate, which is also very hydrophilic and may be contributing to the low contact angles.

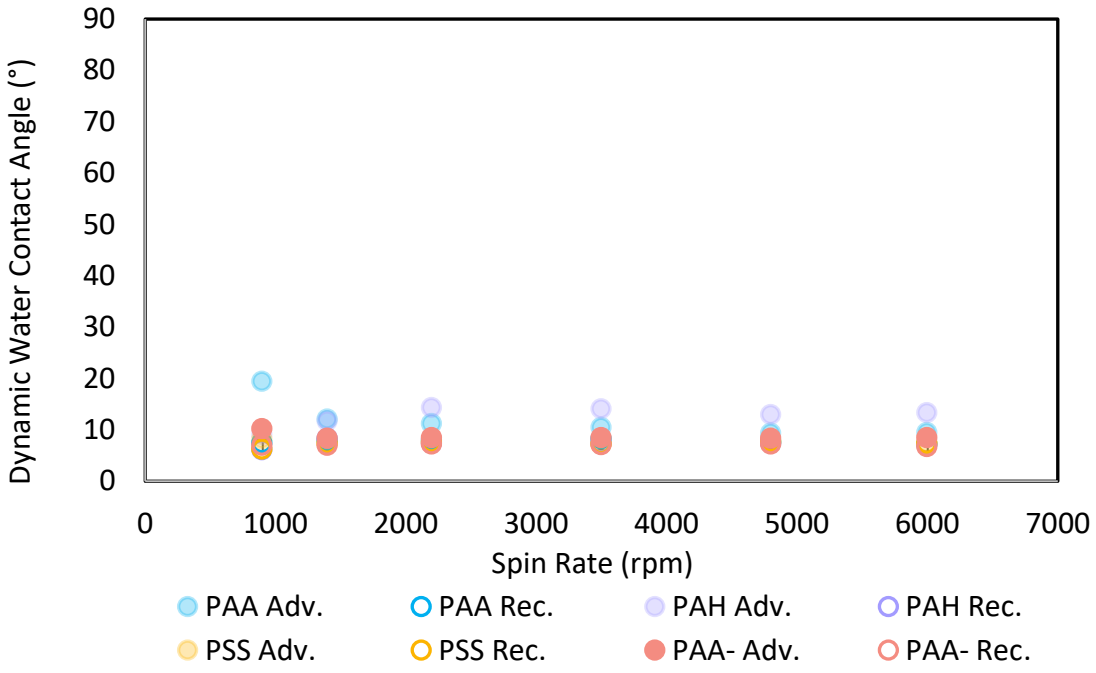

Figure 30. Dynamic water contact angles on 0.1 wt% PAA^- thin films (along with PAA, PAH, and PSS contact angles provided for reference) prepared via spin coating on silicon wafer at various spin rates.

3.3.2.2 Evidence of and Efforts to Mitigate PAA^- Aggregation

Figure 29 shows that the PAA^- spin curve was approximately 1 nm higher than the PAA spin curve across all spin rates. A consistent thickness difference across all spin rates is typically

indicative of a difference in the h_1 layer. In the case of PAA^-, it is hypothesized that this h_1 layer is comprised of aggregates that form upon deprotonation of PAA. This aggregation is attributed to insufficient deprotonation, which results in hydrogen bond donors and acceptors within close proximity. This would allow for intra- and intermolecular hydrogen bonding that may cause originally extended polymer chains to become tightly coiled and form aggregates.

Two approaches to reducing aggregation were investigated based on the theory of incomplete deprotonation. First, increasing the pH of the PAA^- solution was thought to increase the extent of deprotonation and create a chemical environment of excess negative charge in which repulsion of like charge would cause polymer chains to become more extended and less aggregated. Second, boiling the PAA^- solution was expected to increase the mobility of polymer chains and allow OH^- ions into the interior of PAA^- aggregates where they could more completely deprotonate the polymer.

The pKa of PAA is reported to be 4.5-6.5,[22,23,24] so titrating to a pH of approximately 8 was anticipated to sufficiently deprotonate the polymer. However, **Table VIII.** shows that when PAA was titrated to a pH of 8.40, its dispersity drops significantly to 64.3%, a sign of aggregation that may be due to insufficient deprotonation. When titrated to higher pH values closer to 10, the drop in dispersity was significantly less or nonexistent. This supports the theory that supplying an excess of OH^- ions may aid in achieving a more complete state of deprotonation and therefore avoiding aggregation.

When the dispersity dropped drastically for the solution titrated to pH 8.40, boiling aided in reversing the effects of the titration (evidenced by an increase in dispersity from 64.3% to 99.9%). However, for the solutions titrated to approximately pH 10-11, boiling was less effective

in reverting the dispersity of the PAA^- solution to its pre-titration dispersity because there was a less substantial drop in dispersity upon titration.

Another trend that appears in **Table VIII** and that serves as evidence of aggregation is the change in the hydrodynamic size of PAA. For all four PAA solutions, the hydrodynamic size of PAA after initial preparation is approximately 3.5 d.nm. In the cases where there is a drop in dispersity, this drop is accompanied by a decrease in hydrodynamic size, suggesting the polymers go from an extended conformation to a more tightly coiled and aggregated conformation. For the solutions that did not display a drop in dispersity, the hydrodynamic size increased upon titration, suggesting that the extent of deprotonation was more complete, and the intramolecular electrostatic repulsion causes the polymer chain to expand.

Table VIII. pH values, hydrodynamic sizes (by intensity), and dispersity (by volume) of PAA^- solutions at each stage of protonation (initial preparation, titration with NaOH, and boiling) determined using DLS.

pH	State of Preparation	Hydrodynamic Size (d.nm)	Dispersity (by volume)
8.40	PAA (before)	3.380	100%
	PAA^-	1.512	64.3%
	PAA^- Boiled	1.477	99.9%
10.40	PAA (before)	3.713	100%
	PAA^-	3.417	99.7%
	PAA^- Boiled	3.080	99.6%
10.70	PAA (before)	3.521	100%
	PAA^-	6.000	100%
	PAA^- Boiled	5.078	100%
10.50	PAA (before)	3.783	100%
	PAA^-	7.461	100%

Drop casting experiments were performed with 0.1 wt%, 0.01 wt%, and 0.001 wt% PAA^- boiled and not boiled solutions in an attempt to visualize the aggregates present in the PAA^-

solution after they deposit onto the wafer. After diluting the original 0.1 wt% solutions to 0.01 wt% and 0.001 wt%, pH measurements were made to determine the effect of dilution on pH. **Table IX** shows the results of these measurements. The pH of the solutions dropped by approximately 1 pH unit per 10x dilution. Although high pH is predicted to minimize aggregation, no increase in aggregation or aggregate size was observed under optical microscopy upon dilution and subsequent reduction of pH, so this drop in pH was not a source of concern.

Table IX. pH of diluted PAA^- solutions, measured to determine the effect of serial dilution on the pH of the PAA^- solution, which is hypothesized to dictate degree of aggregation.

Concentration	pH
0.1 wt%	10.70
0.01 wt%	9.80
0.001 wt%	8.20

Under optical microscopy, drop casted films of pH 10-11 PAA^- show signs of aggregates regardless of whether the solution was boiled or not (**Table X**). The aggregates appear larger and are present in larger quantities for the drop casted films that were prepared from PAA^- that had not been boiled. This supports the data in **Table VIII** and the hypothesis that boiling may increase the extent of deprotonation and reduce aggregation. However, the clear presence of aggregates in the drop casted films prepared from boiled pH 10-11 PAA^- suggests that boiling does not completely reverse the aggregation induced by deprotonation. Additionally, because the drop casted films were prepared from pH 10-11 PAA^-, this suggests that increasing pH does not significantly reduce aggregation either, which brings into question the reliability of the DLS size and dispersity data in **Table VIII** as an indication of aggregation and its reversal upon increasing pH.

Table X. Optical microscopy images (5x, 10x, and 50x magnification) of pH 10-11 PAA^- thin films prepared by drop casting 0.1 wt%, 0.01 wt% or 0.001 wt% boiled or not boiled PAA^- solution on 2.0 x 2.0 cm^2 silicon wafers.

Method	Conc. (wt%)	5x	10x	50x
Not Boiled	0.1	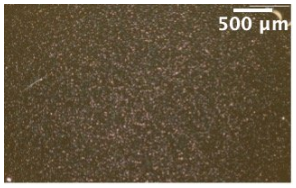	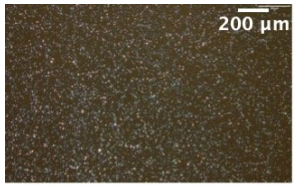	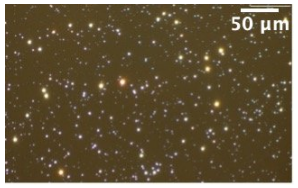
	0.01	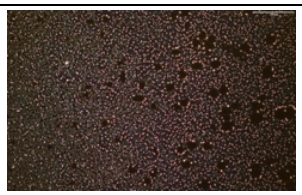	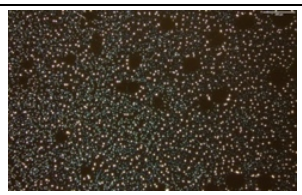	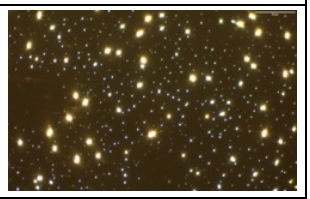
	0.001	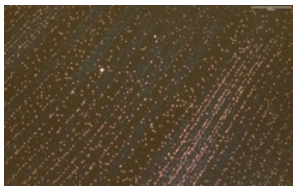		
Boiled	0.1	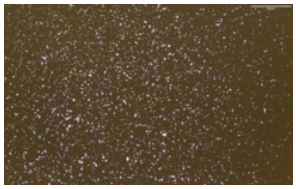	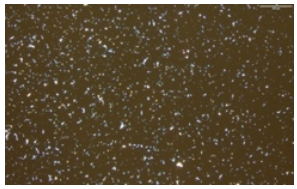	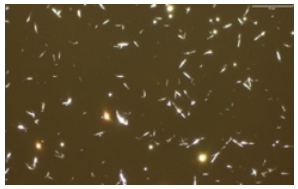
	0.01	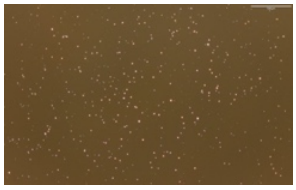	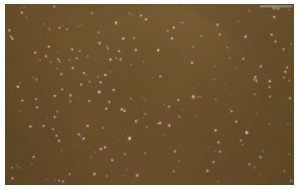	
	0.001		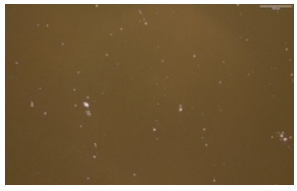	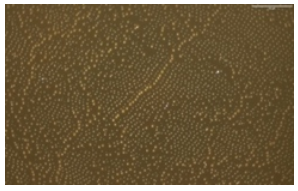

The thickness of the drop casted PAA^- thin films shown in **Figure 31** deviates significantly from what was anticipated based on the calculations below:

$$Thickness = \frac{Volume}{Area}$$

$$Volume\ of\ polymer = \frac{0.1\ g\ PAA^-}{100\ mL} \times 0.100\ mL \times \frac{1\ cm^3}{1\ g} = 1 \times 10^{-4}\ cm^3$$

$$Area = 2.0\ cm \times 2.0\ cm = 4.0\ cm^2$$

$$Thickness = \frac{1 \times 10^{-4}\ cm^3}{4.0\ cm^2} = 2.5 \times 10^{-5}\ cm = 250\ nm$$

Table XI. Calculated thickness (nm) of drop casted PAA^- films.

Concentration	Predicted Drop Casted Film Thickness (nm)
0.1 wt%	250 nm
0.01 wt%	25 nm
0.001 wt%	2.5 nm

Additionally, the thickness of the drop casted film prepared from the 0.1 wt% PAA^- solution that was not boiled is much lower than the thickness of the boiled counterpart. The thickness at 0.1 wt%, for both boiled and not boiled PAA^- solutions, was also expected to be significantly higher than that at 0.01 wt%. Lastly, the extremely large error for the 0.01 wt% boiled condition shows that there were regions of the film that were very thin and others that were significantly thicker, a sign of high roughness. The best way to reconcile these various counterintuitive results is the fact that when PAA^- was drop casted, the liquid layer tends to recede into the corner of the wafer, where it pools and polymer accumulates, thus producing a

film that is not uniformly thick, very rough, and much thinner in the center of the wafer than in the corners.

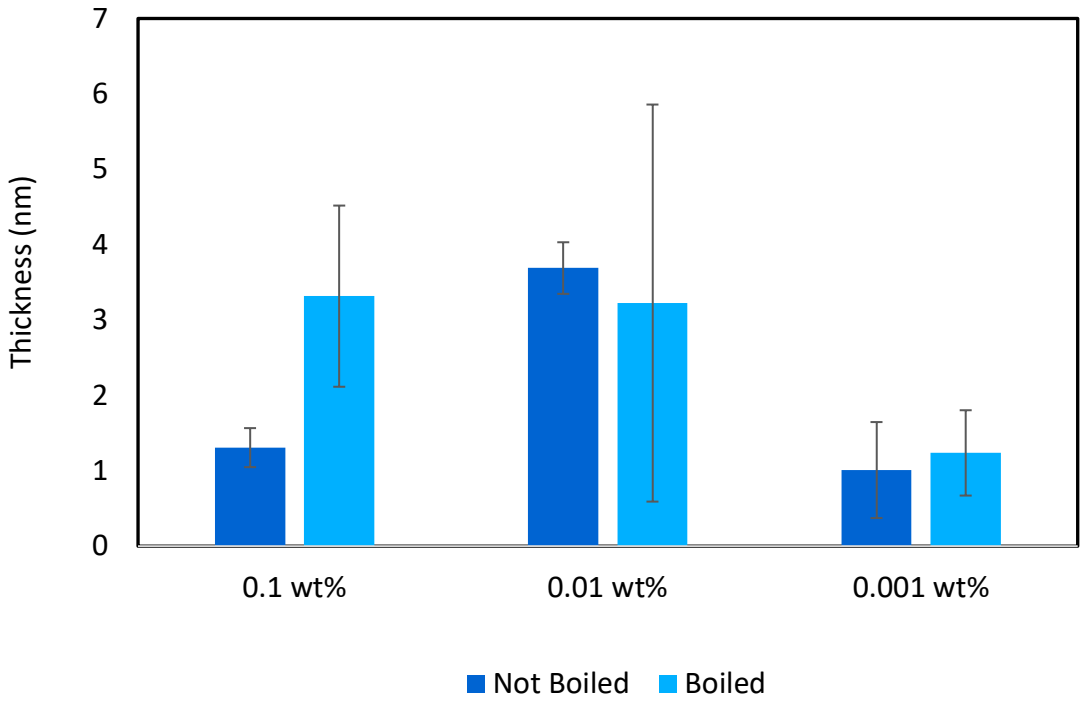

Figure 31. Thickness (nm) of pH 10-11 PAA^- thin films prepared by drop casting 0.1 wt%, 0.01 wt% or 0.001 wt% boiled or not boiled PAA^- solution on 2.0 x 2.0 cm^2 silicon wafers.

3.3.2.3 PAA^- Spin Coating

Figure 32 shows that the spin curves for PAA^- were very similar when the solution was not boiled, regardless of pH. However, at lower spin rates, the spin curves of the boiled systems deviate from those of the systems that did not include boiling. It makes sense that this deviation should occur at lower spin rates because it has been noted previously that at lower spin rates aggregates are not spun off as readily, so the film thickness is significantly greater (recall PAH_{SiO^-} system). However, the fact that the boiled solutions are the ones that have an increased

thickness at lower spin rates contradicts the hypothesis that boiling would mitigate aggregation and the evidence in **Table VIII** and **Table X.** that boiled PAA^- had fewer aggregates. Additionally, the thickest spin curve corresponded to the PAA^- system at the higher pH that had been boiled. This suggests that the combination of boiling and increasing pH worsens aggregation.

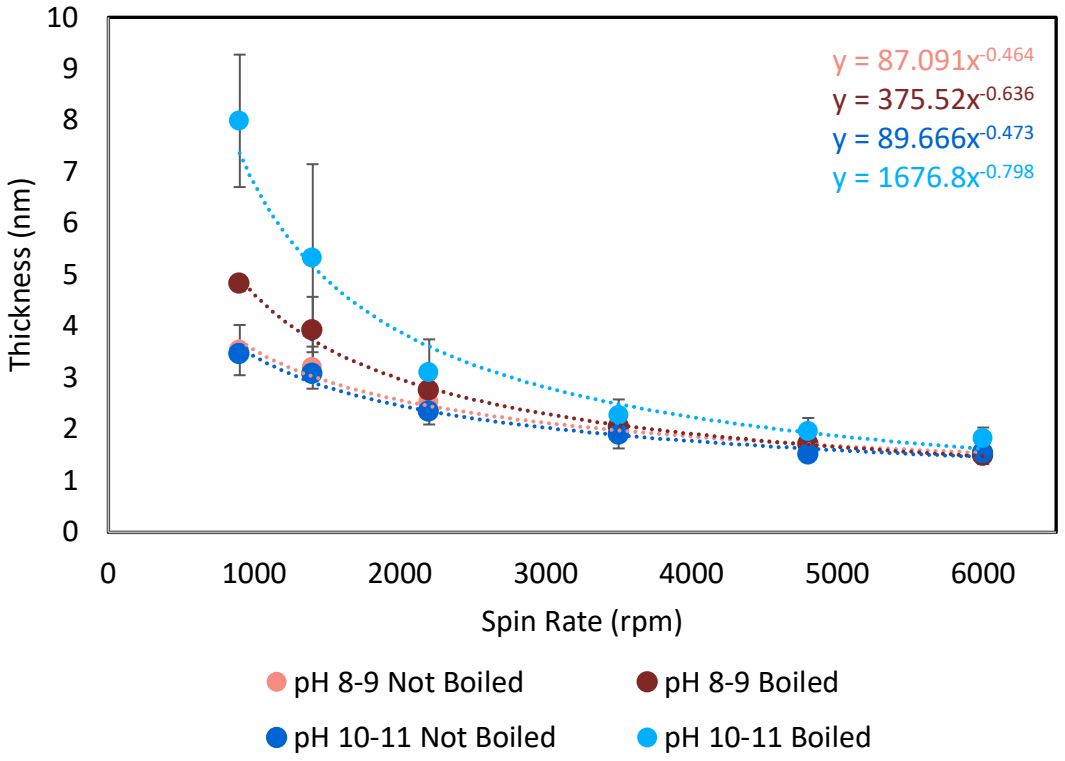

Figure 32. Spin curves of 0.1 wt% PAA^- thin films prepared at various spin rates from 0.1 wt% PAA^- solutions that were titrated to either pH 8-9 or pH 10-11 and either boiled or not boiled.

AFM images of the spin coated PAA^- films produced from either pH 8-9 or pH 10-11 and either boiled or not boiled solutions are shown in **Table XII.** These images show that there are small aggregates on the pH 8-9 boiled films. Although there is no significant evidence of

aggregates on the pH 10-11 boiled films from 1400 rpm to 6000 rpm, there are large aggregates on the 900 rpm films, which explain the significantly higher thickness of the pH 10-11 boiled spin curves at low spin rates (**Figure 32**). The aggregates present on the boiled films in conjunction with the increased thickness of the spin curves of boiled PAA^- at lower spin rates serves as strong evidence of the fact that boiling does not improve aggregation as originally hypothesized.

Table XII. AFM images (data scale 5 nm, aspect ratio 5 µm x 1.25 µm), section analysis, and RMS roughness (in nm) of 0.1 wt% PAA^- thin films prepared by spin coating PAA^- solutions of either pH 8-9 or pH 10-11 that either had or had not been boiled on silicon wafers at various spin rates.

Spin Rate (rpm)	pH 8-9 Not Boiled	pH 8-9 Boiled	pH 10-11 Not Boiled	pH 10-11 Boiled
900	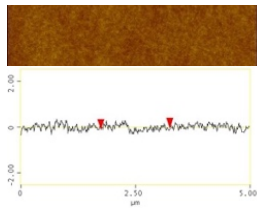 RMS = 0.127	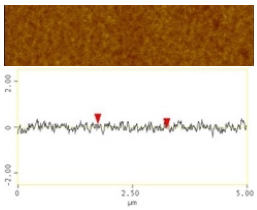 RMS = 0.148	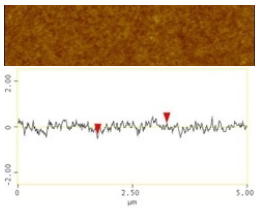 RMS = 0.146	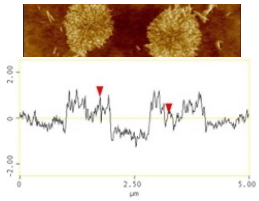 RMS = 0.516
1400	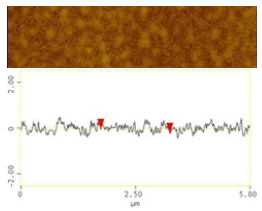 RMS = 0.169	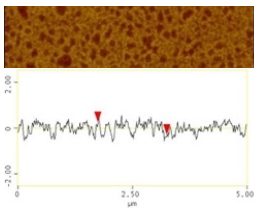 RMS = 0.228	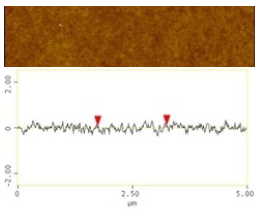 RMS = 0.133	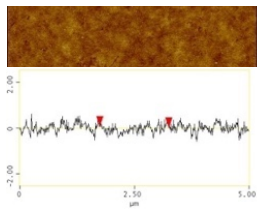 RMS = 0.212

2200	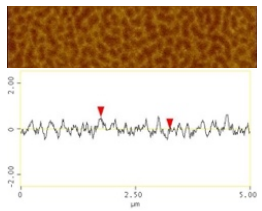 RMS = 0.191	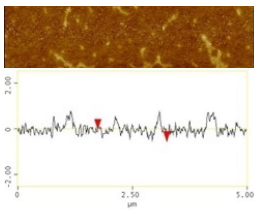 RMS = 0.239	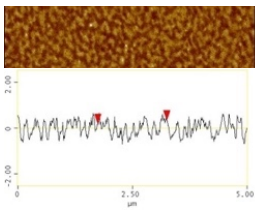 RMS = 0.296	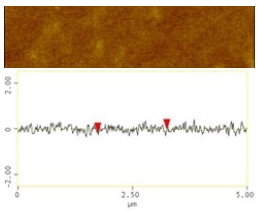 RMS = 0.142
3500	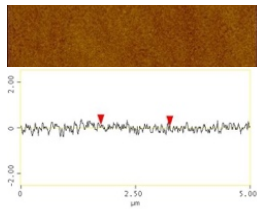 RMS = 0.139	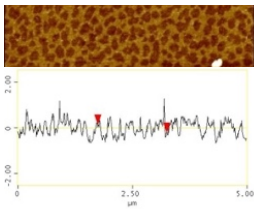 RMS = 0.343	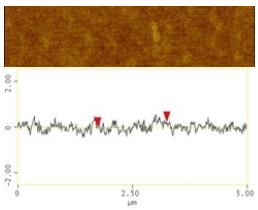 RMS = 0.170	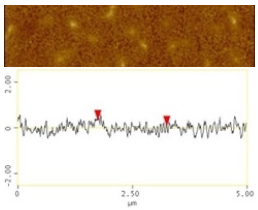 RMS = 0.201
4800	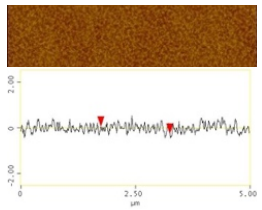 RMS = 0.175	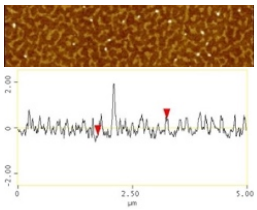 RMS = 0.302	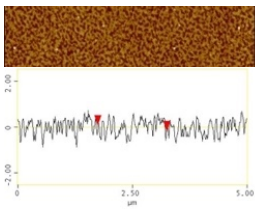 RMS = 0.330	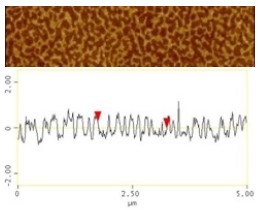 RMS = 0.339
6000	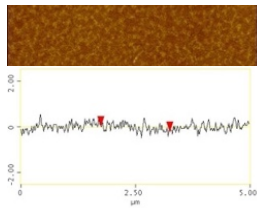 RMS = 0.158	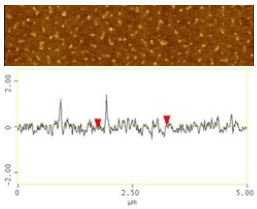 RMS = 0.257	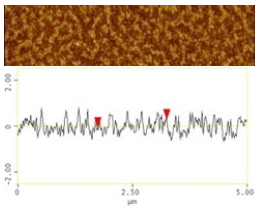 RMS = 0.320	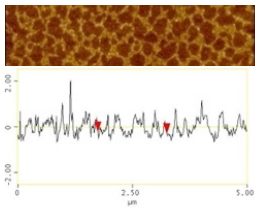 RMS = 0.326

Advancing and receding contact angles on all PAA^- thin films, regardless of pH and whether or not the solution had been boiled are extremely low and consistent across all spin rates. This is evidence of very hydrophilic films. However, the low contact angles may be attributed to different factors depending on the extent of dewetting. AFM images in **Table XII.**

show that at the lower spin rates all the PAA^- thin films appear continuous (except the pH 10-11 boiled film, which is covered in aggregates and whose stability is therefore difficult to determine). For these films, the cause of the low contact angles is the hydrophilic nature of the film, which is comprised of deprotonated PAA^- that is negatively charged. At higher spin rates, the extent of dewetting increases, exposing increasing areas of the superhydrophilic silicon wafer, which also contributes to the low water contact angle. The similarly low water contact angles on PAA^- films reported in **Figure 33** shows that the low contact angle on PAA^- films is reproducible.

Two primary conclusions can be drawn from these DLS, drop casting, and spin coating results. First, there is an abundance of evidence for the presence of aggregates in PAA^- solutions, and these aggregates are very likely to be the source of the 1 nm upward shift of the PAA^- spin curve relative to the PAA spin curve (**Figure 29**). Second, boiling appears to significantly worsen the aggregation of PAA^-, and increasing the pH of the solution to pH 10-11 does little to reduce the extent of aggregation.

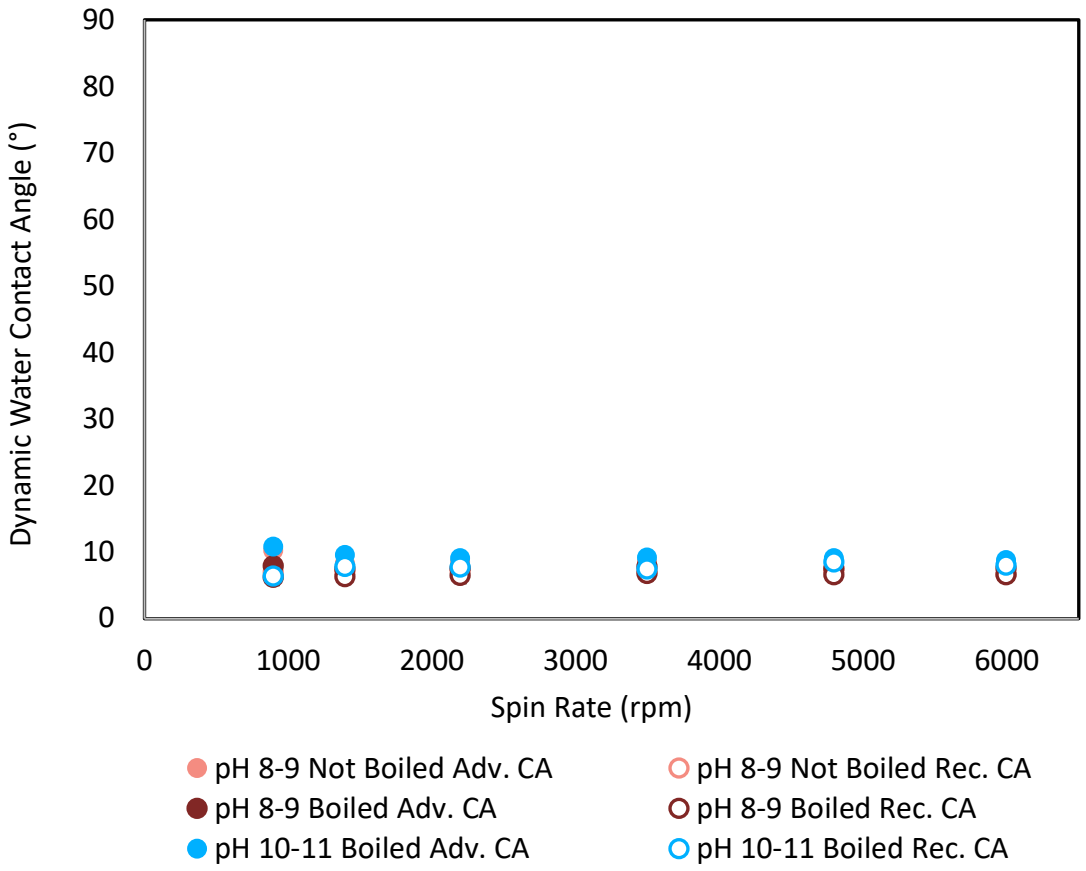

Figure 33. Dynamic water contact angles on 0.1 wt% PAA^- thin films prepared by spin coating PAA^- solutions of either pH 8-9 or pH 10-11 that either had or had not been boiled on silicon wafers at various spin rates.

3.4 Decoupling Polymer-Substrate and Polymer-Polymer Contributions to Thickness

In Section 3.2 it was discussed that the Meyerhofer model's lack of attention to the individual contributions of polymer-substrate and polymer-polymer interactions and its assumption that polymers wet their substrates are two likely sources of inaccuracy in the model's prediction of the thickness of spin coated polymer thin films. To provide further evidence for this claim as well as work towards a more flexible model that better predicts the spin-coated thicknesses of diverse hydrophilic polymers, this section focuses on quantitatively separating the h_1 and h_2 contributions to total film thickness and evaluating the thickness of each component in the context of the known properties of each system. It is hypothesized that subtracting the h_1 contribution at every spin rate along a given spin curve will yield an h_2 spin curve whose exponent is closer to the -0.5 exponent predicted by Meyerhofer because the h_1 contribution has been eliminated, and Meyerhofer did not account for the h_1 layer in his model.

Figure 21 in Section 3.2 displays approximate h_1 thickness values for each polymer based on the assumption that the total film thickness at 6000 rpm is representative of the h_1 layer thickness. However, a different approach to determining h_1 values is to perform a static adsorption experiment, which mimics the spontaneous deposition step of adsorptive spin coating without the subsequent spin deposition. A series of static adsorption experiments were performed with each polymer to obtain a value representative of the h_1 layer, and this was then subtracted from the total thickness at each spin rate on the corresponding polymer's spin curve to generate h_2 spin curves.

Figure 34 shows the h_1 thickness formed by each polymer on the silicon substrate as determined by static adsorption experiments. These experiments were originally performed with

both 0.1 wt% and 0.5 wt% concentrations of each polymer and for 1 minute and 10 minutes; however, it was determined that neither varying polymer concentration nor adsorption time produced significant differences in the h_l layers. All data reported in **Figure 34** are from 10-minute static adsorption experiments using polymer solutions of 0.1 wt% concentration.

The only polymer that spontaneously deposited to form an h_l layer of significant thickness is PVP. This is in good agreement with the PVP spin curve, which is relatively thick at higher spin rates (compared to PVOH 99%H, PAA, PAH, and PSS) where the h_l layer dominates total film thickness. However, the results shown in **Figure 34** do not agree with what was predicted for PVOH 88%H and PAA^- static adsorption. Both PVOH 88%H and PAA^- are expected to display a spontaneously deposited layer of similar thickness to PVP because they are comparable in thickness to PVP at 6000 rpm (**Figure 21**). Contrary to this prediction, PVOH 88%H and PAA^- show negligible spontaneous deposition based on static adsorption experiments (**Figure 34**). This begs the question of what is causing the increased thickness in PVOH 88%H and PAA^- at higher spin rates.

The polymers that are thinner at high spin rates, PVOH 99%H, PAA, PAH, and PSS, all display minimal spontaneous deposition according to the data in **Figure 34**, which is in good agreement with their spin curves. However, the h_l thickness obtained from static adsorption experiments is much smaller than the 6000 rpm thickness for all these polymers (**Figure 21**). Most of these polymers form films approximately 1 nm in thickness when spin coated at 6000 rpm (PVOH 99%H is slightly less at around 0.5 nm) (**Figure 21**), but the statically adsorbed films for each of these polymers fall between 0 and 0.2 nm (**Figure 34**). Therefore, for all polymers, including PVP (which has a 6000 rpm thickness of approximately 1.8 nm and a statically adsorbed thickness of about 1.1 nm), the spontaneously deposited films obtained from

static adsorption experiments are much thinner than what is predicted for the h_1 layer based on the spin coated thickness at 6000 rpm. There are two possible explanations for this:

1. Film thicknesses at 6000 rpm overestimate h_1 layer thickness: If this is the case, it means not all polymer solution is spun off the substrate at 6000 rpm, and there is some h_2 that remains at the highest spin rate, contributing to the total film thickness (i.e. the assumption that film thickness at 6000 rpm is representative of the h_1 layer thickness is inaccurate).
2. Spontaneously deposited films produced in static adsorption experiments underestimate h_1 layer thickness: If this is the case, it means the rinsing steps of the the static adsorption experiments remove some of the h_1 layer that the centrifugal force of spin coating is not strong enough to remove.

There are several reasons why the second of the two explanations is more likely. First, the 6000 rpm thicknesses for each polymer are in better agreement with what is known about each system than the static adsorption thicknesses, which appear to be somewhat random and are difficult to explain in the context of the chemical properties of each system. For example, it makes sense for PVOH 88%H and PVP to have a thicker h_1 due to their hydrophobicity and for PAA^- to have a greater h_1 thickness due to its aggregates. This is reflected in the 6000 rpm thicknesses but not the static adsorption thicknesses, which gives more credit to the former and suggests that it is the statically adsorbed films that underestimate the h_1 thickness.

Additionally, the Milli-Q water control produced a statically adsorbed thickness of nearly 0.2 nm, which is equal to or greater than the statically adsorbed thicknesses of all other films but

PVP. The absence of polymers in Milli-Q water means that any observed thickness is likely due to dust or other contaminants accumulating on the surface of the substrate. Therefore, this control offers a good reference point to act as an indicator of no static adsorption, while also accounting for contaminants that may contribute to observed thickness. The fact that all other polymers except PVP formed h_l layers comparable to or less than this "no static adsorption" reference point suggests that there actually is no polymer adsorbed, and the rinse steps of the static adsorption experiments completely removed all of the h_l layer that formed.

Based on these results, a more nuanced version of the decoupled thickness model is proposed: The h_l layer is comprised of a strongly bound and loosely bound layer. The strongly bound layer is the first layer of polymer to deposit and adsorb to the substrate, and the loosely bound layer is the polymer that deposits on top of this initial layer. The loosely bound layer deposits during the spontaneous deposition step rather than the spin deposition step, so it is still considered part of the h_l layer and does not change as a function of spin rate. Although increasing spin rate does not dislodge the loosely bound layer completely, rinsing the films with water three times as is done in the static adsorption experiments does remove the loosely bound layer.

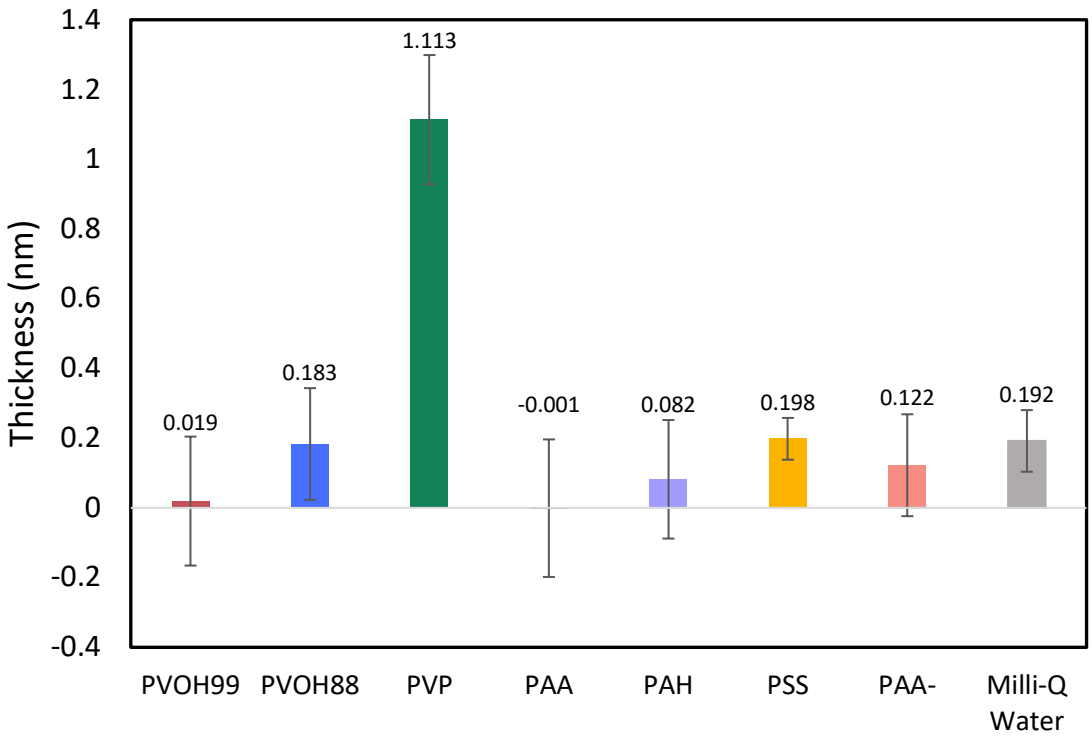

Figure 34. Spontaneously deposited thickness of PVOH 99%H, PVOH 88%H, PVP, PAA, PAH, PSS, and PAA^- thin films as well as a Milli-Q water control prepared via 10-minute static adsorption experiments on silicon wafer.

Although the accuracy of the statically adsorbed film thicknesses reported in **Figure 34** is under scrutiny, the loosely bound layer theory is a recent hypothesis, and there was insufficient time to modify the static adsorption protocol and collect an entirely new set of h_1 layer thicknesses for all polymers. Therefore, the values in **Figure 34** were used to quantitatively isolate the h_2 thickness as a function of spin rate for each polymer by subtracting the values reported in **Figure 34** from the total thickness at each spin rate for the corresponding polymer. The results are shown in **Figure 35**. There are several aspects of **Figure 35** worth noting.

First, the PVP spin curve was the only curve that shifted down significantly because it had the most sizable h_1 value (**Figure 34**). The h_2 spin curve of PVP is similar to the h_2 spin

curves of PAA, PAH, and PSS, suggesting similar polymer-polymer interactions. However, its spin curve exponent changed from -0.382 to -0.708, so the Meyerhofer exponent of -0.5 was not observed for PVP.

Second, the h_2 spin curves for PVOH 99%H and PVOH 88%H do not show a noticeable change in exponent relative to the original spin curves, and therefore still deviate significantly from the -0.5 exponent predicted by the Meyerhofer model. As discussed in Section 3.1, this drastic deviation from -0.5 is likely due to the crystallinity of PVOH, which was not taken into account in the derivation of the Meyerhofer model and which significantly increases polymer-polymer interactions at lower spin rates. The fact that the PVOH 99%H exponent deviates from -0.5 more than that of PVOH 88%H, which is less crystalline, is further evidence for this theory.

Third, most of the polyelectrolytes have a spin curve exponent near the predicted -0.5, with the exception of PAA. Because PAA and PVP are not crystalline, there is no clear explanation for the deviation of their spin curve exponents from -0.5. However, three comments can be made about this deviation. First, if the loosely bound theory is accurate and the h_1 values reported in **Figure 34** and subtracted from the total film thickness at each spin rate are not truly representative of the h_1 thickness for each polymer, then the spin curves shown in **Figure 35** are not true h_2 curves and therefore there may be some inaccuracy in the spin curve exponents displayed in **Figure 35**. Second, even if the spin curves in **Figure 35** are accurate, there is no doubt some variation in the polymer-polymer interactions that dictate the amount of polymer retained on the spinning substrate during spin coating. That is, the Meyerhofer model does not account for variation in the viscous forces of different polymer solutions, and it may be that it is impossible to derive a universal model that can accurately predict the spin coated film thickness of such a wide range of polymers. Third, the Meyerhofer model also assumes that the polymer

wets the substrate. In the case of polymers that dewet their substrate, such as PAA, this assumption is not true and may account for the deviation from Meyerhofer model that is observed **Figure 35**.

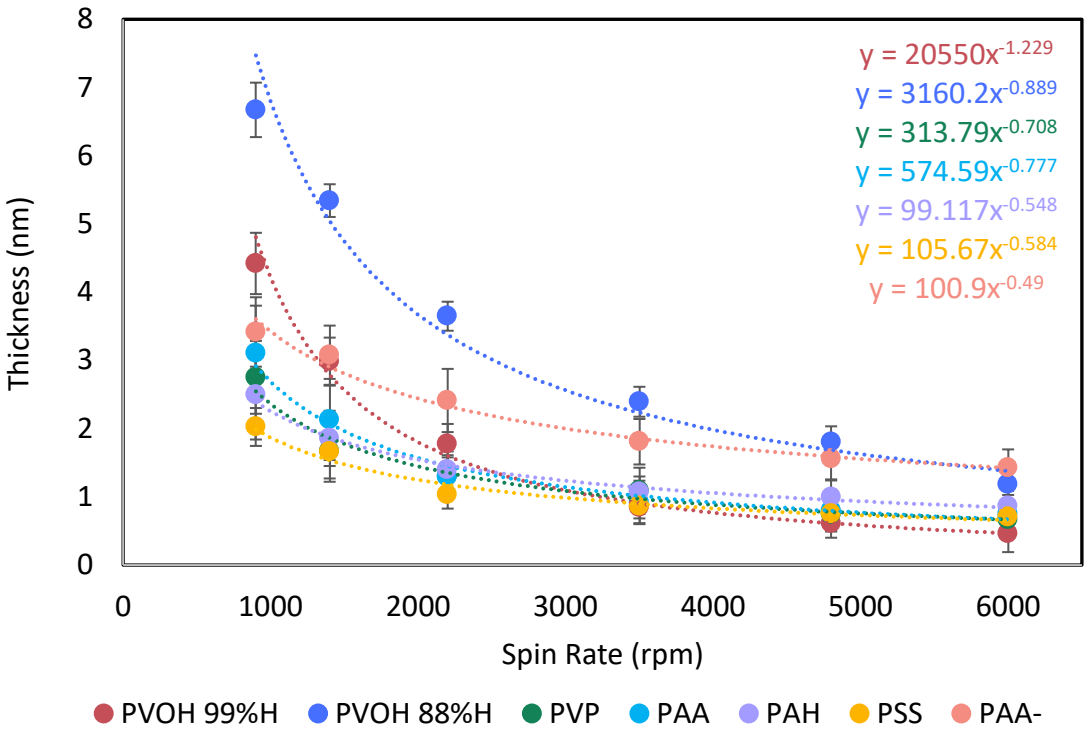

Figure 35. Spin curves of PVOH 99%H, PVOH 88%H, PVP, PAA, PAH, PSS, and PAA^- thin films adjusted by subtracting the corresponding h_1 thickness for each polymer as determined from static adsorption experiments (**Figure 34**).

3.5 Loosely Bound Layer

Figure 36 shows that PAA^- films were thicker than PAA films for corresponding rinse steps, which is likely due to the presence of aggregates in PAA^-. However, the more noteworthy trend exhibited in **Figure 36** is the clear decrease in thickness with increasing number of rinse steps. This confirms a working theory that some or all of the h_l layer is loosely bound to the substrate and can be removed by rinsing the film. This raises the question of what the true h_l layer is and what experimental method can be used to produce it. At the highest spin rate of 6000 rpm, PAA and PAA^- films are approximately 0.75 nm and 1.5 nm, respectively. This suggests that the centrifugal force at the highest spin rate is either not strong enough to dislodge the loosely bound h_l layer or not strong enough to remove it all. For the purpose of producing an h_l layer of reproducible thickness to subtract from a spin curve, it is important to explore different experimental methods of recreating the h_l layer.

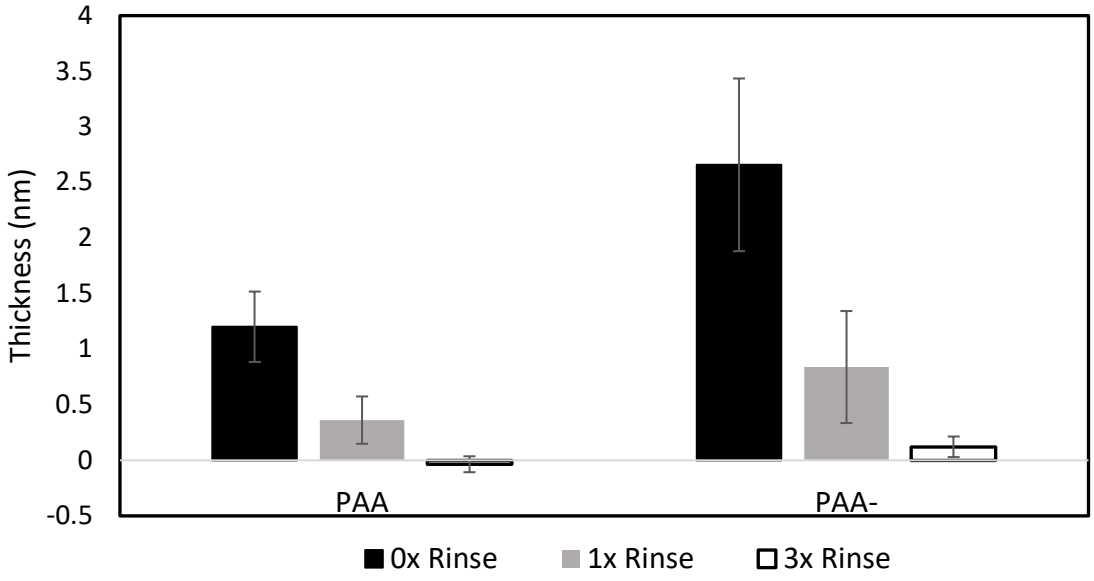

Figure 36. Thickness (nm) of 0.1 wt% PAA and PAA- thin films prepared via static adsorption on silicon wafers followed by 0, 1, or 3 rinse steps.

AFM images of the statically adsorbed PAA and PAA^- films show that only the 0x rinse PAA film was thick enough to dewet (**Table XIII**). The other films were likely too thin to produce a detectable dewetting morphology. Additionally, a few aggregates can be seen on the 3x rinse PAA^- film. If there are aggregates on the 3x rinsed films, it would be expected that there are aggregates on the 0x and 1x rinse PAA^- films as well, so the absence of aggregates in the AFM images of those films likely has to do with where on the sample the image was taken.

Both advancing and receding contact angles are very low on the PAA and PAA^- statically adsorbed thin films, regardless of the number of rinse steps (**Figure 37**). However, there does appear to be a slight decrease in advancing contact angle with increasing number of rinse steps for both PAA and PAA^-. This can be attributed to the thinning of the film and increased exposure of the substrate. Additionally, the PAA^- advancing contact angles are lower than those of PAA, which is consistent with what has been observed previously (**Figure 30**). This is likely due to the negative charge on the PAA^-, which increases its propensity for hydrogen bonding with water.

Table XIII. AFM images (data scale 5 nm, aspect ratio 5 µm x 1.25 µm), section analysis, and RMS roughness (in nm) of PAA and PAA^- thin films prepared via static adsorption on silicon wafers followed by 0, 1, or 3 rinse steps.

Polymer	0x Rinse	1x Rinse	3x Rinse
PAA	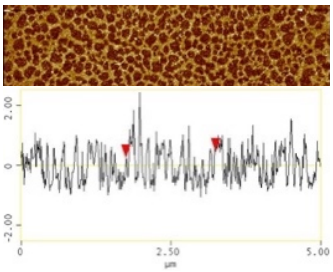 RMS = 0.532	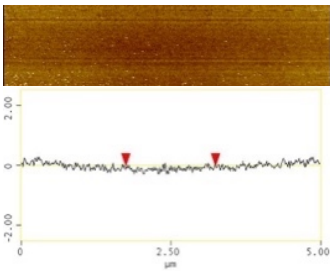 RMS = 0.198	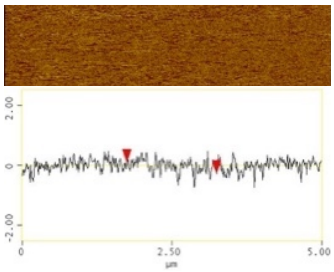 RMS = 0.260
PAA-	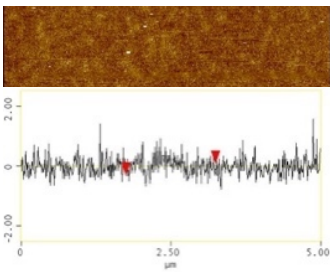 RMS = 0.320	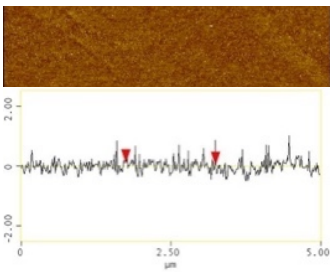 RMS = 0.200	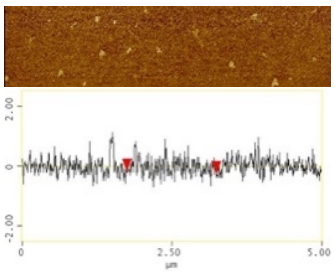 RMS = 0.320

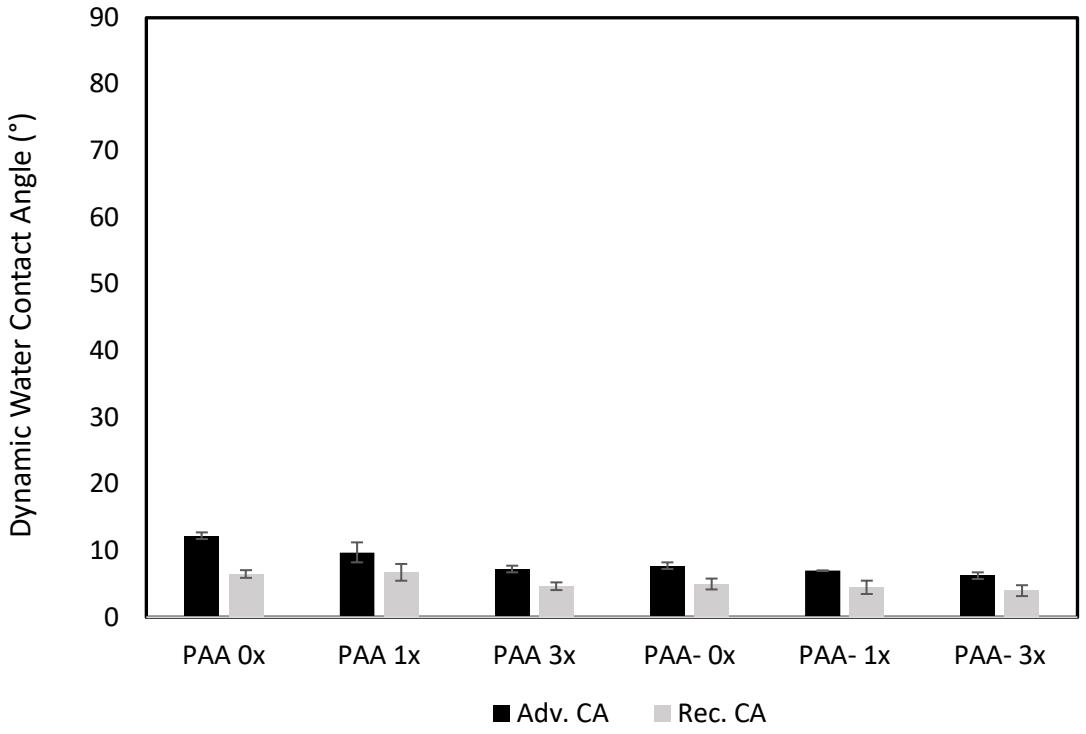

Figure 37. Dynamic water contact angles on 0.1 wt% PAA and PAA^- thin films prepared via static adsorption on silicon wafers followed by 0, 1, or 3 rinse steps.

The statically adsorbed PAA and PAA^- thin films were thermally annealed at 100 °C for 30 minutes to determine whether the h_l layer is stable. Upon annealing, the thickness of all films decreased slightly (**Figure 38**). This may be due to the release of some water trapped in the films upon heating; however a more likely explanation becomes apparent in the context of the AFM images shown in **Table XIV**. All but one of the films show some evidence of aggregates or droplets. This implies that upon heating, the polymer dewetted the surface and collected in small droplets, which are often the final stage of dewetting and indicative of a thermodynamically favorable morphology.[74] Because these droplets represent a small percentage of the area of the substrate, the chances of measuring thickness on or near a droplet is less than the likelihood of measuring bare substrate, which accounts for a much greater percentage of the surface area. This

is a possible explanation for the decrease in thickness after annealing that is displayed in **Figure 38**.

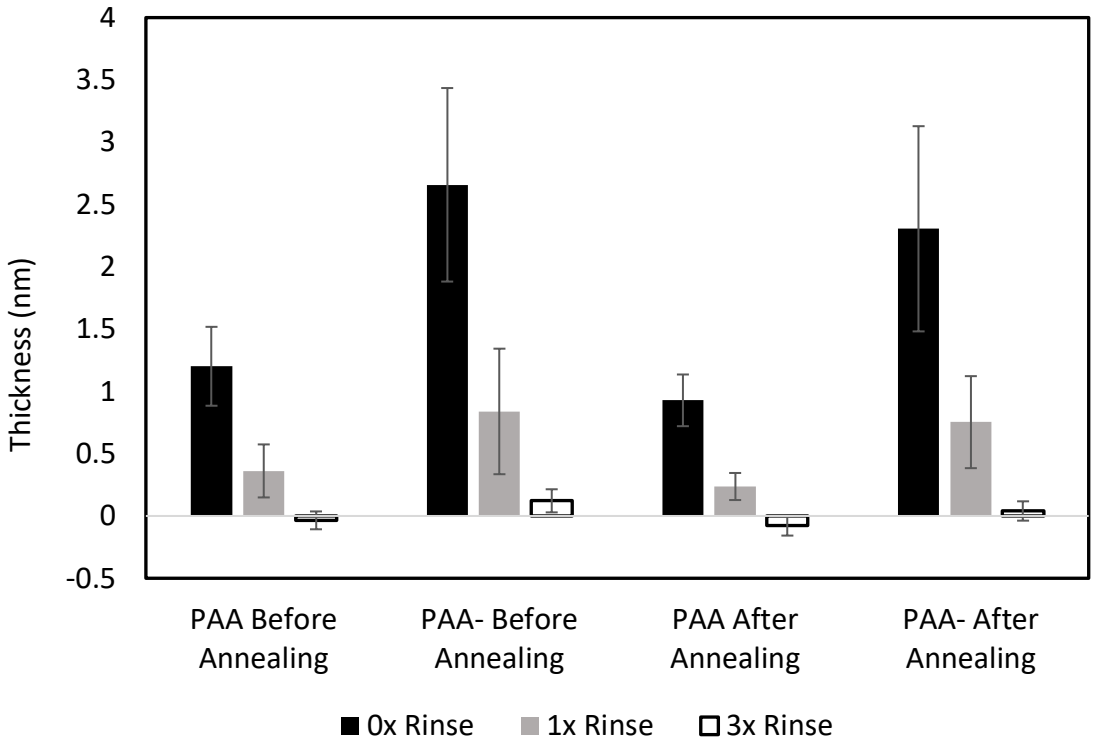

Figure 38. Thickness (nm) of 0.1 wt% PAA and PAA^- thin films prepared via static adsorption on silicon wafers, rinsed 0, 1, or 3 times, and thermally annealed at 100 °C for 30 minutes.

Table XIV. AFM images (data scale 5 nm, aspect ratio 5 µm x 1.25 µm), section analysis, and RMS roughness (in nm) of PAA and PAA^- thin films prepared via static adsorption on silicon wafers, rinsed 0, 1, or 3 times, and thermally annealed at 100 °C for 30 minutes.

Polymer	0x Rinse	1x Rinse	3x Rinse
PAA	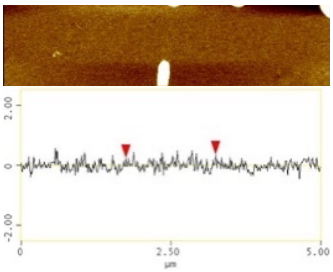 RMS = 0.583	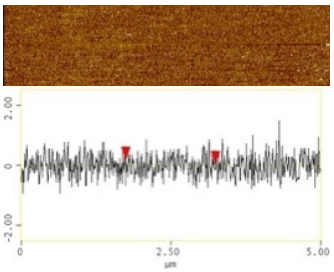 RMS = 0.364	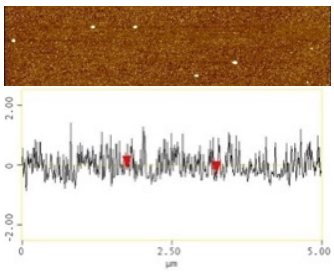 RMS = 0.361
PAA-	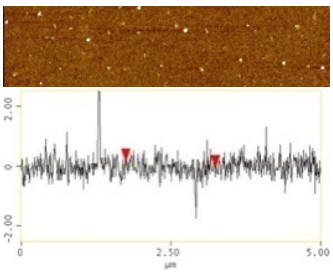 RMS = 0.361	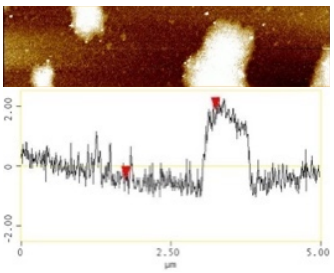 RMS = 0.967	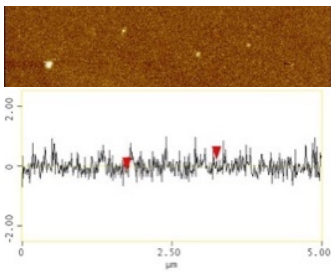 RMS = 0.280

The advancing contact angle on both PAA and PAA^- thin films increased significantly following thermal annealing (**Figure 39**). Upon annealing, polymer mobility increases allowing the polymer chains to adopt a conformation that maximizes hydrogen bonding and electrostatic interactions. This results in orientation of the carboxylate groups inward and the carbon backbone outward towards the surface of the film. The water droplet at the surface of the film interacts with these hydrophobic regions, which results in a greater advancing contact angle than the original drop casted films.

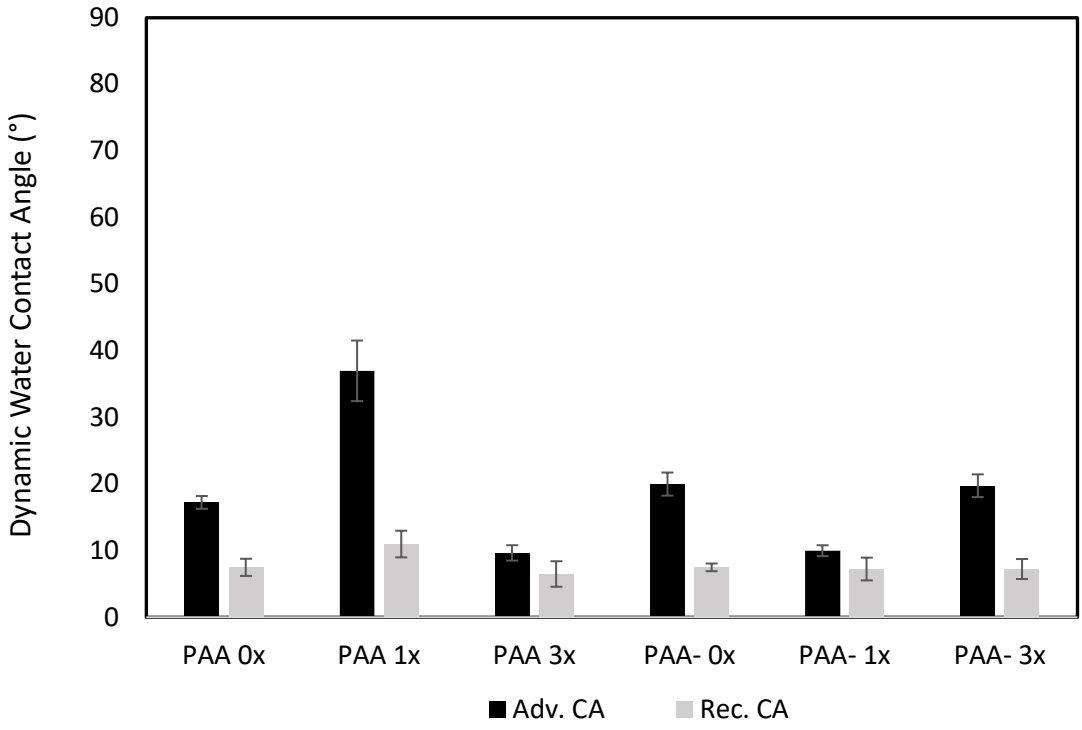

Figure 39. Dynamic water contact angles on PAA and PAA$^-$ thin films prepared via static adsorption on silicon wafers, rinsed 0, 1, or 3 times, and thermally annealed at 100 °C for 30 minutes.

Drop casting experiments were conducted with PAA and PAA$^-$ to compare the extent of aggregation in the two. Because there is no spin or rinsing associated with drop casting, images of drop casted films under optical microscopy offers a visual representation of what is present in solution. **Tables XV** and **XVI** show that there are aggregates on both the PAA and PAA$^-$ films. This contradicts the trend in statically adsorbed thicknesses (**Figure 36**) and the 1 nm upwards shift of the PAA$^-$ spin curve relative to the PAA spin curve (**Figure 29**), which is highly reproducible. The images shown in **Tables XV** and **XVI** are based on only one experiment, so these results should be reproduced both with PAA and PAA$^-$ as well as a polymer known to be

stable on silicon wafer because it is possible that the aggregates seen on the PAA films are dewetted droplets or simply clusters of a polymer known to dewet the silicon substrate.

Table XV. Optical microscopy images (5x, 10x, and 50x magnification) of drop casted 0.1 wt%, 0.01 wt%, or 0.001 wt% PAA thin films on 2.0 x 2.0 cm^2 silicon wafers.

Conc. (wt%)	5x	10x	50x
0.1	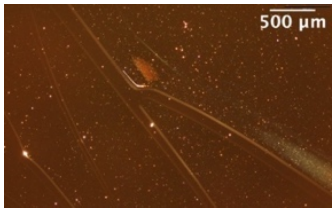	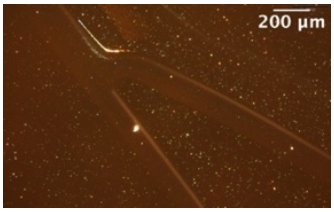	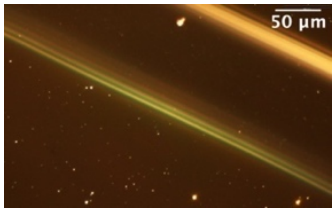
0.01	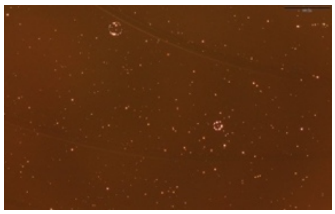	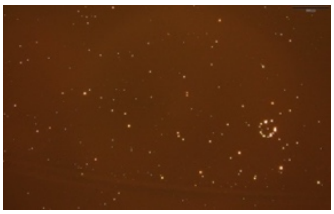	
0.001	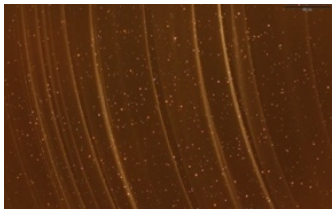		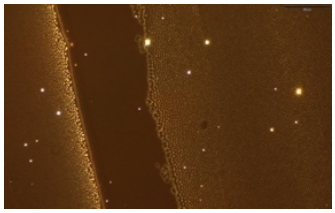

Table XVI. Optical microscopy images (5x, 10x, and 50x magnification) of drop casted 0.1 wt%, 0.01 wt%, or 0.001 wt% PAA^- thin films on 2.0 x 2.0 cm^2 silicon wafers.

Conc. (wt%)	5x	10x	50x
0.1	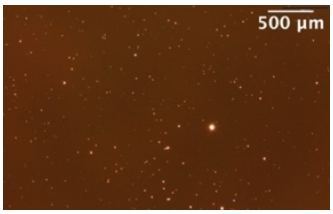	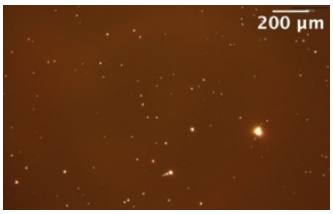	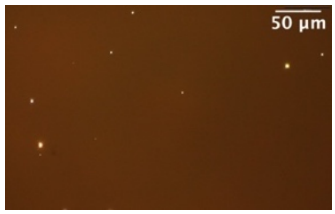
0.01	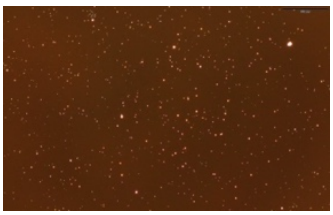	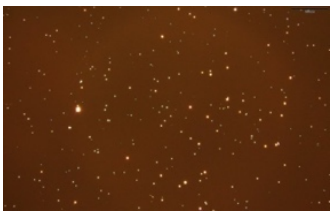	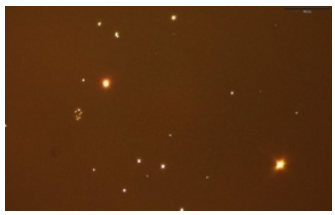
0.001	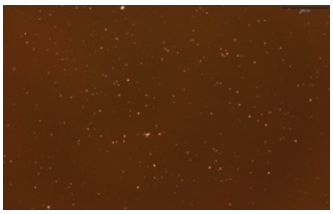	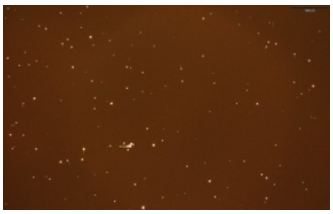	

Figure 40 shows the thickness of the drop casted PAA and PAA^- films prepared from different concentrations of polymer solution. The decrease in thickness with decreasing concentration aligns with expectation, and the decrease in error bars with decreasing thickness indicates a decrease in roughness as the films become thinner. Although the 0.1 wt% PAA and PAA^- films have a comparable thickness, the PAA^- films are thinner than their PAA counterparts at the two lower concentrations. This may be because PAA^- recedes towards the edges and corners of the wafer more than PAA.

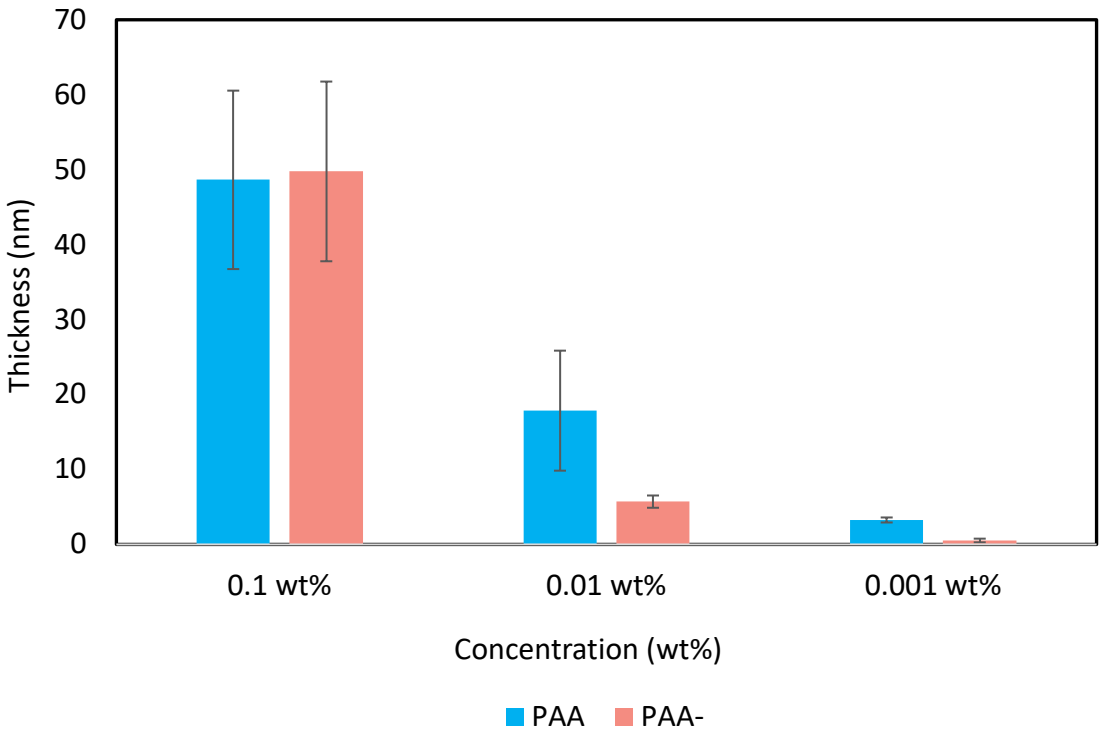

Figure 40. Thickness (nm) of drop casted 0.1 wt%, 0.01 wt%, or 0.001 wt% PAA and PAA^- thin films on 2.0 x 2.0 cm^2 silicon wafers.

Figure 41 shows that the advancing contact angles of water on PAA decrease with decreasing concentration, which is in good agreement with the decrease in film thickness with decreasing concentration (**Figure 40**). With the exception of the advancing contact angle on 0.001 wt% PAA^-, a similar trend is observed for PAA^-. The relatively high advancing contact angle on 0.001 wt% PAA^- is unexpected in light of its extremely thin film thickness (**Figure 40**); however, under 50x magnification, optical microscopy images show a nearly uniform layer of small aggregates comprising the 0.001 wt% PAA^- film. Although the film is thin, this nearly uniform coverage of aggregates may be contributing to the high advancing contact angle on the 0.001 wt% PAA^- film.

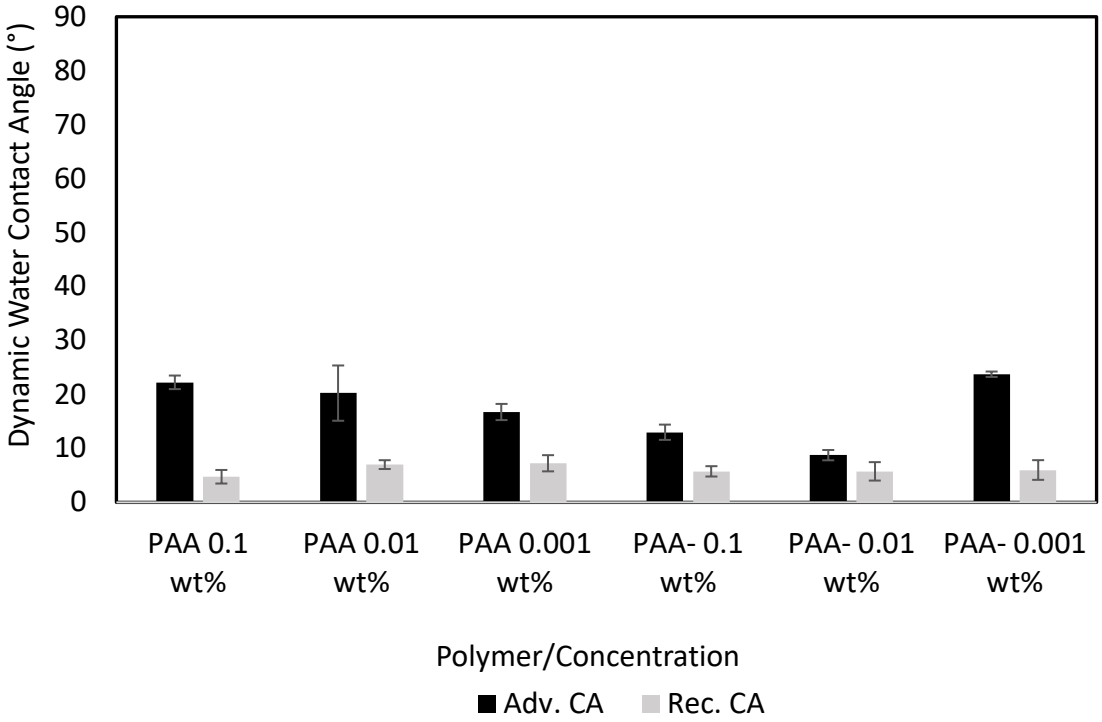

Figure 41. Dynamic water contact angles on drop casted 0.1 wt%, 0.01 wt%, or 0.001 wt% PAA and PAA^- thin films on 2.0 x 2.0 cm^2 silicon wafers.

4. CONCLUSIONS AND FUTURE WORK

The Meyerhofer model for predicting the thickness of spin coated polymer thin films does not account for the distinction between spontaneously deposited polymer and spin deposited polymer. This leads to inaccuracies in film thicknesses predicted by the Meyerhofer model and film thicknesses measured experimentally. The work presented here aims to work towards a more representative model by decoupling spontaneously deposited thickness (h_1) and spin deposited thickness (h_2). In the processes of validating the decoupled thickness model, several polymers were investigated, with the additional aim of probing the effects of crystallinity, hydrophobicity, and polymer charge on the polymer-substrate and polymer-polymer interactions. These interactions are relevant to the decoupled thickness model because they dictate the spontaneously deposited and spin deposited thicknesses, respectively, as well as the stability of the films.

It was determined that PVOH 99%H, PVOH 88%H, and PVP form stable thin films on silicon substrates. This result was confirmed using thermal annealing, after which thin films of all three polymers prepared at a range of spin rates remained continuous. The h_1 layer of PVOH 88%H and PVP was greater than that of PVOH 99%H, according to the thickness of the films prepared at 6000 rpm. This was attributed to the relative hydrophobicity of PVOH 88%H and PVP compared to PVOH 99%H, which is hypothesized to increase polymer-substrate interactions. Additionally, the h_2 thickness of PVOH 99%H and PVOH 88%H at lower spin rates was much higher than that of PVP. This was attributed to the crystallinity of PVOH, which increases the polymer-polymer interactions. None of the three stable polymers had spin curve exponents near the -0.5 value predicted by the Meyerhofer model.

It was determined that PAA, PAH, PSS, and PAA^- form metastable films on silicon substrates. All films dewet to some degree at some, if not all, of the spin rates. However, none of their spin curve exponents are zero, so they are not unstable systems. Although PAH and PSS had spin curve exponents near -0.5, PAA and PAA^- did not. All four polymers produced shallow spin curves, indicating a weak h_2 dependence on spin rate. This is indicative of weak polymer-polymer interactions, which is attributed to the lack of crystallinity and hydrophobicity, along with the repulsive nature of the polymer charge on PAH, PSS, and PAA^-. PAA, PAH, and PSS films all had low thicknesses at the highest spin rate, indicating weak polymer-substrate interactions. This was also attributed to polymer charge and lack of hydrophobicity. PAA^- had a similar h_2 dependence on spin rate as the other metastable polymers but was about 1 nm thicker at all spin rates than the PAA spin curve. This was attributed to the deposition of aggregates, forming an h_1 layer. Although both cohesive and adhesive forces appear to be weak for the metastable polymers, the fact that they all display some degree of dewetting suggests that polymer-polymer interactions are stronger than polymer-substrate interactions. It remains unclear why like-charge repulsion between polymers is a more favorable interaction than adhesion to the substrate, which in theory would be driven by hydrogen bonding.

The pH of PAH was increased from about 3 to about 7 to deprotonate the wafer and create a positive polymer-negative substrate system, and the pH of PAA was increased from about 3 to about 8-10 to create a negative polymer-negative substrate system. Both polymers aggregated upon addition of NaOH, and in both systems the aggregates displayed an affinity for the substrate, producing a significant h_1 layer. At higher spin rates, the larger aggregates were spun off, while the smaller aggregates remained adsorbed to the substrate. Boiling and increasing

pH to 10-11 were tested as methods for mitigating the aggregation of PAA^-; however, when used in conjunction, the two approaches exacerbated the aggregation.

Static adsorption experiments were conducted with PVOH 99%H, PVOH 88%H, PVP, PAA, PAH, PSS, and PAA^- to determine a value for the spontaneously deposited h_1 layer that could be subtracted from each polymer's spin curve to validate the decoupled thickness model. The results were unexpected in the context of the spin curves of each exponent. PVOH 88%H, PVP, and PAA^- all form relatively thick films at 6000 rpm compared to PVOH 99%H, PAA, PAH, and PSS. However, only PVP formed a spontaneously deposited film of significant thickness (~1.2 nm), while PVOH 88%H and PAA^- both formed films of negligible thickness and comparable to PVOH 99%H, PAA, PAH, and PSS. Additionally, the spontaneously deposited thickness for all polymers was thinner than what was projected by their spin curves, even for PVP, which was the thickest of the spontaneously deposited films. These discrepancies brought into question the validity of the static adsorption results. When the h_1 values obtained from static adsorption experiments were subtracted from the corresponding polymer's spin curve at each spin rate, there was no indication of the spin curves shifting towards the -0.5 value predicted by Meyerhofer. This is likely due to the inaccuracies of the h_1 thickness values obtained from static adsorption.

It was hypothesized that the h_1 layer thickness was underestimated by the results of the static adsorption experiments because the protocol involves three rinse steps that likely remove some or all of the h_1 layer. The portion of the h_1 layer that is removed by rinsing was termed the loosely bound layer. The loosely bound layer can comprise either the entire h_1 layer or just a region of the upper part of the h_1 layer (that was last to deposit). The centrifugal force at 6000 rpm is not strong enough to remove the loosely bound layer, which is why the h_1 thickness

predicted by looking at film thickness at the highest spin rate was thicker than the h_1 thickness predicted by static adsorption experiments. To test the loosely bound layer theory, static adsorption with PAA and PAA^- was performed using no, one, or three rinse steps. There was a clear decrease in spontaneously deposited thickness with increasing rinse steps, which supported the theory of the loosely bound layer.

There are several clear next steps for this project. First, repeating the modified static adsorption experiments with fewer rinse steps using the other five polymers (PVOH 99%H, PVOH 88%H, PVP, PAH, and PSS) will confirm whether they also have loosely bound layers that were rinsed off in the original set of static adsorption experiments. If it can be confirmed that the loosely bound layer is the source of the discrepancy in the original static adsorption experiments, the next step is to explore better experimental methods for producing a representative h_1 layer thickness for each polymer. Current possibilities include static adsorption with fewer rinse steps or dilution and spin-removal of solution after static adsorption, which is expected to remove the h_2 layer, but not the h_1 layer. If neither of these methods produce h_1 layers with accurate thicknesses, film thickness at the highest spin rate can be taken to act as a representative h_1 layer thickness value. Once h_1 values have been obtained for each polymer, subtracting these thicknesses from the corresponding spin curve at all spin rates will produce more accurate h_2 spin curves. This should be used to validate the decoupled thickness model and determine whether the spin curve exponents for h_2 spin curves are closer to the predicted -0.5 value. Finally, more work should be dedicated to investigating why hydrogen bonding is not a significant driving force for the adhesion of PAA, PAH, and PSS to the silicon substrate as well as why the repulsive electrostatic interactions between polymer chains are favorable enough to overcome adhesion of these polymers and lead to dewetting.

5. APPENDIX

The dewetting morphologies of spin coated metastable films can vary between samples, especially at lower spin rates. Representative images were selected to be displayed in **Tables V** and **VII**; however, included below are some additional AFM images of PAA, PAH, PSS, and PAA^- thin films that offer a more all-encompassing representation of the possible dewetting morphologies for these systems. Empty cells in **Tables XVII-XX** indicate that there were no additional distinct morphologies.

Table XVII. Supplemental AFM images (data scale 5 nm, aspect ratio 5 µm x 1.25 µm), section analysis, and RMS roughness (in nm) of 0.1 wt% PAA thin films prepared by spin coating on silicon wafer at various spin rates.

Spin Rate (rpm)	Images in Table V	Additional AFM Images, Section Analyses, and RMS Roughness Values	
900	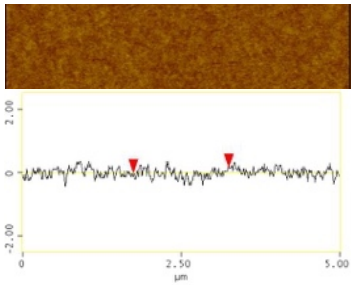 RMS = 0.145		

1400	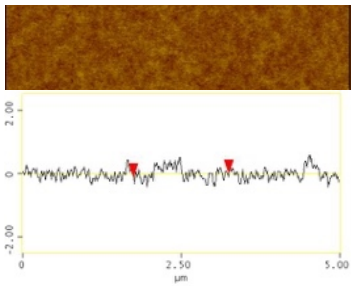 RMS = 0.154		
2200	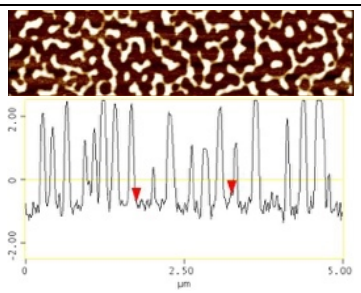 RMS = 1.185		
3500	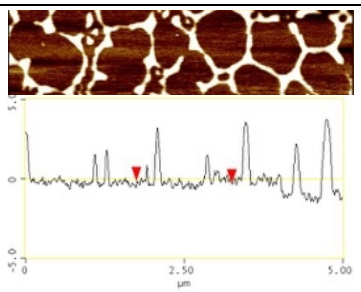 RMS = 1.197		
4800	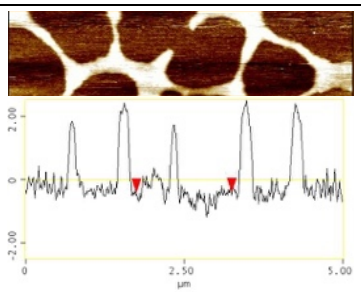 RMS = 1.118	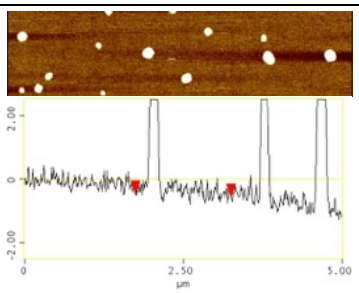 RMS = 0.546	
6000	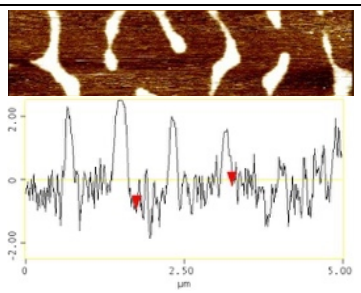 RMS = 1.094	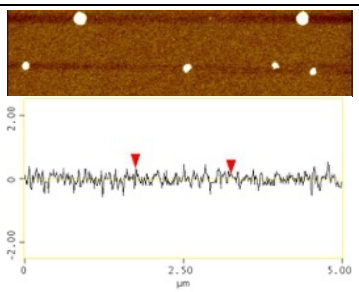 RMS = 0.487	

Table XVIII. Supplemental AFM images (data scale 5 nm, aspect ratio 5 µm x 1.25 µm), section analysis, and RMS roughness (in nm) of 0.1 wt% PAH thin films prepared by spin coating on silicon wafer at various spin rates.

Spin Rate (rpm)	Images in Table V	Additional AFM Images, Section Analyses, and RMS Roughness Values	
900	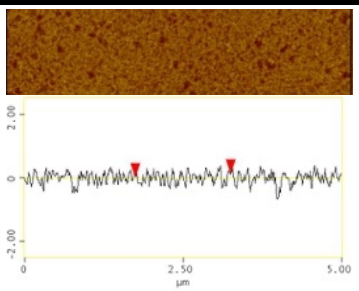 RMS = 0.194	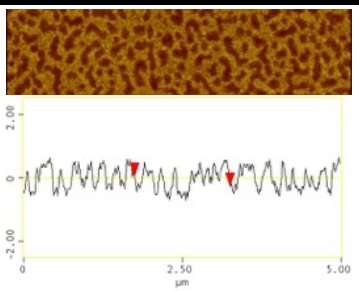 RMS = 0.303	
1400	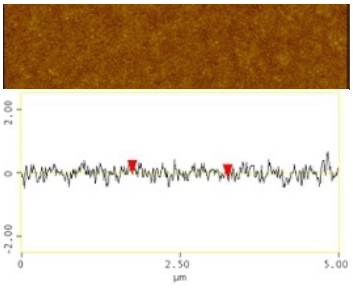 RMS = 0.156	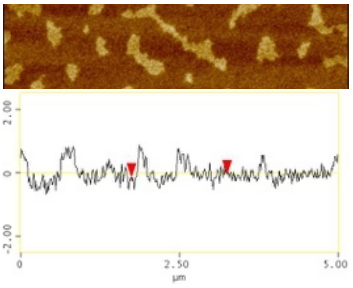 RMS = 0.323	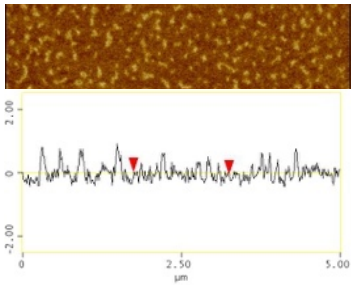 RMS = 0.257
2200	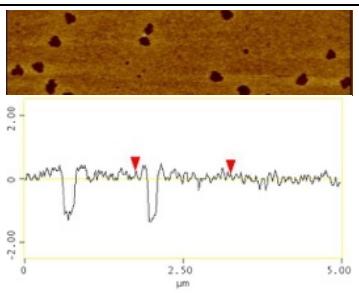 RMS = 0.253	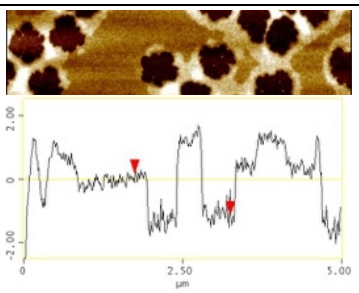 RMS = 0.992	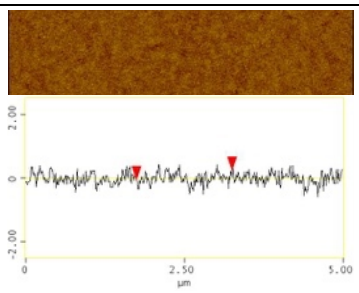 RMS = 0.173
3500	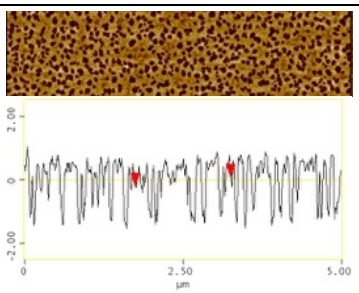 RMS = 0.668		

4800	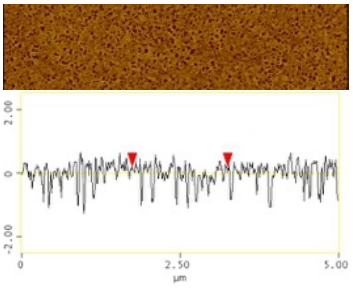 RMS = 0.315		
6000	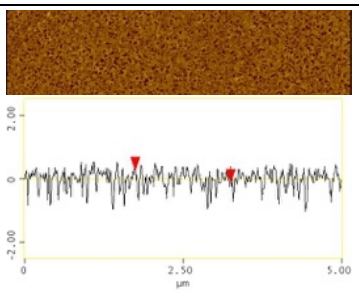 RMS = 0.292		

Table XIX. Supplemental AFM images (data scale 5 nm, aspect ratio 5 µm x 1.25 µm), section analysis, and RMS roughness (in nm) of 0.1 wt% PSS thin films prepared by spin coating on silicon wafer at various spin rates.

Spin Rate (rpm)	Images in Table V	Additional AFM Images, Section Analyses, and RMS Roughness Values	
900	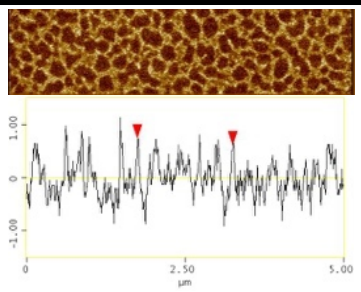 RMS = 0. 0.334	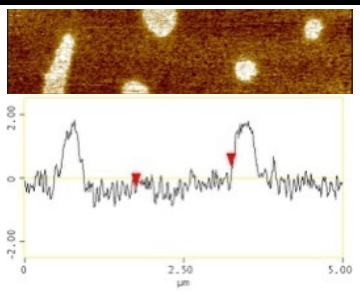 RMS = 0.527	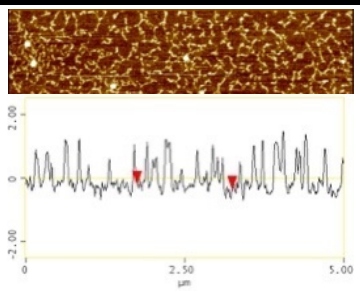 RMS = 0.540

1400	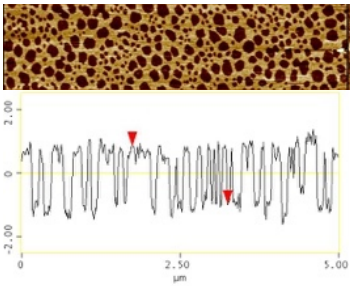 RMS = 0.835		
2200	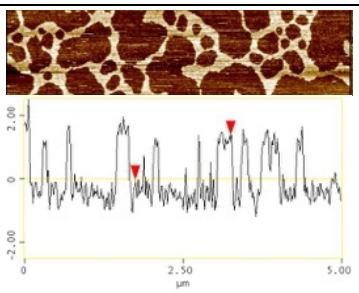 RMS = 0.857		
3500	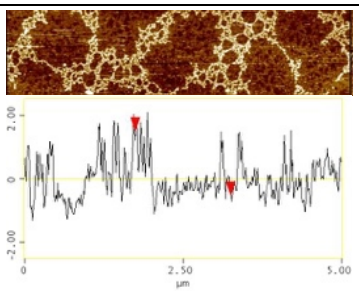 RMS = 0.702		
4800	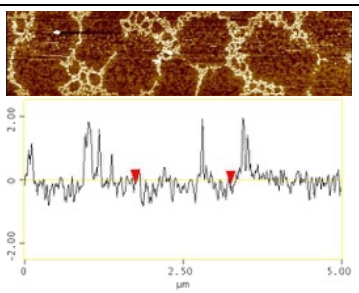 RMS = 1.236		
6000	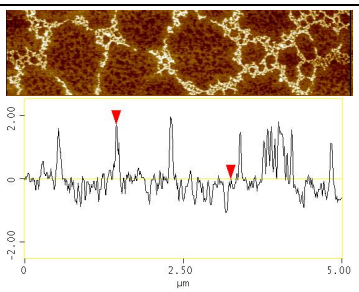 RMS = 0.583		

Table XX. Supplemental AFM images (data scale 5 nm, aspect ratio 5 µm x 1.25 µm), section analysis, and RMS roughness (in nm) of 0.1 wt% PAA^- thin films prepared by spin coating on silicon wafer at various spin rates.

Spin Rate (rpm)	Images in Table VII	Additional AFM Images, Section Analyses, and RMS Roughness Values		
900	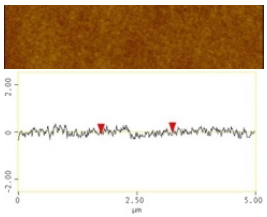 RMS = 0.127	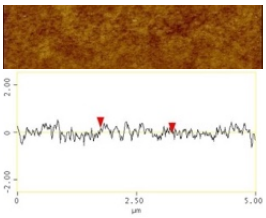 RMS = 0.222		
1400	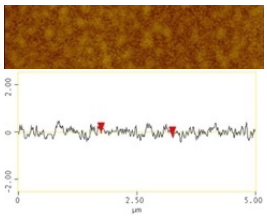 RMS = 0.169	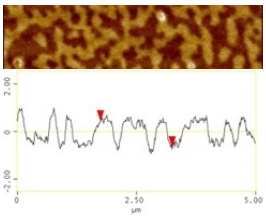 RMS = 0.413	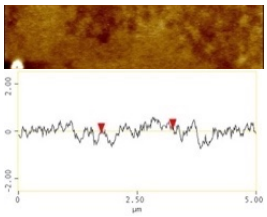 RMS = 0.317	
2200	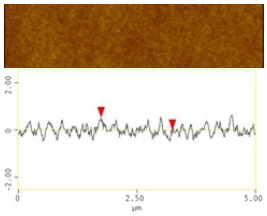 RMS = 0.191	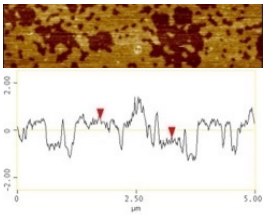 RMS = 0.519	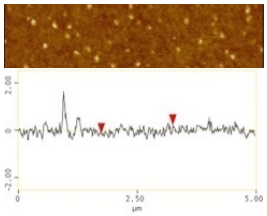 RMS = 0.196	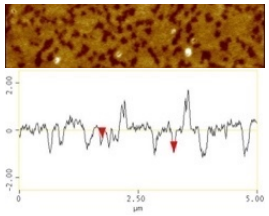 RMS = 0.365
3500	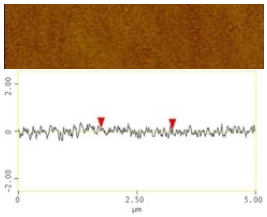 RMS = 0.139	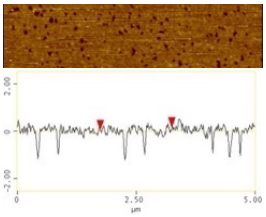 RMS = 0.256	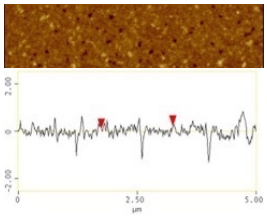 RMS = 0.225	

4800	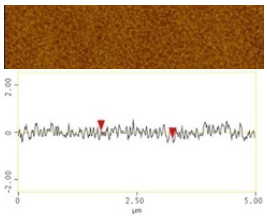 RMS = 0.175	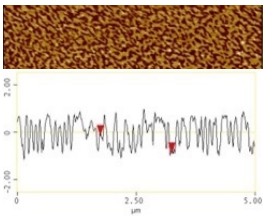 RMS = 0.523		
6000	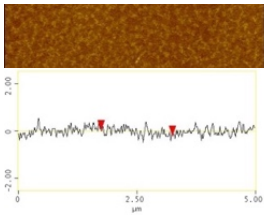 RMS = 0.158	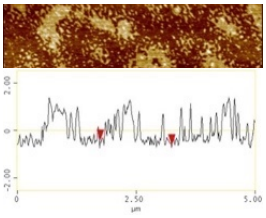 RMS = 0.545		

6. REFERENCES

1. Rao, M. C.; Shekhawat, M. S. A Brief Survey on Basic Properties of Thin Films for Device Application. *Int. J. Mod. Phys.: Conf. Ser.* **2013**, *22*, 576–582.
2. Coatings. https://www.mdpi.com/journal/coatings/special_issues/polymer_thin_film (accessed Apr 21, 2023).
3. De Witt, J. A.; Van de Ven, T. G. Kinetics and Reversibility of the Adsorption of Poly(Vinyl Alcohol) onto Polystyrene Latex Particles. *Langmuir* **1992**, *8* (3), 788–793.
4. Kozlov, M.; Quarmyne, M.; Chen, W.; McCarthy, T. J. Adsorption of Poly(Vinyl Alcohol) onto Hydrophobic Substrates. A General Approach for Hydrophilizing and Chemically Activating Surfaces. *Macromolecules*, **2003**, *36* (16), 6054–6059.
5. Kozlov, M.; McCarthy, T. J. Adsorption of Poly(Vinyl Alcohol) from Water to a Hydrophobic Surface: Effects of Molecular Weight, Degree of Hydrolysis, Salt, and Temperature. Langmuir **2004**, *20* (21), 9170–9176.
6. Barrett, D. A.; Hartshorne, M. S.; Hussain, M. A.; Shaw, P. N.; Davies, M. C. Resistance to Nonspecific Protein Adsorption by Poly(Vinyl Alcohol) Thin Films Adsorbed to a Poly(Styrene) Support Matrix Studied Using Surface Plasmon Resonance. *Anal. Chem.*, **2001**, *73* (21), 5232–5239.
7. Serizawa, T.; Hashiguchi, S.; Akashi, M. Stepwise Assembly of Ultrathin Poly(Vinyl Alcohol) Films on a Gold Substrate by Repetitive Adsorption/Drying Processes. *Langmuir*, **1999**, *15* (16), 5363–5368.
8. Bunn, C. W. Crystal Structure of Polyvinyl Alcohol. *Nature*, **1948**, *161* (4102), 929–930.
9. Mooney, R. C. An X-Ray Study of the Structure of Polyvinyl Alcohol*. *J. Am. Chem. Soc.*, **1941**, *63* (10), 2828–2832.
10. Colvin, B. G. Crystal Structure of Polyvinyl Alcohol. *Nature*, **1974**, *248* (5451), 756–759.
11. Assender, H. E.; Windle, A. H. Crystallinity in Poly(Vinyl Alcohol). 1. an X-Ray Diffraction Study of Atactic PVOH. *Polymer*, **1998**, *39* (18), 4295–4302.
12. Kenney, J. F.; Willcockson, G. W. Structure–Property Relationships of Poly(Vinyl Alcohol). III. Relationships between Stereo-Regularity, Crystallinity, and Water Resistance in Poly(Vinyl Alcohol). *J. Polym. Sci., Part A-1: Polym. Chem.*, **1966**, *4* (3), 679–698.
13. Tadokoro, H.; Seki, S.; Nitta, I. The Crystallinity of Solid High Polymers. i. The Crystallinity of Polyvinyl Alcohol Film. *Bull. Chem. Soc. Jpn.,* **1955**, *28* (8), 559–564.
14. Brydson, J. A. In Plastic materials; Butterworth: Woburn, MA, 1999; 386–397.
15. Horii, F.; Hu, S.; Ito, T.; Odani, H.; Kitamaru, R.; Matsuzawa, S.; Yamaura, K. Cross Polarization/Magic Angle Spinning 13C N.M.R. Study of Solid Structure and Hydrogen

Bonding of Poly(Vinyl Alcohol) Films with Different Tacticities. *Polymer*, **1992**, *33* (11), 2299–2306.

16. Tretinnikov, O. N.; Zagorskaya, S. A. Determination of the Degree of Crystallinity of Poly(Vinyl Alcohol) by FTIR Spectroscopy. *J. Appl. Spectrosc.,* **2012**, *79* (4), 521–526.
17. Miyazaki, T.; Miyata, N.; Yoshida, T.; Arima, H.; Tsumura, Y.; Torikai, N.; Aoki, H.; Yamamoto, K.; Kanaya, T.; Kawaguchi, D.; Tanaka, K. Detailed Structural Study on the Poly(Vinyl Alcohol) Adsorption Layers on a Si Substrate with Solvent Vapor-Induced Swelling. *Langmuir,* **2020**, *36* (13), 3415–3424.
18. Miyazaki, T.; Miyata, N.; Asada, M.; Tsumura, Y.; Torikai, N.; Aoki, H.; Yamamoto, K.; Kanaya, T.; Kawaguchi, D.; Tanaka, K. Elucidation of a Heterogeneous Layered Structure in the Thickness Direction of Poly(Vinyl Alcohol) Films with Solvent Vapor-Induced Swelling. *Langmuir,* **2019**, *35* (34), 11099–11107.
19. Wiśniewska, M. Temperature Effects on the Adsorption of Polyvinyl Alcohol on Silica. *Open Chem.,* **2012**, *10* (4), 1236–1244.
20. Tadros, T. F. Adsorption of Poly (Vinyl Alcohol) on Silica at Various Ph Values and Its Effect on the Flocculation of the Dispersion. *Hydrosols and Rheology,* **1976**, *355*.
21. Segal, T. What is a semiconductor and how is it used? https://www.investopedia.com/terms/s/semiconductor.asp (accessed Apr 21, 2023).
22. What is silicon wafer or silicon substrate? what is it used for? https://waferpro.com/what-is-a-silicon-wafer/ (accessed Apr 21, 2023).
23. Hartmann, E.; Hahn, P. O.; Behm, R. J. Determination of Nanometer Structures and Surface Roughness of Polished Si Wafers by Scanning Tunneling Microscopy. *J. Appl. Phys.,* **1991**, *69* (8), 4273–4281.
24. Morita, M.; Ohmi, T.; Hasegawa, E.; Kawakami, M.; Ohwada, M. Growth of Native Oxide on a Silicon Surface. *J. Appl. Phys.,* **1990**, *68* (3), 1272–1281.
25. Rimola, A.; Costa, D.; Sodupe, M.; Lambert, J.-F.; Ugliengo, P. Silica Surface Features and Their Role in the Adsorption of Biomolecules: Computational Modeling and Experiments. *Chem. Rev.,* **2013**, *113* (6), 4216–4313.
26. Sulpizi, M.; Gaigeot, M.-P.; Sprik, M. The Silica–Water Interface: How the Silanols Determine the Surface Acidity and Modulate the Water Properties. *J. Chem. Theory Comput.*, **2012**, *8* (3), 1037–1047.
27. Benoit, D.; Grimaldi, S.; Robin, S.; Finet, J.-P.; Tordo, P.; Gnanou, Y. Kinetics and Mechanism of Controlled Free-Radical Polymerization of Styrene and n-Butyl Acrylate in the Presence of an Acyclic β-Phosphonylated Nitroxide. *J. Am. Chem. Soc.,* **2000**, *122* (25), 5929–5939.
28. Michaels, A. S.; Morelos, O. Polyelectrolyte Adsorption by Kaolinite. *Ind. Eng. Chem. Res.* **1955**, *47* (9), 1801–1809.
29. Chang, C.; Muccio, D. D.; St. Pierre, T. Determination of the Tacticity and Analysis of the Ph Titration of Poly(Acrylic Acid) by Proton and Carbon-13 NMR. *Macromolecules,* **1985**, *18* (11), 2154–2157.

30. Petrov, A. I.; Antipov, A. A.; Sukhorukov, G. B. Base−Acid Equilibria in Polyelectrolyte Systems: from Weak Polyelectrolytes to Interpolyelectrolyte Complexes and Multilayered Polyelectrolyte Shells. *Macromolecules,* **2003**, *36* (26), 10079–10086.

31. Arkaban, H.; Barani, M.; Akbarizadeh, M. R.; Pal Singh Chauhan, N.; Jadoun, S.; Dehghani Soltani, M.; Zarrintaj, P. Polyacrylic Acid Nanoplatforms: Antimicrobial, Tissue Engineering, and Cancer Theranostic Applications. *Polymers,* **2022**, *14* (6), 1259.

32. Bartlett, P. D.; Altschul, R. The Polymerization of Allyl Compounds. II. Preliminary Kinetic Study of the Peroxide-Induced Polymerization of Allyl Acetate. *J. Am. Chem. Soc.,* **1945**, *67* (5), 816–822.

33. Bartlett, P. D.; Tate, F. A. The Polymerization of Allyl Compounds. Vi. the Polymerization of Allyl-1-D2 Acetate and the Mechanism of Its Chain Termination. *J. Am. Chem. Soc.,* **1953**, *75* (1), 91–95.

34. Volodina, V. I.; Tarasov, A. I.; Spasskii, S. S. Polymerisation of Allyl Compounds. *Russ. Chem. Rev.,* **1970**, *39* (2), 140–155.

35. Harada, S.; Shimizu, K. Process for Producing Polymers of Monoallylamie, U.S. Patent 4,528,347, July 9, 1985.

36. Harada, S.; Hasegawa, S. Process for Producing Monoallylamine Polymer, U.S. Patent 4,504,640, March 12, 1985.

37. Zhao, H. C.; Wu, X. T.; Tian, W. W.; Ren, S. T. Synthesis and Thermal Property of Poly(Allylamine Hydrochloride). *Adv. Mater. Res.,* **2010**, *150-151*, 1480–1483.

38. Fang, M.; Kim, C. H.; Saupe, G. B.; Kim, H.-N.; Waraksa, C. C.; Miwa, T.; Fujishima, A.; Mallouk, T. E. Layer-by-Layer Growth and Condensation Reactions of Niobate and Titanoniobate Thin Films. *Chem. Mater,* **1999**, *11* (6), 1526–1532.

39. Wang, Y.; Yu, A.; Caruso, F. Nanoporous Polyelectrolyte Spheres Prepared by Sequentially Coating Sacrificial Mesoporous Silica Spheres. Angew. Chem., **2005**, *117* (19), 2948–2952.

40. Johnston, A. P. R.; Cortez, C.; Angelatos, A. S.; Caruso, F. Layer-by-Layer Engineered Capsules and Their Applications. *Curr. Opin. Colloid Interface Sci.,* **2006**, *11* (4), 203–209.

41. Keoshkerian, B.; Georges, M. K.; Boils-Boissier, D. Living Free-Radical Aqueous Polymerization. *Macromolecules,* **1995**, *28* (18), 6381–6382.

42. Mannan, M. A.; Fukuda, K.; Miura, Y. Living Radical Polymerization of Sodium 4-Styrenesulfonate Mediated by New Water-Soluble Nitroxides. *Polym. J.,* **2007**, *39* (6), 500–501.

43. Huang, W.; Charleux, B.; Chiarelli, R.; Marx, L.; Rassat, A.; Vairon, J.-P. Synthesis of Water-Soluble Nitroxides and Their Use as Mediators in Aqueous-Phase Controlled Radical Polymerization. *Macromol. Chem. Phys.,* **2002**, *203* (10-11), 1715–1723.

44. Sultana, N.; Chang, H. C.; Jefferson, S.; Daniels, D. E. Application of Conductive Poly(3,4-Ethylenedioxythiophene):Poly(Styrenesulfonate) (PEDOT:PSS) Polymers in Potential Biomedical Engineering. *J. Pharm. Invest.,* **2020**, *50* (5), 437–444.

45. Shahini, A.; Yazdimamaghani, M.; Walker, K. J.; Eastman, M.; Hatami-Marbini, H.; Smith, B.; Ricci, J. L.; Madihally, S.; Vashaee, D. 3D Conductive Nanocomposite Scaffold for Bone Tissue Engineering. *Int. J. Nanomed.,* **2013**, *167*.

46. Guex, A. G.; Puetzer, J. L.; Armgarth, A.; Littmann, E.; Stavrinidou, E.; Giannelis, E. P.; Malliaras, G. G.; Stevens, M. M. Highly Porous Scaffolds of PEDOT:PSS for Bone Tissue Engineering. *Acta Biomater.,* **2017**, *62*, 91–101.

47. Heo, D. N.; Lee, S.-J.; Timsina, R.; Qiu, X.; Castro, N. J.; Zhang, L. G. Development of 3D Printable Conductive Hydrogel with Crystallized Pedot:PSS for Neural Tissue Engineering. *Mater. Sci. Eng., C,* **2019**, *99*, 582–590.

48. Ray, K.; Badugu, R.; Lakowicz, J. R. Polyelectrolyte Layer-by-Layer Assembly to Control the Distance between Fluorophores and Plasmonic Nanostructures. *Chem. Mater.*, **2007**, *19* (24), 5902–5909.

49. Georgianos, P. I.; Liampas, I.; Kyriakou, A.; Vaios, V.; Raptis, V.; Savvidis, N.; Sioulis, A.; Liakopoulos, V.; Balaskas, E. V.; Zebekakis, P. E. Evaluation of the Tolerability and Efficacy of Sodium Polystyrene Sulfonate for Long-Term Management of Hyperkalemia in Patients with Chronic Kidney Disease. *Int. Urol. Nephrol.,* **2017**, *49* (12), 2217–2221.

50. Watling, S. M.; Gehrke, J. C.; Gehrke, C. W.; Zumwalt, R.; Pribble, J. In Vitro Binding of Lithium Using the Cation Exchange Resin Sodium Polystyrene Sulfonate. *Am. J. Emerg. Med.*, **1995**, *13* (3), 294–296.

51. Haaf, F.; Sanner, A.; Straub, F. Polymers of N-Vinylpyrrolidone: Synthesis, Characterization and Uses. *Polym. J.,* **1985**, *17* (1), 143–152.

52. Wan, D.; Satoh, K.; Kamigaito, M.; Okamoto, Y. Xanthate-Mediated Radical Polymerization of n-Vinylpyrrolidone in Fluoroalcohols for Simultaneous Control of Molecular Weight and Tacticity. *Macromolecules,* **2005**, *38* (25), 10397–10405.

53. Guzenko, N. V.; Pakhlov, E. M.; Lipkovskaya, N. A.; Voronin, E. F. Sorption Modification of Fine Silica with Polyvinylpyrrolidone. *Russ. J. Appl. Chem.*, **2001**, *74* (12), 2017–2020.

54. Al-Harbi, L. M.; Kosa, S. A.; Baloch, M. K.; Bhatti, Q. A.; El-Mossalamy, E.-S. E.-B. Adsorption of Polyvinylpyrrolidone over the Silica Surface: As Affected by Pretreatment of Adsorbent and Molar Mass of Polymer Adsorbate. *Int. J. Polym. Sci.,* **2016**, *2016*, 1–9.

55. Robinson, S.; Williams, P. A. Inhibition of Protein Adsorption onto Silica by Polyvinylpyrrolidone. *Langmuir* **2002**, *18* (23), 8743–8748.

56. Cohen Stuart, M. A.; Fleer, G. J.; Bijsterbosch, B. H. The Adsorption of Poly(Vinyl Pyrrolidone) onto Silica. I. Adsorbed Amount. *J. Colloid Interface Sci.* **1982**, *90* (2), 310–320.

57. Cohen Stuart, M. A.; Fleer, G. J.; Bijsterbosch, B. H. Adsorption of Poly(Vinyl Pyrrolidone) on Silica. II. the Fraction of Bound Segments, Measured by a Variety of Techniques. *J. Colloid Interface Sci.,* **1982**, *90* (2), 321–334.

58. Molaei, M.-A.; Osouli-Bostanabad, K.; Adibkia, K.; Shokri, J.; Asnaashari, S.; Javadzadeh, Y. Enhancement of Ketoconazole Dissolution Rate by the Liquisolid Technique. *Acta Pharm.,* **2018**, *68* (3), 325–336.

59. Javadzadeh, Y.; Jafari-Navimipour, B.; Nokhodchi, A. Liquisolid Technique for Dissolution Rate Enhancement of a High Dose Water-Insoluble Drug (Carbamazepine). *Int. J. Pharm.,* **2007**, *341* (1-2), 26–34.

60. Zhang, N.; Wang, C.-X.; Liu, J.-H.; Xing, J.-F.; Dong, A.-J. A Kind of Modified Bovine Serum Albumin with Great Potential for Applying in Gene Delivery. *Chin. Chem. Lett.,* **2013**, *24* (7), 659–662.

61. Panda, H. *Herbal Cosmetics Handbook*; Asia Pacific Business Press Inc.: Delhi, 2015; 278–386.

62. Zinner, D. D.; Jablon, J. M.; Saslaw, M. S. Bactericidal Properties of Povidone-Iodine and Its Effectiveness as an Oral Antiseptic. *Oral Surg., Oral Med., Oral Pathol.,* **1961**, *14* (11), 1377–1382.

63. Bidra, A. S.; Pelletier, J. S.; Westover, J. B.; Frank, S.; Brown, S. M.; Tessema, B. Rapid in-Vitro Inactivation of Severe Acute Respiratory Syndrome Coronavirus 2 (SARS-COV-2) Using Povidone-Iodine Oral Antiseptic Rinse. *J. Prosthodontics,* **2020**, *29* (6), 529–533.

64. Mark, J. E. *Physical Properties of Polymers Handbook*; Springer: Cincinnati, OH, 2007; 208–212.

65. Sepehrianazar, A.; Güven, O. Free Radical Polymerization of Allylamine in Different Acidic Media. *Polym. Polym. Compos.,* **2022**, *30*, 096739112211035.

66. Balding, P.; Borrelli, R.; Volkovinsky, R.; Russo, P. S. Physical Properties of Sodium Poly(Styrene Sulfonate): Comparison to Incompletely Sulfonated Polystyrene. *Macromolecules,* **2022**, *55* (5), 1747–1762.

67. Mark, J. E. *Polymer data handbook*; Oxford University Press: Oxford, 1998.

68. Brinker, C. J.; Hurd, A. J.; Frye, G. C.; Schunk, P. R.; Ashley, C. S. Sol-Gel Thin Film Formation. *J. Ceram. Soc. Jpn.*, **1991**, *99* (1154), 862–877.

69. Bornside, D. E.; Macosko, C. W.; Scriven, L. E. On the Modeling of Spin Coating. *J. Imaging Technol.,* **1987**, *13* (4), 122–130.

70. Jiang, Y.; Minett, M.; Hazen, E.; Wang, W.; Alvarez, C.; Griffin, J.; Jiang, N.; Chen, W. New Insights into Spin Coating of Polymer Thin Films in Both Wetting and Nonwetting Regimes. *Langmuir,* **2022**, *38* (41), 12702–12710.

71. Meyerhofer, D. Characteristics of Resist Films Produced by Spinning. *J. Appl. Phys.*, **1978**, *49* (7), 3993–3997

72. Bornside, D. E.; Macosko, C. W.; Scriven, L. E. Spin Coating of a PMMA/Chlorobenzene Solution. *J. Electrochem. Soc.,* **1991**, *138* (1), 317–320.

73. Daughton, W. J.; Givens, F. L. An Investigation of the Thickness Variation of Spun-on Thin Films Commonly Associated with the Semiconductor Industry. *J. Electrochem. Soc.,* **1982**, *129* (1), 173–179.

74. Berry, M. V. The Molecular Mechanism of Surface Tension. *Phys. Educ.,* **1971**, *6* (2), 79–84.

75. De Gennes, P.-G.; Brochard-Wyart Françoise; Quere, D.; Reisinger, A. *Capillarity and wetting phenomena: Drops, bubbles, pearls, waves*; Springer: New York, NY, 2004.

76. Young, T. An Essay on the Cohesion of Fluids. *Philos. Trans. R. Soc. London,* **1805**, *95*, 65–87.

77. Gentili, D.; Foschi, G.; Valle, F.; Cavallini, M.; Biscarini, F. Applications of Dewetting in Micro and Nanotechnology. *Chem. Soc. Rev.,* **2012**, *41* (12), 4430.

78. Reiter, G. Unstable Thin Polymer Films: Rupture and Dewetting Processes. *Langmuir,* **1993**, *9* (5), 1344–1351.

79. Seemann, R.; Herminghaus, S.; Jacobs, K. Dewetting Patterns and Molecular Forces: A Reconciliation. *Phys. Rev. Lett.,* **2001**, *86* (24), 5534–5537.

80. Sharma, A. Relationship of Thin Film Stability and Morphology to Macroscopic Parameters of Wetting in the Apolar and Polar Systems. *Langmuir,* **1993**, *9* (3), 861–869.

81. Thiele, U.; Mertig, M.; Pompe, W. Dewetting of an Evaporating Thin Liquid Film: Heterogeneous Nucleation and Surface Instability. *Phys. Rev. Lett.* **1998**, *80* (13), 2869–2872.